Mälardalen University Press Dissertations
No. 176

MATHEMATICAL TOOLS APPLIED IN COMPUTATIONAL ELECTROMAGNETICS FOR A BIOMEDICAL APPLICATION AND ANTENNA ANALYSIS

Farid Monsefi

2015

MÄLARDALEN UNIVERSITY
SWEDEN

School of Education, Culture and Communication

ISBN 978-91-7485-200-4
ISSN 1651-4238
Printed by Arkitektkopia, Västerås, Sweden

Mälardalen University Press Dissertations
No. 176

MATHEMATICAL TOOLS APPLIED IN COMPUTATIONAL ELECTROMAGNETICS FOR A BIOMEDICAL APPLICATION AND ANTENNA ANALYSIS

Farid Monsefi

Akademisk avhandling

som för avläggande av teknologie doktorsexamen i matematik/tillämpad matematik vid Akademin för utbildning, kultur och kommunikation kommer att offentligen försvaras tisdagen den 12 maj 2015, 13.15 i Delta, Mälardalens högskola, Västerås.

Fakultetsopponent: associate researcher Jean-Pierre Bérenger, LEAT Universite Nice Sophia Antipolis - CNRS

Akademin för utbildning, kultur och kommunikation

Abstract

To ensure a high level of safety and reliability of electronic/electric systems EMC (electromagnetic compatibility) tests together with computational techniques are used. In this thesis, mathematical modeling and computational electromagnetics are applied to mainly two case studies. In the first case study, electromagnetic modeling of electric networks and antenna structures above, and buried in, the ground are studied. The ground has been modelled either as a perfectly conducting or as a dielectric surface. The second case study is focused on mathematical modeling and algorithms to solve the direct and inverse electromagnetic scattering problem for providing a model-based illustration technique. This electromagnetic scattering formulation is applied to describe a microwave imaging system called Breast Phantom. The final goal is to simulate and detect cancerous tissues in the human female breast by this microwave technique.

The common issue in both case studies has been the long computational time required for solving large systems of equations numerically. This problem has been dealt with using approximation methods, numerical analysis, and also parallel processing of numerical data. For the first case study in this thesis, Maxwell's equations are solved for antenna structures and electronic networks by approximation methods and parallelized algorithms implemented in a LAN (Local Area Network). In addition, PMM (Point-Matching Method) has been used for the cases where the ground is assumed to act like a dielectric surface. For the second case study, FDTD (Finite-Difference Time Domain) method is applied for solving the electromagnetic scattering problem in two dimensions. The parallelized numerical FDTD-algorithm is implemented in both Central Processing Units (CPUs) and Graphics Processing Units (GPUs).

ISBN 978-91-7485-200-4
ISSN 1651-4238

Acknowledgements

I would like to extend my gratitude to the many people who helped me to accomplish this thesis. First and foremost, I would like to thank my supervisor Professor Sergei Silvestrov for his help, professionalism, valuable guidance and support throughout this project. I would also like to gratefully acknowledge my co-supervisor Dr. Magnus Otterskog for his continuous support and encouragement in almost everything in my research work. I am really grateful to my co-supervisor Dr. Linus Carlsson for his support and numerous valuable conversations in theoretical concepts and also his accurate and insightful comments and suggestions about the thesis. I would like to express my deep sincere appreciation to Dr. Miliča Rančić for numerous conversations about electromagnetic modeling and a fruitful collaboration and also for her help and many valuable suggestions.

I have enjoyed the stimulating and friendly working atmosphere at UKK and IDT, Mälardalen University. Special thanks to UKK's Administration for their kind help and taking care of administrative issues. I wish to thank all my colleagues at the Division of Applied Mathematics at Mälardalen University for their support and ideas. I am deeply indebted to Professor Anatoliy Malyarenko for his insightful comments about the thesis, valuable conversations and also Latex implementation of this work. Many thanks goes to Karl Lundengård, Christopher Engström and Jonas Österberg for so much help in many things. Special thanks to Hillevi Gavel for her accurate and careful corrections. I would also like to thank Alex Tumwesigye for his kind help in functional analysis and other related mathematical concepts. I am really grateful to my friend and colleague Dr. Nikola Petrović at IDT and Per Olov Risman, for help and many valuable conversations in this research project. Many thanks goes also to Simon Elgland for a fruitful collaboration in the subject of parallelism.

I would express my sincere gratitude to Mathias Erlandsson who was the first one that presented the Mamacell project to me. Thanks to him I could start this interesting wonderful PhD project. I would also like to thank the

RALF3 project funded by the Swedish Foundation for Strategic Research (SSF), not only for providing the funding which allowed me to undertake this research, but also for giving me the opportunity to attend conferences and meet so many interesting people. During this research I have had the pleasure to meet several people from the RALF3 project. Thank you for all brilliant ideas and conversations.

I would like to thank our family friends Rabizadegans, Modarresis and Liaghats, here in Västerås, for encouraging and supporting me and my family during these years of my research. I gratefully acknowledge my brother-in-law, Dr. Mahmoud Heyrat, for lot of fruitful conversations on Skype about Green's functions and electromagnetism. I am grateful to my friend, Dr. George Fodor for his support and kindness and all the theoretical things I have learned from him.

I am deeply grateful to my brothers and sisters for their love, support and inspiration. As time goes on, I realize more and more clearly the huge impact that Eti and Aliashraf have had on my academic career and my life. I admire you all, each of you in a different way.

Last, but not least, I must express my very profound gratitude to my wife Fathieh and my children Navid and Nicki for providing me with unfailing support and continuous encouragement; for their sacrifice during my years of study and through the process of researching and writing this thesis. This accomplishment would not have been possible without you. Thank you my dearest family, I love you all.

I dedicate this thesis to the memory of my parents Badri Honarmand and Mohammadali Monsefi and my brother Said, whose role in my life was, and remains, immense.

Västerås, March, 2015
Farid Monsefi

This work was done in the frame of the RALF3 project funded by the Swedish Foundation for Strategic Research (SSF).

List of Papers

The present thesis contains the following papers:

Paper A. Monsefi, F., Ekman, J. (2006). Antenna analysis using PEEC and the complex image methods. In: *Proceedings of the Nordic Antenna Symposium*, Linköping, Sweden, 2006.

Paper B. Ekman, J., Monsefi, F. (2006). Optimization of PEEC based electromagnetic modeling code using grid computing. In: *Proceedings of the EMC Europe International Symposium on Electromagnetic Compatibility*, Barcelona, Spain, 2006, 45–50.

Paper C. Monsefi, F., Rančić, M., Aleksić, S., Silvestrov, S. (2014). Sommerfeld's integrals and Hallén's integral equation in data analysis for horizontal dipole antenna above real ground. In: *Proceedings of the 3rd Stochastic Modeling Techniques and Data Analysis International Conference - SMTDA 2014*, Lisbon, Portugal, 2014.

Paper D. Monsefi, F., Rančić, M., Aleksić, S., Silvestrov, S. (2014). HF analysis of thin horizontal central-fed conductor above lossy homogeneous soil. In: *Proceedings of EMC Europe 2014*, Gothenburg, Sweden, 2014, 916–921.

Paper E. Perić, M., Ilić, S., Aleksić, S., Raičević, N., Monsefi, F., Rančić, M., Silvestrov, S. (2014). Analysis of shielded coupled microstrip line with partial dielectric support. In: *Proceedings of XVII-th International Symposium on Electrical Apparatus and Technologies - SIELA 2014*, Bourgas, Bulgaria, 2014.

Paper F. Monsefi, F., Carlsson, L., Rančić, M., Otterskog, M., Silvestrov, S. (2014). Solution of 2D electromagnetic scattering problem by FDTD with optimal step size, based on a discrete norm analysis. In: *Proceedings of 10th International Conference on Mathematical Problems in Engineering, Aerospace and Sciences - ICNPAA 2014*, Narvik, Norway, 2014.

Paper G. Monsefi, F., Elgland S., Otterskog M., Rančić M., Carlsson L., Silvestrov, S. (2014). GPU Implementation of a Biological Electromagnetic Scattering Problem by FDTD. In: *16th ASMDA Conference Proceedings, 30 June-4 July 2015*, Piraeus, Greece.

Parts of the thesis have been presented at the following international conferences:

1. The Nordic Antenna Symposium, Linköping, Sweden, May 30 - June 1, 2006.
2. EMC Europe International Symposium on Electromagnetic Compatibility, Barcelona, Spain, September 6-9, 2006.
3. XVII-th International Symposium on Electrical Apparatus and Technologies - SIELA 2014, Bourgas, Bulgaria, May 29-31, 2014.
4. 3rd Stochastic Modeling Techniques and Data Analysis International Conference - SMTDA 2014, Lisbon, Portugal, June 11-14, 2014.
5. 10th International Conference on Mathematical Problems in Engineering, Aerospace and Sciences - ICNPAA 2014, Narvik, Norway, July 15-18, 2014.
6. EMC Europe 2014, Gothenburg, Sweden, September 1-4, 2014.
7. 16th ASMDA Conference, Piraeus, Greece, 2015.

Parts of the thesis have also been published in the following paper:

- Monsefi, F., Otterskog, M., Silvestrov, S., "*Direct and Inverse Computational Methods for Electromagnetic Scattering in Biological Diagnostics*", Mathematical Physics (math-ph), Cornell University Library.
  URL: http://arxiv.org/find/all/1/all:+AND+farid+monsefi/0/1/0/all/0/1

Contents

1 Introduction

Almost any problem involving derivatives, integrals, or non-linearities cannot be solved in a finite number of steps and thus must be solved by a theoretically infinite number of iterations for converging to an ultimate solution; this is not possible for practical purposes where problems will be solved by a finite number of iterations until the answer is approximately correct. Indeed, the major aspect is, by this approach, finding rapidly convergent iterative algorithms in which the error and accuracy of the solution will also be computed. In computational electromagnetics, a difficult problem like a partial differential equation or an integral equation will be replaced by, for instance, a much simpler system of linear equations. Replacing complicated functions with simple ones, non-linear problems with linear problems, high-order systems by low-order systems and infinite-dimensional spaces with finite-dimensional spaces are applied as other alternatives to solve easier problems that have approximately the same solution to a difficult mathematical model. Numerical modeling of electromagnetic (EM) properties are used in, for example, the electronic industry to:

1. *Ensure functionality of electric systems.* System performance can be degraded due to unwanted EM interference coupling into sensitive parts.

2. *Ensure compliance with electromagnetic compatibility (EMC) regulations and directives.* To prevent re-designs of products and ensure compliance with directives post-production.

3. *Calculate EM properties of tissues inside the human body.* To detect, for example, cancerous tissues.

Methods for determining electromagnetic field quantities, can be classified as experimental, analytical (exact), or numerical (approximate). The experimental techniques are expensive and time-consuming but are still used. The analytic solution of Maxwell's equations involves, among others, *separation of variables* and *series expansion*, but are not applicable in the general case. The numerical solution of the field problems became possible with the availability of high performance computers. The most popular numerical techniques are (1) *Finite difference methods (FDM)*, (2) *Finite element methods (FEM)*, (3) *Moment methods (MoM)*, (4) *Partial element equivalent circuit (PEEC) method.* The differences in the numerical techniques have their origin in the basic mathematical approach and therefore make

one technique more suitable for a specific *class of problems* compared to the others. Typical classes of problems in the area of EM modeling are:

- Printed circuit board (PCB) simulations (mixed circuit and EM problem).
- Electromagnetic field strength and pattern characterization.
- Antenna design.
- Microwave image reconstruction.

Further, the problems presented above require different kinds of analysis in terms of:

- Requested solution domain (time and/or frequency).
- Requested solution variables (currents and/or voltages or electric and/or magnetic fields).

The categorization of EM problems into classes and requested solutions in combination with the complexity of Maxwell's equations emphasizes the importance of using the right numerical technique for the right problem to enable a solution in terms of accuracy and computational effort.

In many disciplines such as image and signal processing, astrophysics, acoustics, quantum mechanics, geophysics and electromagnetic scattering, inverse formulations are solved on a daily basis. The inverse formulation, as an interdisciplinary field, involves people from different fields within natural science. To find out the contents of a given black box without opening it by studying the input and output, would be a good analogy to describe the general inverse problem. Experiments will be carried on to guess and realize the inner properties of the box. It is common to call the contents of the box "the model" and the result of the experiment "the data". The experiment itself is called "the forward modeling". As sufficient information cannot be provided by an experiment, a process of regularization will be needed. The reason to this issue is that there can be more than one model ('different black boxes') that would produce the same data. On the other hand, ill-posed numerical computations will occur in the calculation procedure. Thus, a process of regularization constitutes a major step to solve the inverse problem. Regularization is used at the moment when selection of the most reasonable model is on focus. Computational methods and techniques ought to be as flexible as possible from case to case. A computational technique utilized for small problems may fail totally when it is used to large numerical

domains within the inverse formulation. It is worth noting that 'small' and 'large' are relative concepts and they are changing rapidly with the progress of computer technology. A coefficient matrix of size of hundreds of millions can be considered large if one is using a high-performance computer while, similarly, a coefficient matrix of size of a few thousands can also be considered large if one is working on a workstation. Hence, methodologies and algorithms have to be created for new problems though existing methods are insufficient and computer technology is progressing rapidly. This is the major character of the existing inverse formulation in problems with large numerical domains. There are both old and new computational tools and techniques for solving linear and nonlinear inverse problems. When existing numerical algorithms fail, new algorithms must be developed to carry out nonlinear inverse problems.

Electromagnetic inverse and direct scattering problems are, like other related areas, of equal interest. The electromagnetic scattering theory is about the effect an inhomogeneous medium has on an incident wave where the total electromagnetic field is consisted of the incident and the scattered field. The direct problem in such context is to determine the scattered field from the knowledge of the incident field and also from the governing wave equation deduced from the Maxwell's equations. Even though the direct scattering problem has been thoroughly investigated, the inverse scattering problem has not yet a rigorous mathematical/numerical basis. Because the nonlinearity nature of the inverse scattering problem, one will face ill-posed numerical computation. This means that, in particular applications, small perturbations in the measured data cause large errors in the reconstruction of the scatterer. Some regularization methods must be used to remedy the ill-conditioning due to the resulting matrix equations. Concerning the existence of a solution to the inverse electromagnetic scattering one has to think about finding approximate solutions after making the inverse problem stabilized. A number of methods is given to solve the inverse electromagnetic scattering problem in which the nonlinear and ill-posed nature of the problem are acknowledged. Earlier attempts to stabilize the inverse problem was via reducing the problem into a linear integral equation of the first kind. However, general techniques were introduced to treat the inverse problems without applying any integral equation formulation of the problem.

1.1 Background and Motivation

The vast and increasing applications of antennas within the electronic industry and biomedical applications desires constant mathematical analysis for

new antenna structures. A good design of antenna, based on a mathematical modeling, improves performance of an electronic device or system. In addition, to optimize the radiation energy in an advanced wireless system, the antenna serves as both a directional device and probing device. Antennas have a central role in the microwave technique in which the direct, and inverse electromagnetic scattering problem are solved in a system consisting of several antennas and wave-guides.
In order to guarantee operability of advanced electronic devices and systems, electromagnetic measurements should be compared to results from computational methods. The experimental techniques are expensive and time consuming but are still widely used. Hence, the advantage of obtaining data from tests can be weighted against the large amount of time and expense required to operate such tests. However, in some EM modeling applications like the scattering problem, information from both the numerical solution and experimental data is required and used in, for instance, a least-squares method. Analytic solution of Maxwell's equations offers many advantages over experimental methods but applicability of analytical electromagnetic modeling is often limited to simple geometries and boundary conditions. Analytical solutions of Maxwell's equations by the method of *separation of variables* and *series expansions* have a limited scope and they are not applicable in a general case and rarely in a real-world application. Availability of high performance computers during the last decades has been one of the reasons to use numerical techniques within computational modeling to solve Maxwell's equations also for complicated geometries and boundaries.

Scattering theory has had a major roll in twentieth century mathematical physics. In computational electromagnetics, the direct scattering problem is to determine a scattered field from knowledge of an incident field and the differential equation governing the wave equation. The incident field is emitted from a source, an antenna for instance, against an inhomogeneous medium. The total field is assumed to be the sum of the incident field and the scattered field. The governing differential equation in such cases is the coupled differential form of Maxwell's equations, which will be converted to the wave equation.

In some applications, a model based illustration technique within the microwave range is used to determine EM properties of biological tissues. Appropriate algorithms are used to make it possible for parallel processing of the heavy and large numerical calculation due to the inverse formulation of the problem. The parallelism of the calculations can then be implemented

and performed on GPU:s, CPU:s, and FPGA:s. By the aid of a deeper mathematical analysis and thereby faster numerical algorithms, an improvement of the existing numerical algorithms is expected. The algorithms may be in the the time domain, frequency domain and a combination of both domains.

The main objective of this thesis is to apply mathematical modeling and algorithms for different antenna structures used in EMC applications and biological diagnostic technique. For EMC applications, radiation due to different antenna structures, above and in the proximity of the ground, is investigated. The ground has been assumed as both a perfect conductor and as a lossy medium. In comparison to situations where the ground is acting like a perfect conductor, more complicated mathematical models are desired to analyze antenna structures close to the ground as a lossy medium. In this thesis, this kind of problems are solved by both approximative and numerical methods. For biomedical applications, the EM scattering formulation in two dimensions is solved and analyzed by finite difference approximations. The Finite Difference Time Domain (FDTD) method is used in this thesis to solve the two-dimensional electromagnetic scattering problem, first by a single processor. The electromagnetic scattering problem is, in fact, resembling a so-called *Breast Phantom*. The Breast Phantom is used to simulate human female breast by the microwave technology, detecting cancerous tissues in the breast. To speedup computational time, the FDTD algorithm is then parallelized by CPUs, GPUs, and FPGAs. The long computational time is a crucial issue when solving such kind of electromagnetic scattering problems. The new parallelized algorithms are developed and implemented in MATLAB and Octave to be re-programmed and executed in C, as a more optimized environment; this re-programming is done to suit the algorithms to GPU:s, CPU:s, and FPGA:s. The GPU parallelized algorithm is implemented in OpenCL and CUDA.

2 Related Concepts in Electromagnetism

[1] In constructing the electrostatic model, the electric field intensity vector **E** and the electric flux density vector, **D**, are respectively defined. The fundamental governing differential equations are [10]

$$\begin{aligned} \nabla \times \mathbf{E} &= 0, \\ \nabla \cdot \mathbf{D} &= \rho_v, \end{aligned} \tag{1}$$

where ρ_v is the free charge density. By introducing $\epsilon = \epsilon_r \epsilon_0$ as the the *electric permittivity* where ϵ_r is *relative permittivity*, and $\epsilon_0 = 8.854 \times 10^{-12}$ F/m, the *permittivity of the free space* for a linear and isotropic media, **E** and **D** are related by relation

$$\mathbf{D} = \epsilon \mathbf{E}. \tag{2}$$

The fundamental governing equations for magnetostatic model are

$$\begin{aligned} \nabla \cdot \mathbf{B} &= 0, \\ \nabla \times \mathbf{H} &= \mathbf{J}, \end{aligned} \tag{3}$$

where **B** and **H** are defined as the magnetic flux density vector and the magnetic field intensity vector, respectively. In the above, **J** is conducting current. **B** and **H** are related as

$$\mathbf{H} = \frac{1}{\mu_0 \mu_r} \mathbf{B}, \tag{4}$$

where $\mu_0 \mu_r = \mu$ is defined as the magnetic permeability of the medium which is measured in H/m.; $\mu_0 = 4\pi \times 10^{-7}$ H/m is called *permeability of space* and μ_r is the relative magnetic permeability. The medium in question is assumed to be linear and isotropic. Eqns. (1) and (3) are known as Maxwell's equations in local form and constitute the foundation of electromagnetic theory. As it is seen in the above relations, **E** and **D** in the electrostatic model are not related to **B** and **H** in the magnetostatic model. The coexistence of static electric fields and magnetic electric fields in a conducting medium causes an electromagnetostatic field and a time-varying magnetic field gives rise to an electric field. These are verified by numerous experiments. Static models are not suitable for explaining time-varying electromagnetic phenomenon. Under time-varying conditions it is necessary

[1] The following two chapters are based, to a large extent, on the work presented in [65].

to construct an electromagnetic model in which the electric field vectors **E** and **D** are related to the magnetic field vectors **B** and **H**. In such situations, the equivalent equations are constructed as

$$\nabla \times \mathbf{E} = -\frac{\partial \mathbf{B}}{\partial t}, \tag{5}$$

$$\nabla \times \mathbf{H} = \mathbf{J} + \frac{\partial \mathbf{D}}{\partial t}, \tag{6}$$

$$\nabla \cdot \mathbf{D} = \rho_v, \tag{7}$$

$$\nabla \cdot \mathbf{B} = 0, \tag{8}$$

where **J** is conducting current. As it is seen, the Maxwell's equations above are in differential form. To explain electromagnetic phenomena in a physical environment, it is more convenient to convert the differential forms into their integral-form equivalents. To do this, the Stokes's and divergence theorems can be applied. The Stokes's theorem for an arbitrary vector **A** can be written as

$$\oint_C \mathbf{A} \cdot d\mathbf{l} = \int_S (\nabla \times \mathbf{A}) \cdot d\mathbf{s}, \tag{9}$$

which states that the circulation of a vector field **A** around a (closed) path C is equal to the surface integral of the curl of **A** over the open surface S bounded by C, provided **A** and $\nabla \times \mathbf{A}$ are continuous on S. In Eqn. (9), quantities $d\mathbf{l}$ and $d\mathbf{s}$ are the infinitesimal length and surface, respectively. The divergence theorem, otherwise known as Gauss-Ostrogradsky, is stated as [88]

$$\oint_S \mathbf{A} \cdot d\mathbf{s} = \int_V (\nabla \cdot \mathbf{A}) dv, \tag{10}$$

which means that the volume integral of the divergence of a vector field equals the total outward flux of the vector through the surface that bounds the volume. In Eqn. (10), the volume V is enclosed by the closed surface S and dv and $d\mathbf{s}$ are the infinitesimal volume and infinitesimal surface, respectively.

Now, based on the Stokes's theorem, the integral form of Maxwell's equations can be derived from the two Maxwell's curl equations, stated in general form as [11, 25]

$$\nabla \times \mathbf{E} = -\mathbf{M}_i - \frac{\partial \mathbf{B}}{\partial t}, \tag{11}$$

$$\nabla \times \mathbf{H} = \mathbf{J}_i + \mathbf{J}_c + \frac{\partial \mathbf{D}}{\partial t}, \tag{12}$$

where $\mathbf{M}_i$ is the source magnetic current density (V/m^2), $\mathbf{J}_i$ is the source electric current density (A/m^2), and $\mathbf{J}_c$ is the conduction electric current density (A/m^2). Taking the surface integral of both LHS and RHS of Eqn. (11) yields [11]

$$\iint_S (\nabla \times \mathbf{E}) \cdot d\mathbf{s} = -\iint_S \mathbf{M}_i \cdot d\mathbf{s} - \frac{\partial}{\partial t} \iint_S \mathbf{B} \cdot d\mathbf{s}, \tag{13}$$

which will be reduced to

$$\oint_C \mathbf{E} \cdot d\mathbf{l} = -\iint_S \mathbf{M}_i \cdot d\mathbf{s} - \frac{\partial}{\partial t} \iint_S \mathbf{B} \cdot d\mathbf{s}, \tag{14}$$

by applying the Stokes's theorem given in Eqn. (9). Eqn. (14) is referred to as Maxwell's equation in integral form as derived from Faraday's law which is stated as: The electromotive force appearing at the open-circuited terminals of a loop is equal to the time rate of decrease of magnetic flux linking the loop.

The corresponding integral form of Eqn. (12) can be written as

$$\oint_C \mathbf{H} \cdot d\mathbf{l} = -\iint_S \mathbf{J}_{ic} \cdot d\mathbf{s} + \frac{\partial}{\partial t} \iint_S \mathbf{D} \cdot d\mathbf{s}, \tag{15}$$

in which

$$\mathbf{J}_{ic} = \mathbf{J}_i + \mathbf{J}_c \tag{16}$$

Eqn. (15) is Maxwell's equation in integral form as derived from Ampere's law.

The procedure to obtain the integral form of the other two Maxwell equations, stated as

$$\nabla \cdot \mathbf{D} = q_{ev}, \tag{17}$$

$$\nabla \cdot \mathbf{B} = q_{mv}, \tag{18}$$

in which q_{ev} is electric charge density (C/m^3), and q_{mv} is the magnetic charge density (web/m^3). The procedure to obtain the next integral form of Maxwell's equations is started by taking the volume integral of both sides of Eqn. (17), that is [11]

$$\iiint_V (\nabla \cdot \mathbf{D}) dv = \iiint_V q_{ev} dv \tag{19}$$

By applying the divergence theorem, that is Eqn. (10), on the LHS of Eqn. (19), one can obtain [11]

$$\oint_S \mathbf{D} \cdot d\mathbf{s} = \iiint_V q_{ev} dv, \tag{20}$$

which is Maxwell's electric field equation in integral form as derived from Gauss's law, stated as: The total electric flux through a closed surface is equal to the total charge enclosed.

The divergence theorem, given by Eqn. (10) is applied on the LHS of Eqn. (19) to obtain

$$\oint_S \mathbf{B} \cdot d\mathbf{s} = \rho_m, \tag{21}$$

in which ρ_m is the total magnetic charge. Eqn. (21) is Maxwell's magnetic field equation in integral form as derived from Gauss's law. In fact, there is no magnetic charge in nature but the concept is used as an equivalent to represent physical problems.

Maxwell's equations in a more appropriate form to be applied in this work, are constructed as in the following table.

Maxwell's equations

Differential form	*Integral form*	
$\nabla \times \mathbf{H} = \mathbf{J} + \frac{\partial \mathbf{D}}{\partial t}$	$\oint_C \mathbf{H} \cdot d\mathbf{L} = I + \int_S \frac{\partial \mathbf{D}}{\partial t} \cdot d\mathbf{S}$	(22)
$\nabla \times \mathbf{E} = -\frac{\partial \mathbf{B}}{\partial t}$	$\oint_C \mathbf{E} \cdot d\mathbf{L} = -\int_S \frac{\partial \mathbf{B}}{\partial t} \cdot d\mathbf{S}$	(23)
$\nabla \cdot \mathbf{D} = \rho_v$	$\oint_S \mathbf{D} \cdot d\mathbf{S} = \int_V \rho_v dv$	(24)
$\nabla \cdot \mathbf{B} = 0$	$\oint_S \mathbf{B} \cdot d\mathbf{S} = 0$	(25)

2.1 Green's Functions

When a physical system is subject to some external disturbance, a nonhomogeneity arises in the mathematical formulation of the problem, either in the differential equation, or in the auxiliary conditions, or both. When the differential equation is nonhomogeneous, a particular solution of the equation can be found by applying either the method of undetermined coefficients or the variation of parameter technique. Green's functions[2] are specific functions that develop general solution formulas for solving nonhomogeneous differential equations. Importantly, this type of formulation

[2]George Green, 1793-1841, was one of the most remarkable of nineteenth century physicists, a self-taught mathematician whose work has greatly contributed to modern physics.

gives an increased physical knowledge since every Green's function has a physical significance. This function measures the response of a system due to a point source somewhere on the fundamental domain, and all other solutions due to different source terms are found to be superpositions [3] of the Green's function. Although Green's first interest was in electrostatics, Green's mathematics is nearly all devised to solve general physical problems. The inverse-square law had recently been established experimentally, and George Green wanted to calculate how this determined the distribution of charge on the surfaces of conductors. He made great use of the electrical potential and gave it that name. Actually, one of the theorems that he proved in this context became famous and is nowadays known as Green's theorem. It relates the properties of mathematical functions at the surfaces of a closed volume to other properties inside. The powerful method of Green's functions involves what are now called Green's functions, $G(x, x')$. Applying Green's function method, solution of the differential equation $Ly = F(x)$, by L as a linear differential operator, can be written as

$$y(x) = \int_0^x G(x, x')F(x')dx'. \tag{26}$$

To see this, consider the equation

$$\frac{dy}{dx} + ky = F(x),$$

which can be solved by the standard integrating factor technique to give

$$y = e^{-kx} \int_0^x e^{kx'} F(x')dx' = \int_0^x e^{-k(x-x')} F(x')dx',$$

so that $G(x, x') = e^{-k(x-x')}$. This technique may be applied to other more complicated systems. In general, Green's function is the response of a system to a stimulus applied at a particular point in space or time. This concept has readily been adapted to quantum physics where the applied stimulus is the injection of a quantum of energy. Within electromagnetic computation, it is common practice to use two methods for determining the Green's

[3] Consider a set of functions ϕ_n for $n = 1, 2, ..., N$. If each number of the functions ϕ_n is a solution to the partial differential equation $L\phi = 0$, where L is a linear differential operator with some prescribed boundary conditions, then the linear combination $\phi_N = \phi_0 + \sum_{n=1}^{N} a_n\phi_n$ also satisfies $L\phi = g$. Here, g is a known excitation or source.

function in the cases where there is some kind of symmetry in the geometry of the electromagnetic problem. These are the eigenvalue formulation and the Method of Images. These two methods are described in the following sections, but in order to its importance, the method of the eigenfunction expansion method is, first presented.

Green's Functions and Eigenfunctions

If the eigenvalue problem associated with the operator L can be solved, then one can derive the associated Green's function explicitly. It is known that the eigenvalue problem

$$Lu = \lambda u, \quad a < x < b, \tag{27}$$

with prescribed boundary conditions, has infinitely many eigenvalues and corresponding orthonormal eigenfunctions as λ_n and ϕ_n, respectively, where $n = 1, 2, 3, ...$ Moreover, the eigenfunctions form a basis for the square integrable functions on the interval (a, b). Therefore it is assumed that the solution u is given in terms of eigenfunctions as

$$u(x) = \sum_{n=1}^{\infty} c_n \phi_n(x), \tag{28}$$

where the coefficients c_n are to be determined. Further, the given function f forms the source term in the nonhomogeneous differential equation

$$Lu = f, \qquad u = L^{-1} f$$

where L^{-1} is the inverse operator to the operator L. Now, the given function f can be written in terms of the eigenfunctions as

$$f(x) = \sum_{n=1}^{\infty} f_n \phi_n(x), \tag{29}$$

with

$$f_n = \int_a^b f(\xi)\phi_n(\xi) d\xi. \tag{30}$$

Combining (28), (29), and (30) gives

$$L\left(\sum_{n=1}^{\infty} c_n \phi_n(x)\right) = \sum_{n=1}^{\infty} f_n \phi_n(x). \tag{31}$$

When the linear property associated with superposition principle holds, it can be shown that [62]

$$L\left(\sum_{n=1}^{\infty} c_n \phi_n(x)\right) = \sum_{n=1}^{\infty} c_n L(\phi_n(x)). \tag{32}$$

But

$$\sum_{n=1}^{\infty} c_n L(\phi_n(x)) = \sum_{n=1}^{\infty} c_n \lambda_n \phi_n(x) = \sum_{n=1}^{\infty} f_n \phi_n(x), \tag{33}$$

which finally yields

$$L\left(\sum_{n=1}^{\infty} c_n \phi_n(x)\right) = \sum_{n=1}^{\infty} f_n \phi_n(x). \tag{34}$$

By comparing the above equations, it will be obtained that

$$c_n = \frac{1}{\lambda_n} \text{ and } f_n = \frac{1}{\lambda_n} \int_a^b f(\xi)\phi_n(\xi)d\xi \text{ for } n = 1, 2, 3, ... \tag{35}$$

Further

$$\begin{aligned} u(x) &= \sum_{n=1}^{\infty} c_n \phi_n(x) \\ &= \sum_{n=1}^{\infty} \frac{1}{\lambda_n} \left(\int_a^b f(\xi)\phi_n(\xi)d\xi \right) \phi_n(x). \end{aligned} \tag{36}$$

Now, it is supposed that an interchange of summation and integral is allowed. In this case, (36) can be written as

$$u(x) = \int_a^b \left(\sum_{n=1}^{\infty} \frac{\phi_n(x)\phi_n(\xi)}{\lambda_n} \right) f(\xi)d\xi. \tag{37}$$

On the other hand, by the definition of Green's function, one may write

$$u(x) = L^{-1}f = \int_a^b g(x, \xi)f(\xi)d\xi. \tag{38}$$

By comparing the last two equations, $u(x)$ can be expressed in terms of Green's functions as [62]

$$g(x,\xi) = \sum_{n=1}^{\infty} \frac{\phi_n(x)\phi_n(\xi)}{\lambda_n}, \tag{39}$$

where $g(x,\xi)$ is the Green's function associated with the eigenvalue problem (27) with the differential operator L.

2.2 Method of Images

Solution of electromagnetic field problems is greatly supported and facilitated by mathematical theorems in vector analysis. Maxwell's equations are based on the Helmholtz's theorem where it is verified that a vector is uniquely specified by giving its divergence and curl, within a simply connected region and its normal component over the boundary. This can be proved as a mathematical theorem in a general manner [6]. Solving partial differential equations (PDE) like Maxwell's equations, desires different methods, depending on, for instance, which boundary condition the PDE has and in which physical field it is studied. The Green's function modeling is an applicable method for solving Maxwell's equations for some frequently used cases with different boundary conditions. The issue in this type of formulation is, in the first hand, determining and solving the appropriate Green's function by its boundary condition. Once the Green's function is determined, one may receive a clue to the physical interpretation of the whole problem and hence a better understanding of it. This forms the general manner of applying Green's function formulation in different fields of science. In some cases within electromagnetic modeling, where the physical source is in the vicinity of a perfect electric conducting (PEC) surface and where there is some kind of symmetry in the geometry of the problem, the Method of Images will be a logical and facilitating method to determine the appropriate Green's function. The Method of Images can be used for the problems which include not only PEC surfaces but surfaces of materials with, for instance, dielectric characteristics or with finite specific conductance. The Method of Images is, in its turn, based on the uniqueness theorem verifying that a solution of an electrostatic problem satisfying the boundary condition is the only possible solution [24]. Electric and magnetic field of an infinitesimal dipole in the vicinity of an infinite PEC surface is one of the subjects that can be studied and facilitated by applying the Method of Images. In the following section, the Method of Images is applied to electromagnetic modeling of electrical sources above PEC surface.

2.3 Electric Field of Sources above PEC Surface

It is assumed that an electric point charge q is located at a vertical distance $y = r$ above a large conducting plane that is grounded, see Fig. 1(a) . It

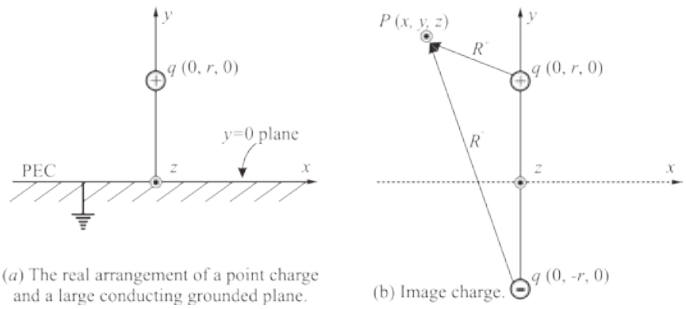

Figure 1: Point charge over a grounded PEC surface.

will be difficult to apply the ordinary field solution in this case but by the image methods, where an equivalent system is presented, it will be considerably easier to solve the original problem. An equivalent problem considers placement of an image point charge $-q$ on the opposite side of the PEC plane, i.e. $y = -r$, see Fig. 1(b). In the equivalent problem, the boundary condition is not changed, that is, the boundary plane is still as $y = 0$, and a solution to the equivalent problem will be the only correct solution. The potential at the arbitrary point $P(x, y, z)$ is [25]

$$\Phi(x, y, z) = \frac{q}{4\pi\epsilon_0}\left(\frac{1}{\sqrt{x^2 + (y - r)^2 + z^2}} - \frac{1}{\sqrt{x^2 + (y + r)^2 + z^2}}\right), \quad (40)$$

which is a contribution from both charges q and $-q$ as

$$\Phi_+(x, y, z) = \frac{q}{4\pi\epsilon_0}\left(\frac{1}{\sqrt{x^2 + (y - r)^2 + z^2}}\right) \quad (41)$$

and

$$\Phi_-(x, y, z) = \frac{-q}{4\pi\epsilon_0}\left(\frac{1}{\sqrt{x^2 + (y + r)^2 + z^2}}\right), \quad (42)$$

respectively. According to the image method, Eqn. (40) gives the potential due to an electric point source above the PEC plane in the region $y > 0$.

The field located at $y < 0$ will be zero; it is indeed the region where the image charge $-q$ is located, see Fig. 1(b).

Now it is assumed that a long line charge of constant charge λ per unit length is located at distance d from the surface of the grounded conductor, occupying half of the entire space, see Fig. 2. It is also assumed that

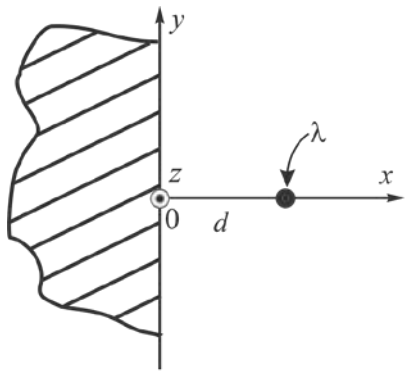

Figure 2: Uniform infinite line charge λ parallel to a semiinfinite grounded conducting plane and perpendicular to the page.

the line charge is parallel to both the grounded plane and to the z-axis in the rectangular coordinate system. Further, the surface of the conducting grounded plane is coincided with yz-plane and x-axis passes through the line charge so that the boundary condition for this system is $\Phi(0, y, z) = 0$ where Φ is defined as the electric potential. This is illustrated in Fig. 2. To find the potential everywhere for this system applying the Method of Images, one may start by converting this system to an equivalent system where the boundary condition of the original problem will be preserved. This will consider a system where the conducting grounded plane vanishes, i.e. a system where the line charge is in the free-space. Adopting the polar coordinate system, the potential at an arbitrary point P, is

$$\Phi(\rho, \phi) = \frac{\lambda}{2\pi\epsilon_0} \ln \left[\frac{(4L_2L_1)^{1/2}}{\rho} \right]. \tag{43}$$

An equivalent problem may consist of a system of two long parallel lines with opposite charges in the free-space at distance $2d$ from each other; the charge densities of the two lines are assumed to be λ and $-\lambda$, respectively. According to the Method of Images, the total potential Φ will be determined by contribution from these two line charges, which respectively are

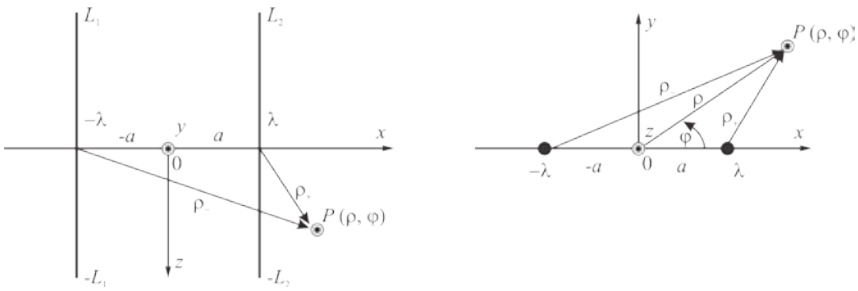

Figure 3: Geometry of two opposite long line charges, λ and $-\lambda$ by a distance of $2d$ from each other and observed as parallel to the paper plane (left) and perpendicular to the paper plane (right).

$$\Phi_+ = \frac{\lambda}{2\pi\epsilon_0} \ln\left[\frac{(4L_2L_1)^{1/2}}{\rho_+}\right] \tag{44}$$

and

$$\Phi_- = -\frac{\lambda}{2\pi\epsilon_0} \ln\left[\frac{(4L_2L_1)^{1/2}}{\rho_-}\right]. \tag{45}$$

The total potential is obtained as a sum of previous two expressions: as

$$\begin{aligned} \Phi &= \Phi_+ + \Phi_- \\ &= \frac{\lambda}{2\pi\epsilon_0} \ln\left(\frac{\rho_-}{\rho_+}\right) \\ &= \frac{\lambda}{2\pi\epsilon_0} \ln\left(\frac{d^2+\rho^2+2d\rho\cos\phi}{d^2+\rho^2-2d\rho\cos\phi}\right). \end{aligned} \tag{46}$$

According to the uniqueness theorem and the Method of Images, Eqn. (46) gives the solution for a long line charge at distance d above the PEC plane. The potential at the left side of the PEC surface will be zero. Electric equipotential lines, due to the line charge λ parallel to the PEC surface are illustrated in Fig. 4.

2.4 Incremental Current Sources

The overall radiation properties of a radiating system can significantly alter in the vicinity of an obstacle. The ground as a lossy medium, i.e. $\sigma \neq 0$, is expected to act as a very good conductor above a certain frequency. Hence,

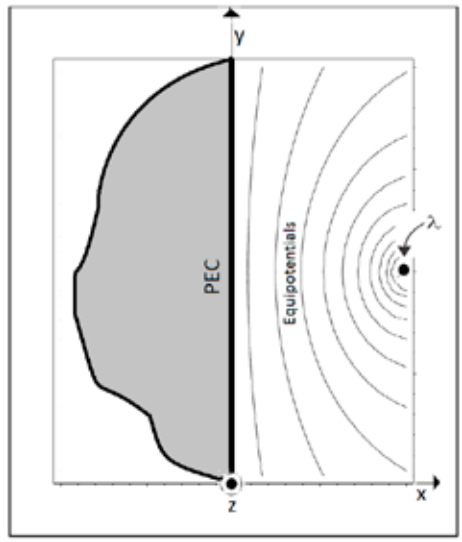

Figure 4: Electric equipotential lines due to the infinitely long line charge λ, parallel to a PEC surface and z-axis.

applying the Method of Images the ground should be assumed as a perfect electric conductor, flat, and infinite for facilitating the analysis. It will also be assumed that any energy from the radiating element towards the ground undergoes reflection, and the total amount of energy is a summation of the reflected and directed (incident) components where the reflected component can be accounted for by the introduction of the image sources. In all of the

following cases, the far-field observation is considered. To find the electric field, radiated by a current element along the infinitesimal length l', it will be convenient to use the magnetic vector potential $\mathbf{A}$ as [10]

$$\mathbf{A}(x,y,z) = \frac{\mu}{4\pi}\int_C \mathbf{I}(x',y',z')\frac{e^{-jkR}}{R}dl' \tag{47}$$

where (x,y,z) and (x',y',z') represent the observation point coordinates and the coordinates of the constant electric current source $\mathbf{I}$, respectively. R is the distance from any point on the source to the observation point; the integral path C is the length of the source, and $k^2 = \omega^2\mu\epsilon$ where μ and ϵ are permeability and permittivity of the medium. By the assumption that an infinitesimal dipole is placed along the z-axis of a rectangular coordinate system, see Fig. 5, plus that it is placed in the origin, one may write $\mathbf{I} = \hat{z}I_0$ for constant electric current I_0, and $x' = y' = z' = 0$. Hence, the distance R will be

$$R = \sqrt{(x-x')^2 + (y-y')^2 + (z-z')^2} = \sqrt{x^2+y^2+z^2}. \tag{48}$$

Knowing that $dl' = dz'$, and by setting $r = \sqrt{x^2+y^2+z^2}$, Eqn. (47) may be written as

$$\mathbf{A}(x,y,z) = \hat{z}\frac{\mu I_0}{4\pi r}e^{-jkr}\int_{-l/2}^{l/2} dz' = \hat{z}\frac{\mu I_0 l}{4\pi r}e^{-jkr}. \tag{49}$$

The most appropriate coordinate system for studying such cases is the spherical coordinate system, so the vector potential in Eqn. (49) should be converted into the spherical components as

$$A_r = A_z\cos\theta = \frac{\mu I_0 l}{4\pi r}e^{-jkr}\cos\theta, \tag{50}$$

$$A_\theta = -A_z\sin\theta = -\frac{\mu I_0 l}{4\pi r}e^{-jkr}\sin\theta, \tag{51}$$

$$A_\phi = 0. \tag{52}$$

In the last three equations, $A_x = A_y = 0$ by the assumption that the infinitesimal dipole is placed along the z-axis. For determining the electric field radiation of the dipole, one should operate the magnetic vector potential $\mathbf{A}$ by a curl operation to obtain the magnetic field intensity $\mathbf{H}_A$ as

$$\mathbf{H}_A = \frac{1}{\mu}\nabla\times\mathbf{A}. \tag{53}$$

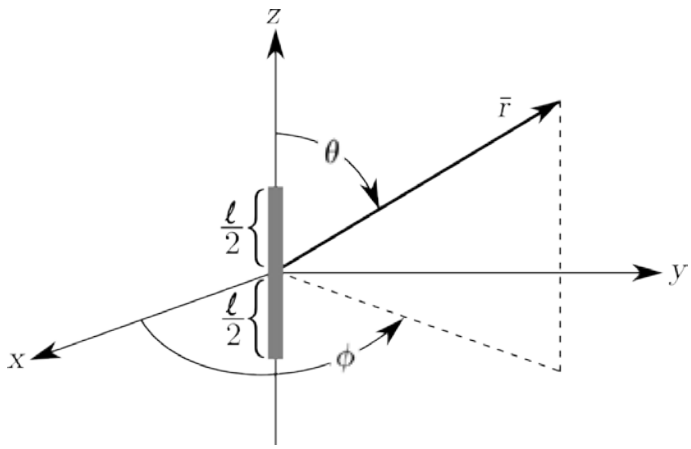

Figure 5: Geometry of a dipole in the origin with incremental electric current.

In spherical coordinate system, Eqn. (53) is expressed as

$$\mathbf{H}_A = \frac{1}{\mu}\left(\hat{r}\frac{1}{r\sin\theta}\left[\frac{\partial}{\partial\theta}(A_\phi\sin\theta) - \frac{\partial A_\theta}{\partial A_\phi}\right] + \frac{\hat{\theta}}{r}\left[\frac{1}{\sin\theta}\frac{\partial A_r}{\partial\phi} - \frac{\partial}{\partial r}(rA_\phi)\right] + \frac{\hat{\phi}}{r}\left[\frac{\partial}{\partial r}(rA_\theta) - \frac{\partial A_r}{\partial\theta}\right]\right).$$

But according to Eqn. (52) and due to spherical symmetry of the problem, where there are no ϕ-variations along the z-axis, the last equation simplifies to [10]

$$\mathbf{H}_A = \frac{1}{\mu}\frac{\hat{\phi}}{r}\left[\frac{\partial}{\partial r}(rA_\theta) - \frac{\partial A_r}{\partial\theta}\right], \tag{54}$$

which together with Eqn. (50) and (51) gives

$$\mathbf{H}_A = \hat{\phi}\frac{kI_0 l\sin\theta}{4\pi r}j\left(1 + \frac{1}{jkr}\right)e^{-jkr}. \tag{55}$$

Further, by equating Maxwell's equations, it will be obtained that

$$\nabla\times\mathbf{H}_A = \mathbf{J} + j\omega\epsilon\mathbf{E}_A. \tag{56}$$

By setting $\mathbf{J} = 0$ in Eqn. (56), it will be obtained that

$$\mathbf{E}_A = \frac{1}{j\omega\epsilon}\nabla\times\mathbf{H}_A. \tag{57}$$

Eqn. (57), together with Eqns. (50)-(52) yields

$$E_r = \eta \frac{I_0 l \cos\theta}{2\pi r^2} \left[1 + \frac{1}{jkr}\right] e^{-jkr}, \tag{58}$$

$$E_\theta = j\eta \frac{kI_0 l \sin\theta}{4\pi r} \left[1 + \frac{1}{jkr} - \frac{1}{kr^2}\right] e^{-jkr}, \tag{59}$$

$$E_\phi = 0, \tag{60}$$

where $\eta = E_\theta / H_\phi$ is called the intrinsic impedance ($= 377 \approx 120\pi$ ohms for the free-space). Stipulating for the far-field region, i.e. the region where $kr >> 1$, the electric field components E_θ and E_r in Eqns. (58)-(60) can be approximated by

$$E_\theta \approx j\eta \frac{kI_0 l \sin\theta}{4\pi r} e^{-jkr}, \tag{61}$$

$$E_r \approx E_\phi = 0, \tag{62}$$

which is the electric far-field solution for an infinitesimal dipole along the z-axis and in the spherical coordinate system. The same procedure may be used to solve the electric field for an infinitesimal dipole along the x-axis where the magnetic vector potential $\mathbf{A}$ is defined as

$$\mathbf{A} = \hat{\mathbf{x}} \frac{\mu I_0 l e^{-jkr}}{4\pi r}. \tag{63}$$

In the spherical coordinate system, the above equation is expressed as

$$A_r = A_x \sin\theta \cos\phi, \tag{64}$$

$$A_\theta = A_x \cos\theta \cos\phi, \tag{65}$$

$$A_\phi = -A_x \sin\phi. \tag{66}$$

It should be mentioned that $A_y = A_z = 0$ due to the placement of the infinitesimal dipole along the x-axis. By far-field approximation, and based on Eqns. (64)-(66), the electric field can be written as

$$E_r \approx 0, \tag{67}$$

$$E_\theta \approx -j\omega A_\theta = -j\omega \frac{\mu I_0 l e^{-jkr}}{4\pi r} \cos\theta \cos\phi, \tag{68}$$

$$E_\phi \approx -j\omega A_\phi = -j\omega \frac{\mu I_0 l e^{-jkr}}{4\pi r} \sin\phi. \tag{69}$$

The electric field, as a whole, will be contributions from both A_θ and A_ϕ which is expressed as

$$E_A \approx -j\omega \left(A_\theta + A_\phi\right) = -j\omega \frac{\mu I_0 l e^{-jkr}}{4\pi r} \left(\cos\theta \cos\phi - \sin\phi\right). \tag{70}$$

2.5 Infinitesimal Dipoles above Grounded PEC Surface

A vertical dipole of infinitesimal length l and constant current I_0, is now assumed to be placed along z-axis at distance h above the grounded PEC surface by an infinite extent, see Fig. 6. The far-zone directed and reflected components in a far-field point P are respectively given by [11]

$$E_\theta^D \approx j\eta \frac{k I_0 l e^{-jkr_1}}{4\pi r_1} \sin\theta_1, \tag{71}$$

and

$$E_\theta^R \approx j\eta \frac{k I_0 l e^{-jkr_2}}{4\pi r_2} \sin\theta_2, \tag{72}$$

where r_1 and r_2 are the distances between the observation point and the two other points, the source and the image locations; the angles θ_1 and θ_2 are related between these lines and the z-axis, as visualized in 6. It is intended to express all the quantities only by the elevation plane angle θ and the radial distance r between the observation point and the origin of the spherical coordinate system. For this purpose, one may utilize the law of cosines and also a pair of simplifications regarding the far-field approximation. The law of cosines gives

$$r_1 = \sqrt{r^2 + h^2 - 2rh\cos\theta}, \tag{73}$$

$$r_2 = \sqrt{r^2 + h^2 - 2rh\cos(\pi - \theta)}. \tag{74}$$

By binomial expansion and regarding phase variations, one may write

$$r_1 = r - h\cos\theta, \tag{75}$$

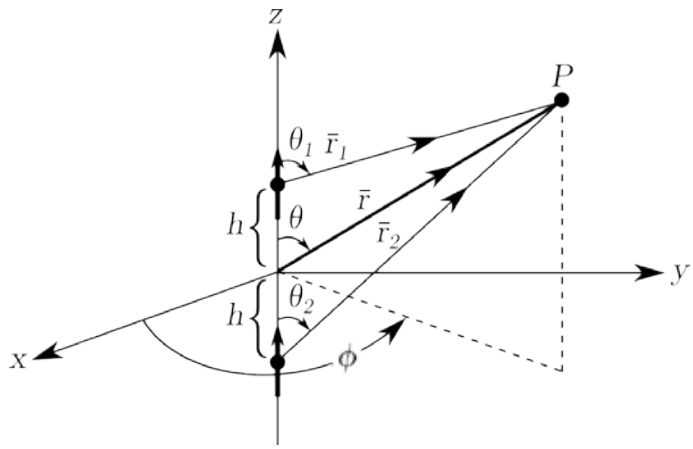

Figure 6: Vertical electric dipole above a PEC surface.

$$r_2 = r + h\cos\theta. \tag{76}$$

By utilizing the far-zone approximation where $r_1 \approx r_2 \approx r$, and all of the above simplifications, it is obtained that

$$E_\theta^{total} = E_\theta^D + E_\theta^R = j\eta\frac{kI_0le^{-jkr}}{4\pi r}\sin\theta\left(e^{+jkh\cos\theta} + e^{-jkh\cos\theta}\right). \tag{77}$$

Finally, after some algebraic manipulations, one may find for $z \geq 0$

$$E_\theta^{total} = j\eta\frac{kI_0le^{-jkr}}{4\pi r}\sin\theta\left[2\cos(kh\cos\theta)\right]. \tag{78}$$

According to the Method of Images, the field will be zero for $z < 0$.

The electric field due to a horizontal electric dipole, positioned above a grounded PEC surface can by a similar process be determined. Considering Fig. 7 and as it is depicted in [11], the total electric field in this context is

$$E^{total} = j\eta\frac{kI_0le^{-jkr}}{4\pi r}\sqrt{1-\sin^2\theta\sin^2\phi}\left[2j\sin(kh\cos\theta)\right], \tag{79}$$

which is valid for $z \geq h, 0 \leq \theta \leq \pi/2$ and $0 \leq \phi \leq 2\pi$, that is, only above the horizontal grounded PEC surface.

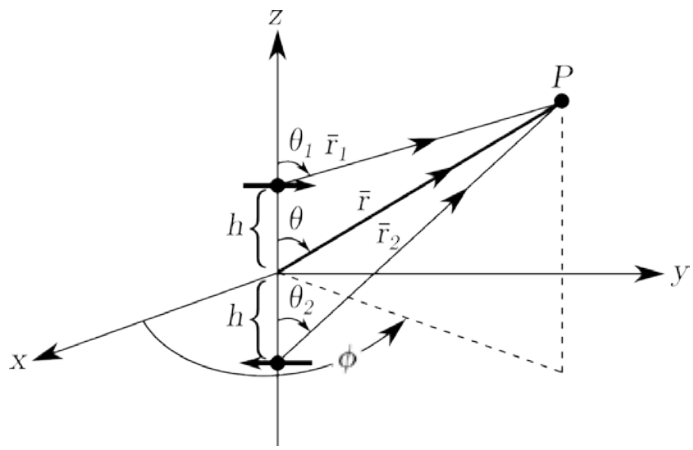

Figure 7: Horizontal electric dipole above a grounded PEC surface.

2.6 Mixed-Potential Integral Equation

Determining Green's functions for stratified media has been, during the last decades, an important and fundamental stage to design of high-frequency circuits. In the case of a layered medium, a so-called *mixed-potential integral equation (MPIE)*, is applied to the associated geometry [67]. MPIE can be solved in both spectral and spatial domain and both solutions require appropriate Green's functions. The Green's functions for multi-layered planar media are represented by the Sommerfeld's integrals whose integrand consists of the Hankel function, and the closed-form spectral-domain Green's functions [26]. A two-dimensional inverse Fourier transformation is needed to determine the spectral-domain Green's functions analytically via the following integral which is along the Sommerfeld's integration path (SIP) and the k_ρ-plane as

$$G = \frac{1}{4\pi} \int_{SIP} dk_\rho k_\rho H_0^{(2)}(k_\rho \rho) \tilde{G}(k_\rho), \tag{80}$$

where $H_0^{(2)}$ is the Hankel function of the second kind; here, G and $\tilde{G}$ are the Green's functions in the spatial and spectral domain. One of the topics in this context is that there is no general analytic solution to the Hankel transform of the closed-form spectral-domain Green's function. Numerical solution of the above transformation integral is very time-consuming, partly due to the slow-decaying Green's function in the spectral domain, partly due to the oscillatory nature of the Hankel function. Dealing with such problem constitutes one of the major topics within the computational electromagnetics for multi-layered media. In many applications, the *Discrete complex image method* (DCIM) is used to handle this numerically time-consuming process. The strategy in this process is to obtain Green's functions in a closed-form as

$$G \cong \sum_{k=1}^{N} a_n \frac{e^{-jkr_m}}{r_m}, \tag{81}$$

where

$$r_m = \sqrt{\rho^2 - b_m^2}, \tag{82}$$

with $j = \sqrt{-1}$, the imaginary unit, will be complex-valued. The constants a_n and b_m are to be determined by numerical processes such as the Prony's method [100, 43]. In dyadic form and by assuming an $e^{j\omega t}$ time dependence,

the electric field at an observation point, defined by the vector $\mathbf{r}$, produced by a surface current $\mathbf{J}$ of a surface S' can be expressed as

$$\begin{aligned}\mathbf{E}(\mathbf{r}) &= -j\omega \int_{S'} \left[\overline{\overline{I}} + \frac{1}{k^2 \nabla\nabla}\right] \frac{\mu e^{-jkR}}{4\pi R} \mathbf{J}(\mathbf{r}, \mathbf{r}') dS' \\ &= \int_{S'} \mathbf{G}(\mathbf{r}, \mathbf{r}') \mathbf{J}(\mathbf{r}, \mathbf{r})' dS', \end{aligned} \tag{83}$$

where $k = \omega\sqrt{\mu\epsilon}$ by μ and ϵ as the electromagnetic characteristics for the layered medium; R is the distance from the source point to the field point. $\overline{\overline{I}}$ is the unit dyad and $\mathbf{G}(\mathbf{r}, \mathbf{r}')$ is defined as the dyadic Green's function. There are different methods to construct the auxiliary Green's function in the case of boundary value problems, which are as a consequence of using mathematics to study problems arising in the real world. The numerical solution of an integral equation has the general property that the coefficient matrix in the ultimate linear equation $Ax = y$ will consist of a dense coefficient matrix A and a relatively fewer number of elements in the unknown vector x. Numerical solution of a general integral equation involves challenges due to the ill-conditioned coefficient matrix A, as a rule and not as an exception; the integration operator to solve a differential equation is a smoothing operator and the differential operator to solve an integral equation will be a non-smooth operator. This is the main reason of the ill-conditioning. Generally, and depending on the kind of problem, there are several numerical methods to handle the ill-conditioning and in the case of solution of Maxwell's equations in the integral form, ill-conditioning will be a problem to handle.[4]

[4]More about integral equations and ill-conditioning in the next sections.

3 Solution of Electromagnetic Fields and Antenna Analysis

Generally, the exact mathematical solution of the field problem is the most satisfactory solution, but in modern applications one cannot find such analytical solution in majority of cases. Analytical methods are limited to solve electromagnetic field problems with simple geometries and as a result one should apply numerical methods to solve problems with complicated geometries. In fact, numerical methods cannot be applied without checking and realizing the limitations in classical analytical methods. In addition, every numerical method involves an analytical simplification to the point where it is easy to apply a certain numerical method. The most commonly used analytical solutions in computational electromagnetics are

- Laplace, and Fourier transforms,
- Perturbation methods,
- Separation of variables (eigenfunction expansion method),
- Conformal mapping,
- Series expansion.

In the next following subsections, several frequently used methods for solving electromagnetic field problems are described.

3.1 Eigenfunction Expansion Method

The method of eigenfunction expansion can be applied to derive the Green's function for partial differential equations by known homogeneous solution. The partial differential equation

$$\begin{aligned} U_{xx} &= \frac{1}{\kappa}U_t + Q(x,t), && 0 < x < L, t > 0, \\ B.C. &: U(0,t) = 0, U(L,t) = 0, && t > 0, \\ I.C. &: U(x,0) = F(x), && 0 < x < L, \end{aligned} \tag{84}$$

with

$$\begin{aligned} Q(x,t) &= \frac{1}{\kappa}K_t(x,t) - q(x,t), \\ F(x) &= f(x) - K(x,0), \end{aligned} \tag{85}$$

features a problem with homogeneous boundary conditions (B.C.) and non-homogeneous initial conditions (I.C.). The Green's function, in this case, can be represented in terms of a series of orthonormal functions that satisfy the prescribed boundary conditions. By using the Method of Separation of Variables, it is assumed that the solution of the partial differential equation may be written in the form [93]

$$U(x,t) = \sum_{n=1}^{\infty} E_n(t)\Psi_n(x), \tag{86}$$

where $\Psi_n(x)$ are eigenfunctions belonging to the associated eigenvalue problem[5]

$$X'' + \lambda X = 0 \tag{87}$$

by prescribed boundary condition (B.C.) and initial conditions (I.C.). In the above equation, $E_n(t)$ are time-dependent coefficients to be determined. It is also assumed that termwise differentiation is permitted. In this case

$$U_t(x,t) = \sum_{n=1}^{\infty} E_n^{'}(t)\Psi_n(x), \tag{88}$$

and

$$U_{xx}(x,t) = \sum_{n=1}^{\infty} E_n(t)\Psi_n''(x),$$

which together with (87) gives

$$U_{xx}(x,t) = -\sum_{n=1}^{\infty} \lambda_n E_n(t)\Psi_n(x). \tag{89}$$

This is a result of applying the superposition principle which can be deduced as $\Psi_n''(x) = -\lambda_n\Psi_n(x)$ from (87). Next, by rewriting the partial differential equation above as

$$\kappa U_{xx} = U_t + \kappa Q(x,t), \tag{90}$$

and inserting the expressions (88) and (89) into the last equation, one can obtain

$$\kappa U_{xx} = \sum_{n=1}^{\infty} [E_n'(t) + \kappa\lambda_n E_n(t)]\Psi_n(x). \tag{91}$$

[5]Clearly $U(x,t)$, satisfies the prescribed homogeneous boundary conditions, since each eigenfunction $\Psi_n(x)$ does.

The right-hand side of the equation above is interpreted as generalized Fourier seriesof the function κU_{xx} for a fixed value of t. Thus, the Fourier coefficients are defined as

$$\begin{aligned} E_n^{'}(t) + \kappa\lambda_n E_n(t) &= \kappa \frac{1}{\|\Psi_n\|^2} \int_0^L Q(x,t)\Psi_n(x)dx, \\ \text{for } n &= 1, 2, ... \end{aligned} \tag{92}$$

where $\|\Psi_n\|$ is defined as the L^2-norm of $\Psi_n(x)$ with the relation

$$\|\Psi_n\|^2 = \int_0^L [\Psi_n(x)]^2 dx, \text{ for } n = 1, 2, ..., \tag{93}$$

Eqn. (91) as a first-order linear differential equation, has the general solution

$$E_n(t) = \left(c_n + \frac{1}{\kappa} \int_0^t exp(\frac{1}{\kappa}\lambda_n) P_n(\tau) d\tau \right) exp(-\frac{1}{\kappa}\lambda_n t), \tag{94}$$

for $n = 1, 2, 3, ...$ It has to be added that c_n are constants. In the equation above, $P_n(t)$ is defined as

$$P_n(t) = \frac{1}{\|\Psi_n\|^2} \int_0^L Q(x,t)\Psi_n(x)dx, \text{ for } n = 1, 2, 3, ... \tag{95}$$

Now, by substituting (94) into (86), it will be obtained that

$$U(x,t) = \sum_{n=1}^{\infty} \left(c_n + \frac{1}{\kappa} \int_0^t exp(\frac{1}{\kappa}\lambda_n) P_n(\tau) d\tau \right) exp(-\frac{1}{\kappa}\lambda_n t)\Psi_n(x). \tag{96}$$

For determining the coefficients c_n, $n = 1, 2, 3, ...$, one shall force Eqn. (95) to satisfy the prescribed initial condition.

3.2 Method of Moments (MoM)

Method of moments (MoM) is based on the integral formulation of the Maxwell's equations [37]. The basic feature makes it possible to exclude the air around the objects in the discretization. The method is usually employed in the frequency domain but can also be applied to the time domain problems. In the MoM, integral-based equations, describing the current distribution on a wire or a surface, are transformed into matrix equations easily solved using matrix inversion. When using the MoM for surfaces, a wire-grid approximation of the surface can be utilized as described in [5]. The wire formulation of the problem simplifies the calculations and is often used for field calculations. The starting point for theoretical derivation is to apply a linear (integral) operator, L, involving the appropriate Green's function $G(\mathbf{r}, \mathbf{r}')$, applied to an unknown function, I, by an equation as [5, 37]

$$LI = f, \tag{97}$$

where f is the known excitation function for the above system. As an example the above equation can be the Pocklington's integral equation [88], describing the current distribution $I(z')$ on a cylindrical antenna, written as

$$\int_a^b I(z')(\frac{\partial^2}{\partial z^2} + k^2)G(z, z')dz' = j\omega\epsilon E_z. \tag{98}$$

Then the unknown function, I, can be expanded into a series of known functions, u_i, with unknown amplitudes, I_i, resulting in

$$I = \sum_{i=1}^{n} I_i u_i, \tag{99}$$

where u_i, are called basis (or expansion) functions. To solve the unknown amplitudes, n, equations are derived from the combination of Eqn. (97) and Eqn. (99) and by the multiplication of n weighting (or test) functions, integrating over the wire length (the cylindrical antenna) and the formulation of a proper inner product [88]. This results in the transformation of the problem into a set of linear equations which can be written in matrix form as

$$[Z][I] = [V], \tag{100}$$

where the matrices, Z, I, and V are referred to as generalized impedance, current, and voltage matrices and the desired solution for the current, I, is

obtained by matrix inversion. Thus, the unknown solution is expressed as a sum of known basis functions whose weighting coefficients corresponding to the basis functions will be determined for the best fit. The same process applied to differential equations is known as the "weighted residual" method [71]. The MoM delivers the result in system current densities **J** and/or voltages at all locations in the discretized structure and at every frequency point (depending on the integral in Eqn. (98)). To obtain the results in terms of field variables, post-processing is needed for the conversion. The well-known computer program *Numerical Electromagnetics Code*, often referred to as NEC [70], utilizes the MoM for calculation of the electromagnetic response for antennas and other metal structures.

3.3 Method of Partial Element Equivalent Circuit (PEEC)

The basis of the Partial Element Equivalent Circuit (PEEC) method originates from inductance calculations performed by Dr. Albert E. Ruehli at IBM T.J. Watson Research Center, during the first part of 1970s [83, 19, 85]. Dr. Ruehli was working with electrical interconnect problems and understood the benefits of breaking a complicated problem into basic partitions, for which inductances could be calculated to model the inductive behavior of the complete structure [83, 20]. By doing so, return current paths need not to be known *a priori* as required for regular (loop) inductance calculations. The concept of partial calculations was first introduced by Rosa [90] in 1908, further developed by Grover [36] in 1946, and Hoer and Love [45] in 1965. However, Dr. Ruehli included the theory of partial coefficients of potential and introduced the partial element equivalent circuit (PEEC) theory in 1972 [82]. Significant contributions of the PEEC method are:

- The inclusion of dielectrics [86],
- The equivalent circuit representation with coefficients of potential [38],
- The retarded partial element equivalent circuit representation [39],
- PEEC models to include incident fields, scattering formulation [39],
- Nonorthogonal PEECs [87].

The interest and research effort of the PEEC method have increased during the last decade. The reasons can be an increased need for combined circuit and EM simulations and the increased performance of computers enabling large EM system simulations. This development reflects on the areas of the

current PEEC research, for example, model order reduction (MOR), model complexity reduction, and general speed up. The PEEC method is a 3D, full wave modeling method suitable for combined electromagnetic and circuit analysis. In the PEEC method, the integral equation is interpreted as the Kirchhoff's voltage law applied to a basic PEEC cell, which results in a complete circuit solution for 3D geometries. The equivalent circuit formulation allows for additional SPICE-type circuit elements to be included. Further, the models and the analysis apply to both the time and the frequency domain. The circuit equations resulting from the PEEC model are easily constructed using a condensed modified loop analysis (MLA) or modified nodal analysis (MNA) formulation [44]. In the MNA formulation, the volume cell currents and the node potentials are solved simultaneously for the discretized structure. To obtain field variables, post-processing of circuit variables is necessary. This section gives an outline of the nonorthogonal PEEC method as fully detailed in [87]. In this formulation, the objects, conductors and dielectrics, can be both orthogonal and non-orthogonal quadrilateral (surface) and hexahedral (volume) elements. The formulation utilizes a global and a local coordinate system where the global coordinate system uses orthogonal coordinates x, y, z where the global vector $\mathbf{F}$ is of the form $\mathbf{F} = F_x\hat{\mathbf{x}} + F_y\hat{\mathbf{y}} + F_z\hat{\mathbf{z}}$. A vector in the global coordinates are marked as $\mathbf{r_g}$. The local coordinates a, b, c are used to separately represent each specific possibly non-orthogonal object and the unit vectors are $\hat{\mathbf{a}}$, $\hat{\mathbf{b}}$, and $\hat{\mathbf{c}}$, see further [87]. The starting point for the theoretical derivation is the total electric field on the conductor expressed as

$$\mathbf{E}^i(\mathbf{r_g}, t) = \frac{\mathbf{J}(\mathbf{r_g}, t)}{\sigma} + \frac{\partial \mathbf{A}(\mathbf{r_g}, t)}{\partial t} + \nabla\phi(\mathbf{r_g}, t), \tag{101}$$

where $\mathbf{E}^i$ is the incident electric field, $\mathbf{J}$ is the current density in a conductor, $\mathbf{A}$ is the magnetic vector potential, ϕ is the scalar electric potential, and σ is the electrical conductivity. The dielectric areas are taken into account as an excess current with the scalar potential using the volumetric equivalence theorem. By using the vector potential $\mathbf{A}$ and scalar potential ϕ one can formulate the integral equation for the electric field at a point $\mathbf{r_g}$ which is to be located either inside a conductor or inside a dielectric region according

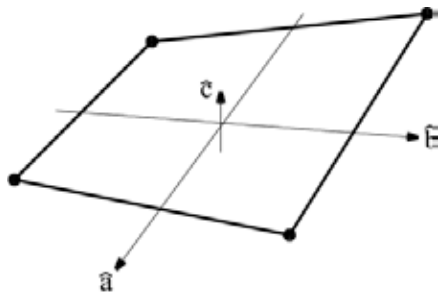

Figure 8: Nonorthogonal element created by the mesh generator with associated local coordinate system.

to [30]

$$\begin{aligned}\mathbf{E}^i(\mathbf{r_g},t) &= \frac{\mathbf{J}(\mathbf{r_g},t)}{\sigma} \\ &+ \mu\int_{v'} G(\mathbf{r_g},\mathbf{r_g}')\frac{\partial \mathbf{J}(\mathbf{r_g}',t_d)}{\partial t}dv' \\ &+ \epsilon_0(\epsilon_r-1)\,\mu\int_{v'} G(\mathbf{r_g},\mathbf{r_g'})\frac{\partial^2\mathbf{E}(\mathbf{r_g}',t_d)}{\partial t^2} \\ &+ \frac{\nabla}{\epsilon_0}\int_{v'} G(\mathbf{r_g},\mathbf{r_g}')q(\mathbf{r_g}',t_d)dv'.\end{aligned} \tag{102}$$

Eqn. (102) is the time domain formulation which can easily be converted to the frequency domain using the Laplace transform operator $s = \frac{\partial}{\partial t}$ and where the time retardation τ will transform to $e^{-s\tau}$. The PEEC integral equation solution of the Maxwell's equations is based on the total electric field in (101). An integral or inner product is used to reformulate each term of (102) into the circuit equations. This inner product integration converts each term into the fundamental form $\int \mathbf{E}\cdot d\mathbf{l} = V$ where V is the voltage or potential difference across the circuit element. It can be shown how this transforms the sum of the electric fields in (101) into the Kirchhoff's Voltage Law (KVL) over a basic PEEC cell. Fig. 9 details the (L_p,P,τ)PEEC model for the metal patch in Fig. 8 when discretized using four edge nodes (solid dark circles). The model in Fig. 9 consists of:

- partial inductances (L_p) which are calculated from the volume cell discretization using a double volume integral.
- coefficients of potentials (P) which are calculated from the surface cell discretization using a double surface integral.

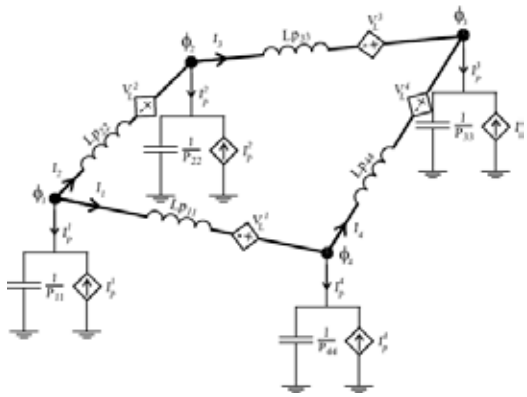

Figure 9: (L_p,P,τ)PEEC model for metal patch in Fig. 8 discretized with four edge nodes. Controlled current sources, I_p^n, account for the electric field coupling and controlled voltage sources, V_L^n, account for the magnetic field coupling.

- retarded controlled current sources, to account for the electric field couplings, given by $I_p^i = \frac{p_{ij}}{p_{ii}} I_C^j(t - t_{d_{ij}})$ where $t_{d_{ij}}$ is the free space travel time (delay time) between surface cells i and j,
- retarded current controlled voltage sources, to account for the magnetic field couplings, given by $V_L^n = Lp_{nm} \frac{\partial\, I_m(t-t_{d_{nm}})}{\partial t}$, where $t_{d_{nm}}$ is the free space travel time (delay time) between volume cells n and m.

Using the MNA method, the PEEC model circuit elements can be placed in the MNA system matrix during evaluation by the use of correct matrix stamps [44]. The MNA system, when used to solve frequency domain PEEC models, can be schematically described as

$$\begin{array}{rcl} j\omega \boldsymbol{P}^{-1} V - \boldsymbol{A}^T I & = & I_s, \\ \boldsymbol{A} V - (\boldsymbol{R} + j\omega \boldsymbol{L}_p) I & = & V_s, \end{array} \tag{103}$$

where: $\boldsymbol{P}$ is the coefficient of potential matrix, $\boldsymbol{A}$ is a sparse matrix containing the connectivity information, $\boldsymbol{L}_p$ is a dense matrix containing partial inductances, elements of the type Lp_{ij}, $\boldsymbol{R}$ is a matrix containing the volume cell resistances, V is a vector containing the node potentials (solution), elements of the type ϕ_i, I is a vector containing the branch currents (solution), elements of the type I_i, I_s is a vector containing the current source excitation, and V_s is a vector containing the voltage source excitation. The first row in the equation system in (103) is the Kirchhoff's current law for

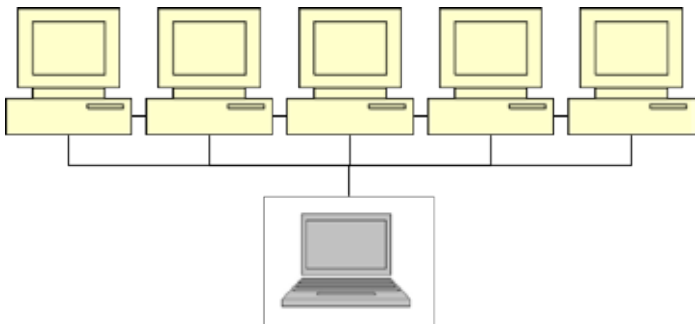

Figure 10: The test environment for implementation of the Grid-PEEC by several executors and the manager.

each node while the second row satisfies the Kirchhoff's voltage law for each basic PEEC cell (loop). The use of the MNA method when solving PEEC models is the preferred approach since additional active and passive circuit elements can be added by the use of the corresponding MNA stamp. For a complete derivation of the quasi-static and full-wave PEEC circuit equations using the MNA method, see for example [31].

Grid Computing and the PEEC Method

Partial element equivalent circuit (PEEC) models [83, 84, 85] are ideal for solving mixed circuit and electromagnetic problems. However, the nonorthogonal PEEC formulation [87] is computationally demanding for partial element computations since semi-analytic computation routines can not be used. Worse case is for PEEC-based frequency domain, full-wave solvers that require the partial elements to be recomputed at each frequency step. Different speed-up approaches for PEEC have been presented, for instance, using wavelet transform [3] and fast multipole method [4]. To deal with optimization of an existing frequency domain, nonorthogonal PEEC-based code, parallel computation by Grid-PEEC is applied. The purpose is to speed up both the calculation of the nonorthogonal partial elements and the solution of the frequency domain systems. In the applied Grid-PEEC, three different groups of accounts are defined as Executors, Users, and Administrators. For implementation of the Grid-PEEC, a test environment was provided in which the test was preformed with different numbers of executors (1, 2, 6, 12 and 20), see Fig. 10. The modified code works as follows:

1. Manager performs:

- parsing and meshing,
- calculations of $\mathbf{A}$ and $\mathbf{R}$,
- setup $\mathbf{I}_S$ and $\mathbf{V}$,
- check how many executors.

2. Partition calculation of coefficients of potentials on the connected executors (fill $\mathbf{P}$). Keep track of non-fill-ins.

3. Partition calculations of partial inductances on the connected executors (fill $\mathbf{L}$). Keep track of non-fill-ins.

4. Solve eq. (103) on the executors. Collect the results.

Antenna Analysis Applying the PEEC and Image Methods

The partial element equivalent circuit (PEEC) method has been developed from the VLSI inductance calculations in the early 70s. Electric and magnetic field of an electric dipole in the vicinity and within an infinite perfect electric conductor (PEC), or dielectric plane are subjects that can be studied and facilitated applying the image method (IM) and the complex image method (CIM) [92, 100]. Due to a layered medium, the idea of the CIM is to transform the problem into a combination of the source dipole and image dipoles with real and complex locations in space and in the absence of the layered medium, see Fig. 11. The radiation dyadic integral is expressed as

$$\bar{E}(\mathbf{r},\omega) = -j\omega\mu \left[\overline{\overline{I}} + \frac{1}{\beta^2}\right] \int \overline{\overline{G}}(\mathbf{r},\mathbf{r}')d\mathbf{r}', \tag{104}$$

where ω and μ are the angular frequency and permeability, respectively. $\mathbf{r}$ is the observation point distance to the origin and $\mathbf{r}'$ is the distance from the origin to the source point. The identity dyad $\overline{\overline{I}}$ is defined as $\overline{\overline{I}} = \hat{x}\hat{x}+\hat{y}\hat{y}+\hat{z}\hat{z}$. The radiation integral in (104) gives the solution of the Maxwell's equations in terms of a Green's function formulation. The Green's function in this case will be a 3×3 matrix of functions, or dyadic as

$$\overline{\overline{G}} = \left[\overline{\overline{I}} + \frac{1}{\beta^2}\nabla\nabla\right] \frac{e^{j\beta|\mathbf{r}-\mathbf{r}'|}}{4\pi|\mathbf{r}-\mathbf{r}'|}. \tag{105}$$

The integral in (104) is strongly singular, which makes the numerical integration very time-consuming. For the case of an infinitesimal vertical dipole above a dielectric half-plane, Eqn. (104) can be rewritten as

$$E_z(z) = \frac{1}{j\omega\epsilon_0} \int_{z'} \left(\beta_0^2 + \frac{\partial^2}{\partial z^2}\right) G_A^{zz} I(z')dz', \tag{106}$$

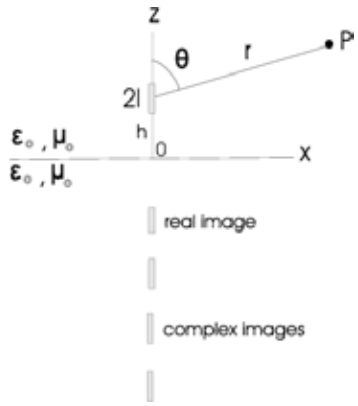

Figure 11: Real and complex images for a vertical dipole above a dielectric plane.

where β_0 is the free-space wave-number and G_A^{zz} is the dyadic Green's function for the vector potential A. It is shown that the dyadic Green's function in the above equation takes the form of a Sommerfeld-type integral for an infinitesimal vertical dipole located at (x', y', z') above a dielectric half-space of the relative permittivity ϵ_r [13]. This is an slowly convergent integral that is cumbersome to solve numerically. However, by the CIM, this dyadic Green's function can be solved much easier in terms of spherical wave components as [92]

$$G_A^{zz} = \frac{e^{-j\beta_0 R_s}}{4\pi R_s} - K\frac{e^{-j\beta_0 R_q}}{4\pi R_q} + \sum_{i=1}^{N} \frac{e^{-j\beta_0 R_i}}{4\pi R_i} \quad , N = 3...5, \tag{107}$$

where $K = (1-\epsilon_r)/(1+\epsilon_r)$, and R_s, R_q, and R_i are distances from the source point, real image point (quasidynamic image), and i-th image respectively to the field point. The classical image solution of an infinitesimal vertical dipole above a PEC plane can be derived where the third term in (107) vanishes. This Green's function is

$$G_A^{zz} = \frac{e^{-j\beta_0 R_s}}{4\pi R_s} - \frac{e^{-j\beta_0 R_q}}{4\pi R_q}. \tag{108}$$

Applying the image methods, the input impedance of a horizontal dipole above a PEC plane, as described in [10], can be calculated as a summation of self- and mutual impedances. For determining the input impedance of a horizontal dipole located above a PEC plane, a side-by-side configuration

can be applied. For this case, the self-impedance Z_{11} will be computed as $Z_{11} = R_{11} + jX_{11}$ where R_{11} and X_{11} are input- resistance and reactance. The mutual impedance for a side-by-side dipole configuration is computed as $Z_{21} = R_{21} + jX_{21}$ where R_{21} and X_{21} are the mutual- resistance and reactance. This computation of the input impedance is based on the current at the input.

Partial Element Calculations Applying PEEC and IM

Based on the PEEC method, the coefficients of potential are obtained by [30]

$$p_{ij} = \frac{1}{S_i S_j \epsilon} \int_{S_j} \int_{S_i} G(\mathbf{r}_i, \mathbf{r}_j) dS_j dS_i, \tag{109}$$

where S_i and S_j are the surface areas of cell i and j, created in the PEEC discretization. Applying (108), the Green's function in the above case, i.e. in the case of a vertical dipole above a PEC plane, is shown to be [92] $G = G_{free-space} - G_{image}$ where

$$G_{free-space} = \frac{1}{4\pi|\bar{r}_i - \bar{r}_j|}, \quad G_{image} = \frac{1}{4\pi|\bar{r}_i - \bar{r}_q|}, \tag{110}$$

in which $|\bar{r}_i - \bar{r}_j|$ and $|\bar{r}_i - \bar{r}_q|$ represent respectively the distances to the field point from the source point and to the quasidynamic image, i.e. the distance between the source point and its classical real image. This means that each element in the matrix for partial element potential coefficients p_{ij} includes the subtraction $G_{free-space} - G_{image}$. Determining the total partial self- and mutual inductances for a structure above a PEC plane will be analogous to that of the partial coefficients of potential [64], that is

$$L_{total} = L_{free-space} - L_{image}, \tag{111}$$

where the elements in the matrix $L_{free-space}$ are the partial self- and mutual inductances for the physical segments; L_{image} is the matrix including partial mutual inductances between the physical segments and their images.

3.4 Finite Difference Time-Domain (FDTD) Method

In this section the Finite Difference Time Domain (FDTD) method is described. The method is widely used within EM modeling mainly due to its simplicity. The FDTD method can be used to model arbitrarily heterogeneous structures like printed circuit boards (PCBs) and the human body.

In the FDTD method finite difference equations are used to solve Maxwell's equations for a restricted computational domain. The method requires the whole computational domain to be divided, or discretized, into volume elements (cells) for which Maxwell's equations have to be solved. The volume element sizes are determined by considering two main factors [5]:

1. *Frequency.* The cell size should not exceed $\frac{\lambda}{10}$, where λ is the wavelength corresponding to the highest frequency in the excitation.
2. *Structure.* The cell sizes must allow the discretization of thin structures.

The volume elements are not restricted to cubical cells, parallelepiped cells can also be used with a side to side ratio not exceeding $1:3$, mainly to avoid numerical problems [22]. In many cases, the resulted FDTD method is based according to the well-known Yee formulation [101]. However, there are other FDTD methods which are not based in the Yee cell and thus have another definition of the field components. To be able to apply Maxwell's equations in differential form to the Yee cell, the time and spatial derivatives using finite difference expressions will result in the FDTD equations [95]. The equations are then solved by:

1. Calculating the electric field components for the complete structure.
2. Advancing in time by $\frac{\Delta t}{2}$.
3. Calculating the magnetic field components for the complete structure based on the electric field components calculated in 1.
4. Advancing in time by $\frac{\Delta t}{2}$ and continuing to 1.

The FDTD method delivers the result in field variables, $\mathbf{E}$ and $\mathbf{H}$, at all locations in the discretized domain and at every time point. To obtain structured currents and voltages post-processing is needed for the conversion.

Leap-Frog Algorithm for Two-Dimensional (FDTD)

By the 2D-FDTD applied in this work, the staggered field quantities are based on a "leap-frog" time-update strategy where the magnetic and electric fields are computed in an altering manner. The method of the Central Differences is used in the FDTD to approximate the first-order derivatives in which the general derivative is written as [40]

$$\frac{\partial f(x)}{\partial x} = \frac{f\left(x + \frac{\Delta x}{2}\right) - f\left(x - \frac{\Delta x}{2}\right)}{\Delta x} + O(\Delta x^2) \tag{112}$$

or

$$\frac{\partial f(x)}{\partial x} \approx \frac{f\left(x+\frac{\Delta x}{2}\right)-f\left(x-\frac{\Delta x}{2}\right)}{\Delta x}. \tag{113}$$

To reduce the three-dimensional Maxwell's equations into special forms with faster solution, a two-dimensional analysis is widely used. In this manner, the two-dimensional domain will be described in a mathematical sense though any radiating electromagnetic field takes place in the three-dimensional physical space. By assuming that there is no variation in the electromagnetic field in the z-direction, the curl form of

$$\nabla \times \mathbf{H} = \mathbf{J} + \frac{\partial \mathbf{D}}{\partial t}$$

in Maxwell's equations can be expanded as [88]

$$-\mu \frac{\partial H_x}{\partial t} = \frac{\partial E_z}{\partial y}, \tag{114}$$

$$\mu \frac{\partial H_y}{\partial t} = \frac{\partial E_z}{\partial x}, \tag{115}$$

$$\frac{\partial E_z}{\partial t} = \frac{1}{\epsilon}\left(\frac{\partial H_y}{\partial x} - \frac{\partial H_x}{\partial y} - \sigma E_z\right) \tag{116}$$

where the current density $\mathbf{J}$ is expressed as σE_z [88]. Eqns. (114)-(116) are referred to as Transverse Magnetic (TM) fields, or TM polarization fields, implying that the electromagnetic fields lie only in the xy-plane. Different electromagnetic field directions for the TM polarization are illustrated in Fig. 12, applying 2D-FDTD discretization. Consider a uniformly rectangular grid, $\Omega = [0,a] \times [0,b]$ where each grid cell has dimensions Δx and Δy along each Cartesian axis. In this work, Δx and Δy have been chosen of equal size. By defining Δt as the time-step, in the domain $(t,x,y) \in [0,T] \times \Omega$ for $T > 0$, the following notation will be used in the 2D-FDTD formulation [89]

$$x_i = i\Delta x,\ x_{i+\frac{1}{2}} = x_i + \frac{1}{2}\Delta x,\ i = 0,1,2,...,I-1,\ x_I = a, \tag{117}$$

$$y_j = j\Delta y,\ y_{j+\frac{1}{2}} = y_j + \frac{1}{2}\Delta y,\ j = 0,1,2,...,J-1,\ y_J = b, \tag{118}$$

$$t^n = n\Delta t,\ t^{n+\frac{1}{2}} = t^n + \frac{1}{2}\Delta t,\ n = 0,1,2,...,N-1,\ N\Delta t = T. \tag{119}$$

where I, J and N are positive integers so that the electric field at the spatial location $(i\Delta x, j\Delta y)$ and the time-step $t^n = n\Delta t$ is then denoted by

$$\mathbf{E}(i\Delta x, j\Delta y, n\Delta t) = \mathbf{E}^n_{i,j} \tag{120}$$

Using the FDTD method, the TM polarization formulation in Eqns. (114)-(116), will be then substituted by the following difference equations [89]

$$H_{x_{i,j+\frac{1}{2}}}^{n+\frac{1}{2}} = H_{x_{i,j+\frac{1}{2}}}^{n-\frac{1}{2}} - \frac{\Delta t}{h\mu_0}\left[E_{z_{i,j+1}}^{n} - E_{z_{i,j}}^{n}\right], \tag{121}$$

$$H_{y_{i+\frac{1}{2},j}}^{n+\frac{1}{2}} = H_{x_{i+\frac{1}{2},j}}^{n-\frac{1}{2}} + \frac{\Delta t}{h\mu_0}\left[E_{z_{i+1,j}}^{n} - E_{z_{i,j}}^{n}\right], \tag{122}$$

$$E_{z_{i,j}}^{n+1} = E_{z_{i,j}}^{n} + \frac{\Delta t}{h\epsilon_0}\left[H_{y_{i+\frac{1}{2},j}}^{n+\frac{1}{2}} - H_{y_{i-\frac{1}{2},j}}^{n+\frac{1}{2}} - H_{x_{i,j+\frac{1}{2}}}^{n+\frac{1}{2}} + H_{x_{i,j-\frac{1}{2}}}^{n+\frac{1}{2}}\right] - \frac{\Delta t}{h\epsilon_0} J_{z_{i,j}}^{n+\frac{1}{2}}, \tag{123}$$

where $h = \Delta x = \Delta y$ and J_z can be a source due to an incident plane wave. The recursive update equations (121-123) are referred to as leap-frog time-update strategy in which $E_{z_{i,j}}^{n+1}$ relies on $H_{y_{i+\frac{1}{2},j}}^{n+\frac{1}{2}}$ and $H_{y_{i-\frac{1}{2},j}}^{n+\frac{1}{2}}$ along the y-axis and $H_{x_{i,j+\frac{1}{2}}}^{n+\frac{1}{2}}$ and $H_{x_{i,j-\frac{1}{2}}}^{n+\frac{1}{2}}$ along the x-axis; these are spatially centered about $E_{z_{i,j}}^{n+1}$. This is illustrated in Figs. 12-13. On the other hand, the magnetic field quantities along both x and y-axis are updated at $n + \frac{1}{2}$, i.e., at the previous time-step for all space samples. The electric field quantities are then updated at time step $n + 1$ for all space samples, and so on.

To simulate unbounded problems by the FDTD method, an Absorbing Boundary Condition (ABC) should be designed. In [68] a so-called second-order accurate ABC is proposed to resolve the unboundedness of the problem. To find a stable maximum time-step, a combination of theory and numerical experimentation is often the only way to proceed. To approximate the solution of a partial differential equation (PDE), one should analyze the problem by three important concepts which are *consistency, convergence,* and *stability.* By definition, a finite difference (FD) scheme is convergent if the point-wise error tends to zero as both the spatial and temporal step-sizes, for example Δx and Δt, tend to zero. However, it may be cumbersome to prove convergence for many numerical schemes. In fact, the order of convergence gives a good indication to how well a solution of an FD scheme approximates the exact solution of a differential equation. An FD scheme is consistent if the truncation error tends to zero as the spatial and temporal step-sizes tend to zero. Truncation error gives therefore a rate to how well the exact solution of a differential equation satisfies the FD scheme. In addition, truncation error is an accessible rate to determine the accuracy of an FD scheme whose formal order of accuracy is defined by the order of its truncation error. Similar to the point-wise error, the truncation error is an accessible rate to the accuracy for an FD scheme. The point-wise

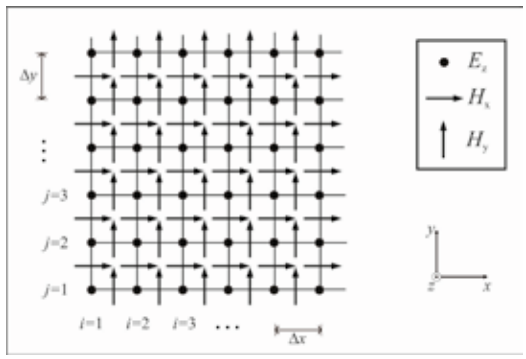

Figure 12: 2D-FDTD mesh for the transverse magnetic polarization.

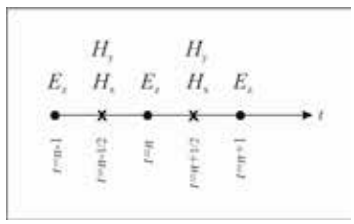

Figure 13: Leap-frog scheme used in 2D-FDTD for the transverse magnetic polarization.

error in an FD scheme shall grow unboundedly with time if the FD scheme is not stable. According to the *Lax Equivalence Theorem*, a consistent FD scheme, approximating the exact solution, is convergent if and only if the FD scheme is stable [59]. The three-dimensional FDTD algorithm is stable according to *Courant-Fredrichs-Lewy* or *CFL stability condition* in which the time-step is bounded by the limit [96]

$$\Delta t \leq \frac{1}{c_0} \frac{1}{\sqrt{\frac{1}{(\Delta x)^2} + \frac{1}{(\Delta y)^2} + \frac{1}{(\Delta z)^2}}}. \tag{124}$$

However, in the 2D-FDTD algorithm in this work, the CFL stability condition (124) reduces to

$$\Delta t \leq \frac{h}{c_0} \frac{1}{\sqrt{2}}, \tag{125}$$

where $h = \Delta x = \Delta y$. By choosing Δt, Δx, and Δy based on the CFL stability condition, the 2D-FDTD algorithm will be convergent, according to the Lax Equivalence Theorem [18]. In problems applying central-finite differences, one does not know the order of convergence even though the standard central-difference algorithm converges with an error of order h^2; h being the cell size. The order of convergence will decrease due to singular behavior of the solution in problem with geometries possessing sharp edges of metallic conductors and dielectrics [28]. The next step will then be to determine the order of convergence which is introduced by an error analysis and defining a semi-norm.

To determine the order of convergence in the 2D-FDTD algorithm, an error analysis is used. A good way to visualize errors when they are expected to behave like some power of the spatial discretization, is to write the error ϵ as [59]

$$\epsilon(h) \approx C\,(h)^p \tag{126}$$

where h is the cell size and C is a constant independent of h. Then by taking logarithm of both sides of (235), namely

$$\ln|\epsilon\,(h)| \approx \ln|C| + p \ln|h| \tag{127}$$

the error ϵ, on a log-log scale, behaves linearly with a slope which is equal to the order of convergence p. The next step in the process of determining the order of convergence is to define a semi-norm.

Let X be a vector space. Then, for every $u, v \in X$, and every $c \in \mathbb{R}$, a

semi-norm $|||.||| : X \to \mathbb{R}_+$ satisfies

$$\begin{aligned} N_1 &: |||u||| \geq 0 \\ N_2 &: |||cu||| = |c| \cdot |||u||| \\ N_3 &: |||u+v||| \leq |||u||| + |||v||| \end{aligned}$$

Let also P be an observation point. By defining the semi-norm $|||u||| = |u(P)|$ in this section, the goal is to show that the error $\varepsilon_h = |||u_h - u_{h/2}|||$ has order of convergence 2, where u_h is the numerical 2D-FDTD solution to the electric field $\mathbf{E}$ in the observation point P; $h = \Delta x = \Delta y$ is the spatial cell size in meter. Having (126) and (127) in mind, it will be shown that the error will be reduced by reducing the step size. Assume that

$$|||u_h - u_{\frac{h}{2}}||| \leq C \cdot h^k \tag{128}$$

where C is some constant (independent on k), and the integer k is to be determined by the above semi-norm; $u_{\frac{h}{2}}$ is the solution of the problem by a halved-cell size $\frac{h}{2}$. The discretized semi-norm will then be used to investigate how the order of convergence in the 2D-FDTD algorithm changes by halving the spatial step size h. The procedure for investigating a point-wise convergence in the point P is started by taking logarithm of both sides of Eqn. (128), that is

$$\begin{aligned} \ln\left(|||u_h - u_{\frac{h}{2}}|||\right) &\leq \ln\left(C \cdot h^k\right) \\ &= \ln(C) + \ln\left(h^k\right) \\ &= k\ln(h) + \ln(C). \end{aligned} \tag{129}$$

Eqn. (129) can be interpreted as a linear equation in the general form of $\eta = k\xi + m$, where $m = \ln(C)$, $\xi = \ln(h)$, and $\eta = \ln\left(|||u_h - u_{\frac{h}{2}}|||\right)$. The problem of determining the order of convergence is now converted to determine the slope k in the linear equation of $\eta = k\xi + m$. The left hand-side of Eqn. (129) will then be found by running the computer program for different step sizes h. That is, at each step in the algorithm, the spatial step size h (i.e. ξ-values) is halved.

4 Direct Electromagnetic Scattering Problem

Scattering theory has had a major roll in the twentieth century mathematical physics. The theory is concerned with the effect an inhomogeneous medium has on an incident particle or wave. The direct scattering problem is to determine a scattered field u^s from a knowledge of an incident field u^i and the differential equation governing the wave equation. The incident field is emitted from a source, an antenna for example, against an inhomogeneous medium. The total field is assumed to be the sum of the incident field u^i and the scattered field u^s. The governing differential equations in such cases are Maxwell's equations that will be converted to the wave equation. Generally, the direct scattering problems depend heavily on the frequency of the wave in question. In particular, the phenomenon of diffraction is expected to occur if the wavelength $\lambda = 2\pi/k$ is very small compared to the smallest observed distance; k is the wavebumber. Thus, due to the scattering obstacle, an observable shadow with sharp edges is produced. Obstacles which are small compared with the wavelength disrupt the incident wave without any identifiable shadow. Two different frequency regions are therefore defined based on the wavebumber k and a typical dimension of the scattering objects a. The set of k values such that $ka >> 1$ is called the *high frequency region* and the set of k values where $ka \leq 1$ is called the *resonance region*. The distinction between these two frequency regions is due to the fact that the applied mathematical methods in the resonance region differ greatly from the ones used in the high frequency region.

One of the first issues to think about when studying the direct scattering problem is the *uniqueness* of the solution. Then, by having established uniqueness, the existence of the solution and a numerical approximation of the problem must be analyzed and handled. The uniqueness of the solution will be discussed in the next section.

4.1 Uniqueness of the Solution

Within the electromagnetic field theory there are two fundamental governing differential equations for electrostatics in any medium. These are [25]:

$$\nabla \cdot \mathbf{D} = \rho_v, \tag{130}$$

$$\nabla \times \mathbf{E} = 0, \tag{131}$$

where $\mathbf{D}$ and $\mathbf{E}$, are the electric flux density and electric field intensity, as defined earlier; ρ_v is free charge per unit volume. Because $\mathbf{E}$ is rotation-free,

a scalar electric potential Φ can be defined such that

$$\mathbf{E} = -\nabla\Phi. \tag{132}$$

Combining (130) and (132) yields

$$\nabla \cdot (\epsilon\nabla\Phi) = -\rho_v, \tag{133}$$

where ϵ is the permittivity due to linear isotropic medium in which $\mathbf{D} = \epsilon\mathbf{E}$. The above equations will finally result in

$$\nabla^2\Phi = \frac{-\rho_v}{\epsilon}. \tag{134}$$

Eqn. (134) is called the *Poisson's equation*. In this equation ∇^2 is *Laplacian*. If there is no charge in the simple medium, i.e. $\rho_v = 0$, then Eqn. (134) will be converted into

$$\nabla^2\Phi = 0, \tag{135}$$

which is called the *Laplace's equation*. The concept of uniqueness has arisen when solving the Laplace's or Poisson's equation by different methods. Depending on the complexity and the geometry of the problem, one may use analytical, numerical, or experimental methods. The question is whether all of these methods will give the same solution. This may be reformulated as: Is the present particular solution of the Laplace's or Poisson's equation, satisfying the boundary conditions, the only solution? The answer will be yes by relying on the uniqueness theorem. Irrespective of the method, a solution of the problem satisfying the boundary conditions is the only possible one.

In connection with the concept of the uniqueness, two theorems are extensively discussed within the computational electromagnetics [6]. These are:

Theorem 1. *A vector is uniquely specified by giving its divergence and its curl within a simply connected region and its normal component over the boundary.*

Theorem 2. *A vector* $\mathbf{V}$ *with both source and circulation densities vanishing at infinity may be written as the sum of two parts, one of which is irrotational, the other solenoidal.*

A field $\mathbf{A}$ is irrotational if $\nabla \times \mathbf{A} = 0$ and solenoidal if $\nabla \cdot \mathbf{A} = 0$. A proof of the uniqueness theorem due to the Laplace's equation is given in

[89]. The theorem (2) is called the Helmholtz's theorem. The theorems (1) and (2) can together be interpreted as: "*a solution of the Poisson's equation (134) and Eqn. (135) (as a special case), which satisfies a given boundary condition, is a unique solution*" [25]. In [10], there is another interpretation of the uniqueness theorem:

"*A field in a lossy region is uniquely specified by the sources within the region plus the tangential components of the electric field over the boundary, or the tangential components of the magnetic field over the boundary, or the former over part of the boundary and the latter over the rest of the boundary*". Hence, according to the uniqueness theorem, the field at a point in space will be sufficiently determined by having information about the tangential electric field and the tangential magnetic field on the boundary. This means that to determine the field uniquely, one of the following alternatives must be specified [97]:

- $\hat{n} \times \hat{E}$ everywhere on S,
- $\hat{n} \times \hat{H}$ everywhere on S,
- $\hat{n} \times \hat{E}$ on a part of S and $\hat{n} \times \hat{H}$ on the rest of S,

with S as the boundary of the domain. Directly related to the electromagnetic obstacle scattering two other theorems can be found in [27]. These are:

Theorem 3. *Assume that D_1 and D_2 are two perfect conductors such that for one fixed wavebumber the electric far-field patterns for both scatterers coincide for all incident directions and all polarizations. Then $D_1 = D_2$.*

Theorem 4. *Assume that D_1 and D_2 are two perfect conductors such that for one fixed incident direction and polarization the electric far field patterns of both scatterers coincide for all wavebumbers contained in some interval $0 < k_1 < k < k_2 < \infty$. Then $D_1 = D_2$.*

As depicted in the above theorems, the scattered wave depends analytically on the wavebumber k.

4.2 Solution of the Direct Electromagnetic Scattering Problem

The simplest problem in the direct scattering problem is scattering by an impenetrable obstacle D. Then, the total field u can be determined by [27]

$$\nabla^2 u + k^2 n(x) u = 0 \ \ in \ \mathbb{R}^3, \tag{136}$$

$$u(x) = e^{ikx\cdot d} + u^s(x), \tag{137}$$

$$\lim_{r\to\infty} r(\frac{\partial u^s}{\partial r} - iku^s) = 0, \tag{138}$$

in which $r = |x|$, and $n = c_0^2/c^2$ is the refractive index due to the square of the sound speeds. By the assumption that the medium is absorbing and also assuming that $1 - n$ has *compact support*, n will be complex-valued [27]. For the homogeneous host medium, $c = c_0$, and for the inhomogeneous medium, $c = c(x)$. Depending on obstacle properties, different boundary conditions will be assumed. Eqn. (138) is called *Sommerfeld radiation condition*. Acoustic wave equations possessing such kind of boundary condition guarantee that the scattered wave is outgoing.

Within the computational electromagnetics for the scattering problem, the incident field by the time-harmonic electromagnetic plane wave can be expressed as

$$E^i(x,t) = ik(d\times p)\times d e^{i(kx\cdot d-\omega t)}, \tag{139}$$

$$H^i(x,t) = ik(d\times p) e^{i(kx\cdot d-\omega t)}, \tag{140}$$

where ω is the radial frequency, ϵ_0 the electric permittivity in vacuum, μ_0 the magnetic permeability in vacuum, d the direction of propagation and p the polarization. Assuming variable permittivity but constant permeability, the electromagnetic scattering problem is now to determine both the electric and magnetic field according to

$$\begin{aligned} \nabla\times E - ikH = 0 \ \ \text{in} \ \mathbb{R}^3, \\ \nabla\times H + ikn(x)E = 0 \ \ \text{in} \ \mathbb{R}^3, \end{aligned} \tag{141}$$

where $n = \varepsilon/\varepsilon_0$ is the refractive index by the ratio of the permittivity $\epsilon = \epsilon(x)$ in the inhomogeneous medium; n will have a complex value if the medium is conducting. It is assumed that $1 - n$ has compact support. The total electromagnetic field is determined by

$$E(x) = (i/k)\nabla\times\nabla\times p e^{ikx\cdot d} + E^s(x), \tag{142}$$

$$H(x) = \nabla\times p e^{ikx\cdot d} + H^s(x), \tag{143}$$

so that

$$\lim_{r\to\infty}(H^s \times x - rE^s) = 0, \tag{144}$$

where Eqn. (144) is called the *Silver-Müller radiation condition*. The electromagnetic scattering by a perfect obstacle D is now to find an electromagnetic field such that [27]

$$\nabla E - ikH = 0, \;\; \nabla H - ikE = 0 \;\; \text{in } \mathbb{R}^3 \setminus \bar{D}, \tag{145}$$

$$E(x) = (i/k)\nabla \times \nabla \times pe^{ikx\cdot d} + E^s(x), \tag{146}$$

$$H(x) = \nabla \times pe^{ikx\cdot d} + H^s(x), \tag{147}$$

$$\nu \times \nabla E = 0 \;\; \text{on } \partial D, \tag{148}$$

$$\lim_{r\to\infty}(H^s \times x - rE^s) = 0, \tag{149}$$

where ν is the unit outward normal on ∂D. Eqns. (145) are called the *time harmonic Maxwell's equations*. The above formulation is called the *direct electromagnetic scattering problem*. The method of integral equations is a common method to investigate the existence of a numerical approximation of the direct problem. The integral equation associated with the electromagnetic scattering problem due to Eqns.(141)-(143) is given by [27]

$$E(x) = \frac{i}{k}\nabla \times \nabla \times pe^{ikx\cdot d} - k^2 \int_{\mathbb{R}^3} \Phi(x,y)m(y)E(y) \tag{150}$$
$$+\nabla \int_{\mathbb{R}^3} \frac{1}{\nu(y)} \nabla n(y) \cdot E(y)\Phi(x,y)dy, \quad x \in \mathbb{R}^3,$$

where

$$\Phi(x,y) = \frac{1}{4\pi} \frac{e^{ik|x-y|}}{|\, x-y \,|}, \;\; x \neq y, \tag{151}$$

and $m := 1 - n$; if E is the solution of Eqn. (151), one can define

$$H(x) = \frac{1}{ik}\nabla \times E(x). \tag{152}$$

Letting x tend to the boundary of D and introducing a as a tangential density to be determined, one can verify that a will be a solution for E in the following boundary integral equation [27]:

$$E^s(x) = \nabla \times \int_{\partial D} a(y)\Phi(x,y)ds(y), \;\; x \in \mathbb{R}^3 \setminus \bar{D} \tag{153}$$
$$H^s(x) = \frac{1}{ik}\nabla \times E^s(x), \;\; x \in \mathbb{R}^3 \setminus \bar{D}.$$

In this formulation, the boundary integral equation in Eqns. (153) will be used to solve Eqns. (141)-(143). The fact is that the integral equation is not uniquely solvable if k^2 is a Neumann eigenvalue of the negative Laplacian in D [9]. The numerical solution of boundary integral equations in scattering theory is generally a much challenging area and a deeper understanding of this topic requires knowledge in different areas of functional analysis, stochastic processes, and scientific computing. In fact, the electromagnetic inverse medium problem is not entirely investigated and numerical analysis and experiments have yet to be done for the three dimensional electromagnetic inverse medium.

5 Inverse Electromagnetic Scattering Problem

The inverse scattering problem is, in many areas, of equal interest as the direct scattering problem. Inverse formulation is applied on a daily basis in many disciplines such as image and signal processing, astrophysics, acoustics, geophysics and electromagnetic scattering. The inverse formulation, as an interdisciplinary field, involves people from different fields within natural science. To find out the contents of a given black box without opening it, would be a good analogy to describe the general inverse problem. Experiments will be carried out to guess and realize the inner properties of the box. It is common to call the contents of the box "the model" and the result of the experiment "the data". The experiment itself is called "the forward modeling." As sufficient information cannot be provided by an experiment, a process of regularization will be needed. The reason to this issue is that there can be more than one model ('different black boxes') that would produce the same data. On the other hand, improperly posed numerical computations will arise in the calculation procedure. A regularization process in this context plays a major roll to solve the inverse problem.

5.1 Analytic Formulation of the Inverse Scattering Problem

As in the direct formulation, the permittivity ϵ has a constant value, in inverse scattering formulation ϵ has to be assumed as room-dependent. Assuming $\epsilon = 1$ outside a sphere with radius R, and $\epsilon \neq 1$ inside, the following equation can be deduced by starting from Maxwell's equations and some vector algebra [57]

$$\nabla \times (\nabla \times \mathbf{E}(\mathbf{r}, \omega)) - \omega^2 \epsilon_0 \mu_0 \epsilon(\mathbf{r}) \mathbf{E}(\mathbf{r}, \omega) = \mathbf{0}, \tag{154}$$

where $\mathbf{r}$ is the room variable and the scatterer material with volume V_s is assumed to be non-magnetic, i.e. $\mu = 1$; no other current sources except induced current generated by the incident field $\mathbf{E}^i$ are assumed to exist either. By introducing a dimensionless quantity χ_e, known as the *electric susceptibility*, a new equation will be introduced as

$$\mathbf{D} = \epsilon_0(1 + \chi_e(\mathbf{r}))\mathbf{E}(\mathbf{r}, \omega) = \epsilon_0 \epsilon(\mathbf{r}) \mathbf{E}(\mathbf{r}, \omega) = \epsilon \mathbf{E}(\mathbf{r}, \omega) \tag{155}$$

where $\mathbf{D}(\mathrm{C/m^2})$ is defined as *electric displacement*, see previous sections. By Eqn. (155), it is easy to see that

$$\epsilon(\mathbf{r}) = 1 + \chi_e(\mathbf{r}). \tag{156}$$

A dielectric medium is, by definition, linear if χ_e is independent of $\mathbf{E}$ and homogeneous if χ_e is independent of space coordinates. In fact, the electric susceptibility χ_e gives the dielectric deviation between the free-space and other dielectric media in the case of inverse scattering problem. It is equal to zero in the free-space on the outside of the sphere with radius R and distinct from zero inside. The sphere in fact contains the scatterer with the volume V_s. In addition, it is assumed that the medium contained in the volume V_s is not *dispersive*, i.e. χ_e inside the volume V_s is not dependent on the frequency ω. In the case of the inverse electromagnetic scattering problem, the goal is to determine the function $\chi_e(\mathbf{r})$ by experimentally obtained incident electric field E^i and scattered electric field E^s and the total field $E = E^i + E^s$. This process is started by re-writing the Eqn. (154) as

$$\nabla \times (\nabla \times \mathbf{E}(\mathbf{r}, \omega)) - k^2 \mathbf{E}(\mathbf{r}, \omega) = k^2 \chi_e(\mathbf{r}) \mathbf{E}(\mathbf{r}, \omega) \tag{157}$$

where

$$k^2 = \omega^2 \epsilon_0 \mu_0 \tag{158}$$

in which k is the wavebumber associated with vacuum as the surrounding medium. Due to the incident field $\mathbf{E}^i$, a current will be induced in V_s with the associated current density $\mathbf{J}_s$, which can be expressed as [57]

$$\mathbf{J}_s = -j\omega\epsilon_0 \chi_e \mathbf{E}. \tag{159}$$

By the aid of this induced current density, the scattered electric field can be expressed as [57]

$$\mathbf{E}^s(\mathbf{r}) = [k^2 + \bigtriangledown\bigtriangledown] \cdot \int_{V_s} \frac{e^{jk|\mathbf{r}-\mathbf{r}'|}}{4\pi|\mathbf{r}-\mathbf{r}'|} \chi_e(\mathbf{r}') \mathbf{E}(\mathbf{r}') dv', \quad \mathbf{r} \notin V_s, \tag{160}$$

where $j = \sqrt{-1}$As it is seen in Eqn. (160), the integral deals with the inside of the scatterer which is unobservable by experimentally measuring the electric field. Both the scattered and the incident electric field can be measured at the outside of the scatterer and the unknown electric field inside the integral should be determined in different situations. In the cases where $\mathbf{E}^s << \mathbf{E}^i$, there are different methods to approximate the integral in Eqn. (160). In the *Born* approximation, the dielectric properties of the scatterer can be determined by a three-dimensional inverse Fourier transforming of the far-field $\mathbf{F}$ in certain directions and for any frequency [57]. This means that for the experimentally given incident plane wave with propagation vector $\hat{\mathbf{k}}_i$, one has

$$\mathbf{E}^i(\mathbf{r}) = \mathbf{E}_0 e^{jk\hat{k}_i \cdot \mathbf{r}}, \tag{161}$$

and for a fixed point k, a three-dimensional Fourier transform of the function χ_e can be calculated in a point $k(\hat{\mathbf{k}}_i - \hat{\mathbf{r}})$, that is [57]

$$\int_{V_s} \chi_e(\mathbf{r}') e^{jk(\hat{\mathbf{k}}_i - \hat{\mathbf{r}})\cdot\mathbf{r}'} dv' = \frac{4\pi}{k^3} \frac{\mathbf{F}(\hat{\mathbf{r}})}{\hat{\mathbf{r}} \times (\mathbf{E}_0 \times \hat{\mathbf{r}})}, \tag{162}$$

where the far-field scattering amplitude (measured data in the far-field) is

$$\mathbf{F}(\hat{\mathbf{r}}) = \hat{\mathbf{r}} \times (\mathbf{E}_0 \times \hat{\mathbf{r}}) \frac{k^3}{4\pi} \int_{V_s} \chi_e(\mathbf{r}') e^{jk(\hat{\mathbf{k}}_i - \hat{\mathbf{r}})\cdot\mathbf{r}'} dv'. \tag{163}$$

As depicted in Eqn. (162), in the Born approximation the problem is linearized with substitution of the unknown field in the integral by the given incident field. In the *Rytov* approximation, the polarization field is assumed to be almost unchanged and the phase of the field is interpreted as all the scattering, that is

$$\mathbf{E}(\hat{\mathbf{r}}) = \mathbf{E}_0 e^{jk\psi(\mathbf{r})}, \tag{164}$$

where $\psi(\mathbf{r})$ is the field phase as

$$\psi(\mathbf{r}) = \hat{\mathbf{k}}_i \cdot \mathbf{r} + \psi_s(\mathbf{r}), \tag{165}$$

in which $\psi_s(\mathbf{r})$ is the deviations from $\hat{\mathbf{k}}_i$, i.e., the phase associated with the incident field. By application of some vector algebra and by the aid of an approximation, (157) can be written as [57]

$$2\mathbf{E}_0(\hat{\mathbf{k}}_i \cdot \nabla\psi(\mathbf{r})) - (\mathbf{E}_0 \cdot \nabla\psi_s(\mathbf{r}))\hat{\mathbf{k}}_i = \chi_e(\mathbf{r})\mathbf{E}_0, \tag{166}$$

that yields

$$\begin{aligned} 2\hat{\mathbf{k}}_i \cdot \nabla\psi(\mathbf{r}) &= \chi_e(\mathbf{r}), \\ \mathbf{E}_0 \cdot \nabla\psi_s(\mathbf{r}) &= 0, \end{aligned} \tag{167}$$

using which the electric susceptibility χ_e can be determined by the following process. By introducing new Cartesian coordinates ξ and η, it will be possible to have the directions of $\hat{k}_i$ lying in, for example, the xy-plane so that the $\eta\xi$-plane is perpendicular to the xy-plane, see Fig. 14. Hence:

$$\begin{aligned} \xi &= x\cos\phi + y\sin\phi, \\ \eta &= -x\sin\phi + y\cos\phi, \end{aligned} \tag{168}$$

where ϕ is the rotation angle between the two coordinate systems of xy and $\eta\xi$.

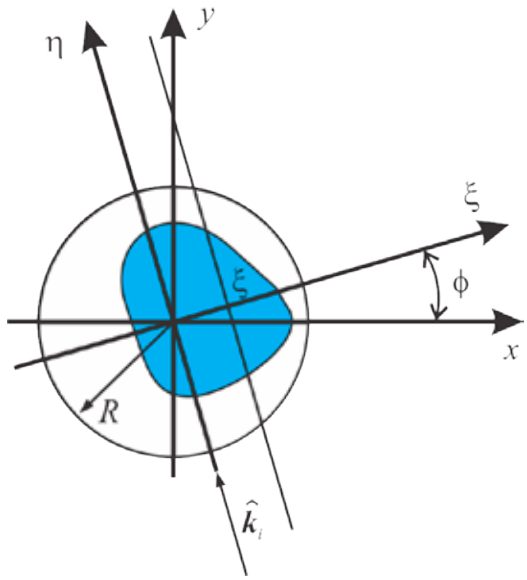

Figure 14: New Cartesian coordinate system building the $\eta\xi$-plane.

Finally, the phase ψ_s can be expressed, by the Rytov approximation as [57]

$$\psi_s(\xi, \phi) = \frac{1}{2} \int_{-\infty}^{+\infty} \chi_e(x, y) d\eta. \tag{169}$$

Two methods are frequently used to obtain $\chi_e(x, y)$ from Eqn. (169): the method of *Projection* and the method of *Integral Equation*. Following, the method of Projection is briefly explained.

The general inverse formulation of determining dielectric properties $f(x, y)$ of the scatterer is in the form of the following integral [57]

$$u_\phi(\xi) = \int_{-\infty}^{\infty} f(x, y) d\eta = \int_{-\infty}^{\infty} \int_{-\infty}^{\infty} f(x, y) \delta(\xi - \rho \cdot \hat{\xi}) dx dy, \tag{170}$$

where $\rho = \hat{\mathbf{x}}x + \hat{\mathbf{y}}y$ is a two-dimensional regional vector and δ, Dirac's delta distribution. The coordinates ξ and η are associated with the directions $\hat{\xi}$ and $\hat{\eta}$ according to

$$\begin{aligned} \hat{\xi} &= \hat{\mathbf{x}} \cos\phi + \hat{\mathbf{y}} \sin\phi, \\ \hat{\eta} &= -\hat{\mathbf{x}} \sin\phi + \hat{\mathbf{y}} \cos\phi. \end{aligned} \tag{171}$$

According to this formulation of inverse electromagnetic scattering, the data is actually the Fourier transform $\mathfrak{F}$ of the dielectric properties of the scatterer in question. This means

$$\mathfrak{F}\{u_\phi(p)\} = \hat{u}_\phi(p) = \int_{-\infty}^{\infty} u_\phi(\xi) e^{ip\xi} d\xi, \tag{172}$$

where p is a Fourier variable related to ξ. Eqn. (172) and (170) yield

$$\hat{u}_\phi(p) = \int_{-\infty}^{\infty} e^{ip\xi} \int_{-\infty}^{\infty} \int_{-\infty}^{\infty} f(x,y)\delta(\xi - \rho \cdot \hat{\xi}) dx dy d\xi. \tag{173}$$

Using the Dirac's delta distribution properties, (173) can be written as

$$\hat{u}_\phi(p) = \int_{-\infty}^{\infty} \int_{-\infty}^{\infty} f(x,y) e^{ip\rho\cdot\hat{\xi}} dx dy. \tag{174}$$

The unknown dielectric properties $f(x,y)$ can now be determined by inverse Fourier transforming of (174), that is [57]

$$f(x,y) = \frac{1}{4\pi^2} \int_{-\infty}^{\infty} \int_{-\infty}^{\infty} \hat{f}(\mathbf{p}) e^{-j\rho\cdot\mathbf{p}} dp_x dp_y, \tag{175}$$

where

$$\hat{f}(\mathbf{p}) = \hat{u}_\phi(p), \quad \text{for } p \geq 0. \tag{176}$$

Expressed in the Cartesian coordinates, the vector $\mathbf{p}$ can be written as

$$\mathbf{p} = \hat{\mathbf{x}} p_x + \hat{\mathbf{y}} p_y. \tag{177}$$

5.2 Numerical Solution of the Inverse Electromagnetic Scattering Problem

As the direct scattering problem has been thoroughly investigated, the inverse scattering problem has not yet a rigorous mathematical/numerical basis. Because of the nonlinear nature of the inverse scattering problem, one will face improperly posed numerical computation in the inverse calculation process. This means that, in many applications, small perturbations in the measured data cause large errors in the reconstruction of the scatterer. Some regularization methods must be used to remedy the ill-conditioning due to the resulting matrix equations. Concerning the existence of a solution to the inverse electromagnetic scattering one has to think about finding approximate solutions after making the inverse problem stabilized. A number

of methods is given to solve the inverse electromagnetic scattering problem in which the nonlinear and ill-posed nature of the problem are acknowledged. Earlier attempts to stabilize the inverse problem was via reducing the problem into a linear integral equation of the first kind. However, general techniques were introduced to treat the inverse problems without applying an integral equation. The process of regularization is used at the moment when selection of the most reasonable model is on focus. Computational methods and techniques ought to be as flexible as possible from case to case. A computational technique utilized for small problems may fail totally when it is used for large numerical domains within the inverse formulation. New methodologies and algorithms would be created for new problems since existing methods are insufficient. This is the major characteristics of the existing inverse formulation in problems with large numerical domains. There are both old and new computational tools and techniques for solving linear and nonlinear inverse problems. Linear algebra has been extensively used within linear and nonlinear inverse theory to estimate noise and efficient inverting of large and full matrices. As different methods may fail, new algorithms must be developed to carry out nonlinear inverse problems. Sometimes, a regularization procedure may be developed for differentiating between correlated errors and non-correlated errors. The former errors come from linearization and the latter from the measurement. To deal with the nonlinearity, a local regularization will be developed as the global regularization will deal with the measurement errors. There are researchers who have been using integral equations to reformulate the inverse obstacle problem as a nonlinear optimization problem. In some approaches, a priori is assumed such that enough information is known about the unknown scattering obstacle D [51, 52, 53]. Then, a surface Γ is placed inside D such that k^2 is not a Dirichlet eigenvalue of the negative Laplacian for the interior of Γ. Then, assuming a fixed wavebumber k and a fixed incident direction d, and also by representing the scattered field u^s as a single layer potential [27]

$$u^s(x) = \int_\Gamma \phi(y)\Phi(x,y)dS(y), \tag{178}$$

where $\phi \in L^2(\Gamma)$ is to be determined; $L^2(\Gamma)$ is the space of all *square integrable functions* on the boundary Γ. The far field pattern u_∞ is then represented as

$$u_\infty(\hat{x};d) = \frac{1}{4\pi}\int_\Gamma e^{-ik\hat{x}\cdot y}\phi(y)\Phi(x,y)dS(y), \quad \hat{x} \in \Omega \tag{179}$$

where Ω is the unit sphere, and $\hat{x} = x/|x|$. By the aid of the given (measured) far field pattern u_∞, one can find the density ϕ by solving the ill-posed integral equation of the first kind in Eqn. (179). This method is described thoroughly in [54, 55, 56].

In another method it is assumed that the given (measured) far field u_∞ for all $\hat{x}$, and $d \in \Omega$ is given. The problem is now to determine a function $g \in L^2(\Omega)$ such that

$$\int_\Omega u_\infty(\hat{x}; d)g(d)dS(d) = \frac{1}{ki^{p+1}}Y_p(\hat{x}), \quad \hat{x} \in \Omega, \tag{180}$$

where p is an integer and k is fixed; Y_p is a spherical harmonic of order p [6]. It can be shown that solving the ill-posed integral equation (180) leads, in special conditions, to the nonlinear equation [27]

$$\int_\Omega e^{ikr(a)a\cdot d}g(d)dS(d) = -h_p^{(1)}(kr(a))Y_p(\hat{x}), \quad a \in \Omega, \tag{181}$$

in which r is to be determined, and where $x(a) = r(a)a$; h_p^1 is the spherical Hankel function of the first kind of order p [6]. In [14], this method is developed and applied to the case of the electromagnetic inverse obstacle problem.

Optimization of the Inverse Problem

A linear inverse problem can be given in the form of finding $\mathbf{x}$ such that $\mathbf{A}x = \mathbf{b} + \mathbf{n}$, where $\mathbf{b}$, $\mathbf{x}$, and $\mathbf{n}$ are vectors, and A is a matrix; $\mathbf{n}$ is the noise which has to be minimized by different so-called *regularization* methods. Within the field of image processing, a forward model is defined as an unobservable input x^* which returns as an observable output $\mathbf{b}$. Here, the forward problem is modeled by a forward model, and the inverse problem will be an approximation of x^* by $\hat{x}$. The forward process is, in other words, a mapping from the image to error-free data, $\bar{d}$, and the actual corrupted data, d; the noise n is the difference $\bar{d} - d$. The corruption in such context is due to small round off error by a computer representation and also by inherent errors in the measurement process.

The collection of values that are to be reconstructed is referred to as the *image*. Denoting f as the image, the forward problem is the mapping from the image to the quantities that can be measured. By the forward mapping denoted by A, the actual data d can be denoted by

$$d = A(f) + n, \tag{182}$$

where A may be either linear or nonlinear mapping. Accordingly, the inverse problem can now be interpreted as finding the original image given the data, and the information from the forward problem.

Well-posed and Ill-posed Problems

As the image and data are infinite-dimensional (continuous) or finite-dimensional (discrete), there will be several classifications. Image and data can be both continuous; they can also be both discrete, or the former continuous, the latter discrete, and vice versa. However, each of the cases is approximated by a discrete-discrete alternative as computer implementation is in a discrete way. The other mentioned alternatives are always an idealization of the problem. According to Hadamard [33], the inverse problem to solve

$$A(f) = d \tag{183}$$

is a *well-posed* problem if

- a solution exists for any data d,
- there is a unique solution in the image space,
- the inverse mapping from d to f is continuous.

In addition, an *ill-posed* problem is where an inverse does not exist because the data is outside the range of A. Other interpretations of the above three conditions is *an ill-posed problem, i.e, a problem in which small changes in data may cause large changes in the image.* To stabilize the solution of ill-conditioned and rank-deficient problems, the concept of *singular value decomposition (SVD)* is widely used. The reason is that relatively small singular values can be dropped, which makes the process of computation less sensitive to perturbations in data. Another important application of the SVD is the calculation of the condition number of a matrix which is directly related to ill-posed problems.

Singular Value Decomposition

In connection with rank-deficient and ill-posed problems, it is convenient to describe singular value expansion of a kernel due to an integral equation. This calculation is by means of the singular value decomposition (SVD). All the difficulties due to ill-conditioning of a matrix will be revealed by

applying SVD. Assuming $A \in \mathbb{R}^{m \times n}$ be a rectangular or square matrix and letting $m \geq n$, the SVD of A is a decomposition in form of

$$A = U\Sigma V^T = \sum_{i=1}^{n} u_i \sigma_i v_i^T, \tag{184}$$

where the orthonormal matrices $U = (u_1, ..., u_n) \in \mathbb{R}^{m \times n}$ and $V = (v_1, ..., v_n \in \mathbb{R}^{n \times n})$ are such that $U^T U = V^T V = I_n$ [40]. The diagonal matrix $\Sigma = diag(\sigma_1, ..., \sigma_n)$ has decreasing nonnegative elements such that

$$\sigma_1 \geq \sigma_2 \geq ... \geq \sigma_n \geq 0, \tag{185}$$

where the vectors u_i and v_i are the *left and right singular vectors* of A, respectively; σ_i are called the *singular values* of A which are, in fact, the nonnegative square roots of the eigenvalues of $A^T A$. Columns of U and A are orthonormal eigenvectors of AA^T and $A^T A$ respectively. The rank of a matrix is equal to the number of nonzero singular values, and a singular value of zero indicates that the matrix in question is rank-deficient. One of the most significant applications of matrix decomposition by SVD is within parallel matrix computations. The SVD has other important applications within the area of scientific computing. Some of them are as follows [40]:

- solving linear least squares of ill-conditioned and rank-deficient problems,
- calculation of orthonormal bases for range and null spaces,
- calculation of condition number of a matrix,
- calculation of the Euclidean norm.

As an example, the Euclidean norm of a matrix can be calculated by SVD as the first element in (185), i.e. σ_1. This value is indeed the first (and the largest) singular value, positioned on the diagonal matrix Σ, that is:

$$\sigma_{max} = \|A\|_2 = \max_{x \neq 0} \frac{\|Ax\|_2}{\|x\|_2}. \tag{186}$$

With respect to the Euclidean norm in (186), and also the smallest singular value, both calculated by the SVD procedure, one can determine the condition number of the matrix A by

$$cond(A) = \frac{\sigma_{max}}{\sigma_{min}}, \tag{187}$$

with σ_{min} as the smallest element on the diagonal matrix Σ in (184).

Regularization

With an origin in the *Fredholm integral equation* of the first kind as [6]

$$f(x) = \int_a^b K(x,t)\phi(t)dt, \tag{188}$$

with $f(x)$ and $K(x,t)$ known and $\phi(t)$ unknown, most inverse problems describe the continuous world. The *kernel* K represents the response functions of an instrument (determined by known signals), and f represents measured data; ϕ represents the underlying signal to be determined. Integral equations can also result from *the method of Green's functions* [81] and the *boundary element methods* [58] for solving differential equations. The *existence* and *uniqueness* of solutions to integral equations is more complicated in comparison to algebraic equations. In addition, the solution may be highly sensitive to perturbations in the input data f. The reason to sensitivity lies in the nature of the problem that has to do with determining the integrand from the integral; this is just the opposite integration operator which is a smoothing process. Such an integral operator with a smooth kernel K, i.e., a kernel that does not possess singularities, has zero as an eigenvalue [40]. This means that there are nonzero functions that will be annihilated under the integral operator. Solving for ϕ in (188) tends to introduce high-frequency oscillation as the integrand contains ϕ as an arbitrary function and the smooth kernel K. The sensitivity in the process of solving integral equations of type (188) is inherent in the problem and it has not to do with the method of solving. For an integral operator with a smooth kernel by having zero as an eigenvalue, additional information may be required. The reason to this is that using a more accurate quadrature rule leads to an ill-conditioned linear equation system, which thereby results into a more erratic solution. To handle the ill-conditioning in such context, several numerical methods have been used. In *truncated singular value decomposition* the solution of the ultimate linear equation system $Ax = y$ is computed by using the singular value decomposition of A. In this process, small singular values of A are omitted from the solution; the small singular values of A reflects and generates in fact ill-conditioning when solving the ultimate linear equation system.

The method of *regularization* solves a minimization problem to obtain a physically meaningful solution. Starting from the Fredholm integral equation in (188) and introducing $m(t)$ as the model and letting $b = [b_1, ..., b_n]^T$

be the vector of the measured data, a connection between m and b will be

$$b_i = \int_D K(s_i, t)m(t)dt + \epsilon_i, \tag{189}$$

where $K(s,t)$ is still the smooth kernel, and ϵ_i is the measurement noise; D is the domain of the integration. The goal is now to find the model m assuming that the noisy data b is given. The problem (189) becomes a well-posed least-squares system if it will be discretized with a number of parameters M which is smaller than N. As a disadvantage, this discretization makes the solution lie in a small subspace which does not always fit the problem. However,choosing a discretization with a number of parameters M bigger than N, the discrete system will possess some of the characteristics of the continuous system.

Two different methods have been used to discretize Eqn. (189) [99]. The first method uses a quadrature rule to approximate the integral in Eqn. (189), that is

$$\int_D K(s_j, t)m(t)dt \approx \sum_{i=1}^{M} w_i K(s_j, t)m(t_i)\triangle(t_i). \tag{190}$$

This discretization results into a rectangular system like

$$b = Ax + \epsilon, \tag{191}$$

where $A_{ji} = w_i K(s_j, t_j)$ and $x = m(t_i)$ which is a vector in $\mathbb{R}^M$. The second method uses discretization by the *Galerkin* methods in which the model m is described by

$$m = \sum_{i=1}^{M} x_i \psi_i(s), \tag{192}$$

where $\psi_i(s)$ for $i = 1, 2, ..., m$ is an orthonormal set of basis functions. The integral in Eqn. (190) can now be written as

$$\int_D K(s_j, t)m(t)dt = \sum_{i=1}^{M} x_i \int_D K(s_j, t)\psi_i(t)dt, \tag{193}$$

which is in the same form as in Eqn. (191), that is $b = Ax + \epsilon$, in which x is a vector of coefficients and

$$A_{ji} = \int_D K(s_j, t)\psi_i(t)dt. \tag{194}$$

The "trade-off" is of importance to think about when selecting discretization methods in computational work; as quadrature methods are easier to implement, the Galerkin method gives more accurate results and requires fewer unknowns to obtain the same accuracy. However, the major issue to think about in this stage is that the matrix A is, as a rule, ill-conditioned and to get rid of ill-conditioning, regularization is needed for the solution of the problem. In the following section, two different methods for regularization are presented. They are the *Tikhonov* regularization and regularization by the *subspace* methods.

Tikhonov Regularization

According to Tikhonov, the problem of finding x as a solution to $b = Ax + \epsilon$ can be substituted by a minimization problem as [99]

$$\min \ \phi(\beta, x) = \|Ax - b\|^2 + \beta\|Wx\|^2,$$

$$\text{Subject to } x$$

where $\phi(\beta, x)$ is called the *global objective function*. In this formulation $\|Ax - b\|^2$ is the *data misfit* and $\|Wx\|^2$ is called the *model objective function*; β is a *penalty parameter* as a parameter that determines how well the solution is fitted with data. By adjusting β, the solution will fit the data in an optimal way. By differentiating the problem in (194) with respect to x and setting the differentiation to zero, a solution will be achieved, that is

$$(A^T A + \beta W^T W)x = A^T b. \tag{195}$$

It is shown that the penalty parameter β is found by solving

$$\|b - Ax(\beta)\|^2 = \|(I - A(A^T A + \beta I)^{-1} A^T)b\|^2, \tag{196}$$

where I is the identity matrix. Inversion or decomposition of the term $(A^T A + \beta I)^{-1}$ is costly in this equation and this constitutes a major challenge in finding the solution. In the context of inverse problems, the *Tikhonov* regularization is used to damp the singular vectors, which are associated with small singular values in the problem, formulated as a singular value decomposition [99]. Referred to Eqn. (196) and with the matrix A decomposed by singular value decomposition as

$$A = U\Sigma V^T, \tag{197}$$

one can find out that

$$(A^TA + \beta I)x = (V\Sigma^2V^T + \beta I)x = V(\Sigma^2 + \beta I)V^Tx = V\Sigma U^Tb. \quad (198)$$

Multiplying both sides in V^T in (198) and by other simplifications, x can be found as

$$x = V\Sigma^{-1}(\Sigma^2 + \beta I)^{-1}\Sigma^2U^Tb. \quad (199)$$

Having (199) in vector form, it can be written as

$$x = \sum_{i=1}^{N} \frac{\lambda_i^2}{\lambda_i^2 + \beta}\frac{b^Tu_i}{\lambda_i}v_i. \quad (200)$$

Introducing a function $f_T(\lambda)$ as

$$f_T(\lambda) = \frac{\lambda^2}{\lambda^2 + \beta}, \quad (201)$$

which is called the *Tikhonov filter function*, Eqn. (200) will be rewritten as

$$x = \sum_{i=1}^{N} f_T(\lambda_i)\frac{b^Tu_i}{\lambda_i}v_i. \quad (202)$$

In fact, the Tikhonov filter function in (201), "filters" the singular vectors which are associated with small singular values [99]. These vectors are in their turn associated with λ^2 which are much smaller than β as the penalty parameter. The Tikhonov regularization is a fundamental process in inverse problems.

Subspace Regularization

For more efficiency, the Tikhonov regularization can be extended by the *Subspace* regularization method. In fact, the Tikhonov regularization solutions require a long time and considerable memory. Any shortcut like discretizing the problem with fewer parameters, leads to an overdetermined system for a solution to $b = Ax + \epsilon$. As a consequence, a coarse discretization will not fit the problem as the solution is forced into a small subspace [99]. The challenge in such context will be to transform the problem into a small appropriate one by choosing a new subspace S_k in the minimization problem of

$$\begin{aligned} &\min \ \|Ax - b\|^2, \\ &\text{Subject to } \ x \in S_k \end{aligned} \quad (203)$$

where $A : R^M \longrightarrow R^N$. Subspace regularization is involved with definition of the $k-$dimensional subspace S_k for $k < N$ such that $S_k = Span(V_k)$. Hence, the original problem of (203) is now converted into an equivalent minimization problem of the least-square system of

$$AV_k z = 0. \tag{204}$$

In fact, a more realistic formulation in this context is to solve a minimization problem of (203) by defining a subspace S_k with $k << N < M$ that leads to a well-posed overdetermined system by choosing a small enough k and a good choice of S_k. There are different methods in which the subspace is chosen such that it is spanned by singular values.

6 Medical Diagnostics and Microwave Tomographic Imaging by Applying Electromagnetic Scattering

The main objective of this section is to investigate biological imaging algorithms by solving the direct, and inverse electromagnetic scattering problem due to a model based illustration technique within the microwave range. A well-suited algorithm will make possible fast parallel processing of the heavy and large numerical calculation of the problem's inverse formulation. The parallelism of the calculations can then be performed and implemented on GPU:s, CPU:s, and FPGA:s. By the aid of mathematical/analytical methods, and thereby faster numerical algorithms, an improvement of the existing algorithms is also expected to be developed. These algorithms may be in time domain, frequency domain, and a combination of both.

There is a potential in the microwave tomographic imaging for providing information about both physiological state and anatomical structure of the human body. By several strong reasons the microwave tomographic imaging is assumed to be tractable in medical diagnostics: the energy in the microwave region is small enough to avoid ionization effects in comparison to X-ray tomography. Furthermore, tissue characteristics such as blood content, blood oxygenation, and blood temperature cannot be differentiated by the density-based X-ray tomography. The microwave tomography can be used instead of determining tissue properties by means of complex dielectric values of tissues. It is shown that the microwave tissue dielectric properties are strongly dependent on physiological condition of the tissue [91]. The dependence of the tissue dielectric properties plays a major roll to open opportunities for microwave imaging technology within medical diagnostics. In such context, the interesting thing to think about is, always, how the old electromagnetic scattering computations can be improved by smarter faster mathematical/numerical algorithms. In addition, there are promising methods providing a good compromise between rapidity and cost why there is a potential interest for microwave imaging in biomedical applications. The area of the research is rather new so that new approaches and new methods are expected to be developed for tomographic imaging.

The inverse electromagnetic scattering should be solved in order to produce a tomographic image of a biological object. In this process, the dielectric properties of the object under test are deduced from the measured scattered field due to the object and a known incident electric field. Nonlinearity relations arise between the scattered field and multiple paths through

the object. Approximations are used to linearize the resulting nonlinear inverse scattering problem. As this problem is ill-posed, the existence and uniqueness of the solution and also its stability should be established [42].

6.1 Direct and Inverse Formulation in Biological Imaging

A two-dimensional prototype microwave tomographic imaging system composed of 64 antennas (a circular antenna array) with the operating frequency in 2450 MHz is considered in [91]. The antennas are located on the perimeter of a cylindrical microwave chamber with an internal diameter of 360 mm which can be filled with various solutions, including deionized water. By separating the antennas into emitters and receivers, the influence of the emitter signal is assumed to be avoided. The sequential radiation from 32 emitters and $16-20$ receiving antennas, is measured. The antennas are used with a narrow radiation pattern in the vertical direction for creating a two-dimensional slice of the three-dimensional object under test (OUT). Special waveguides are also used to get a wider horizontal projection. The amplitude and the phase of the scattered field due to the OUT is also measured. The OUT is located in the media with a constant complex dielectric permittivity. In addition, the magnetic permeability is assumed to be constant everywhere. The dielectric properties of the OUT which is assumed to be an infinite cylindrically symmetric object with volume V is investigated. The situation is finally modeled by the following integral equation [91]

$$\begin{aligned} \frac{j}{k^2-k_0^2} - \int_v Gj dV &= E^i, \quad \text{inside V} \\ \int_v Gj dV &= E^s, \quad \text{outside V} \end{aligned} \tag{205}$$

where

$$k^2 = (\frac{\omega'}{c})^2 \epsilon\mu_0, \quad k_0^2 = (\frac{\omega'}{c})^2 \epsilon_0\mu_0$$

in which

$$\begin{cases} E^i, & \text{Incident field;} \\ E^s, & \text{Scattered field;} \\ G, & \text{Green's function;} \\ j, & \text{Polarization current.} \end{cases}$$

Eqns. (205) describe the OUT with unknown dielectric characteristics ϵ which is illuminated from the circular antenna array; the scattered field is received by the receiving antennas on the same antenna array. As the

ill-posed problem for the inverse system of determining ϵ in Eqns. (205), approximation methods should be chosen. In [91] a modified Rytov's approximation is used. Born approximation is also used for the above inverse problem concerning the objects with high contrast of ϵ. In this case, the Rytov's approximation gives better results. The algorithm in [91] gives an accurate solution of the inverse problem in two-dimensional cases including image reconstruction of a phantom consisted of a semisoft gel cylinder. The gel phantom is immersed into the working chamber after being cooled in a refrigerator. It is shown that the dielectric situation inside the working chamber is affected by the temperature gradients. In addition, the dielectric properties of the phantom are also affected by non-isothermic conditions in the working chamber. Assuming that the frequency range from 2 to 8 GHz gives the most suitable results for microwave imaging [61], there are technical difficulties in building a tomographic system for the whole body concerning the frequency range. One of the reasons is that the acquisition time would be unrealistically long. However, at the lower frequency of about 0.9 GHz suitable spatial resolution is achieved. In summary, the multifrequency range from 0.9 to 3 GHz is optimal for microwave tomographic imaging [91]. In [15], a suitable method for quasi real-time microwave tomography for biomedical applications is presented. By simulating a focusing system characterized by small field depth and a variable focal length, a tomographic process is achieved in this work. The organ under test, which constitutes the scatterer, transforms the divergent wavefront from the focusing system into a convergent wavefront. An image, corresponding to a thin organ slice, from the divergent wavefront can be derived. By changing the focal length, different slices can be obtained resulting into a cross-section of the organ. From the measured field distribution, the slice images are deduced. Letting d and D be the length of the organ and the distance between the observation line and the slice, respectively, the length of the observation domain will be $2D + d$. The equivalent currents $\mathbf{J}$, responsible for the scattered field is [15]

$$\mathbf{J}(x, y) = (k^2(x, y) - k_m^2)\mathbf{E}_t(x, y), \tag{206}$$

where $\mathbf{E}_t(x, y)$ and $k(x, y)$ are the total field and the wavenumber inside the organ, respectively; k_m is the wavenumber of the homogeneous surrounding medium. For cylindrical objects, illuminated by a plane wave, the scattered field $\mathbf{E}_S$ is determined by [15]

$$\mathbf{E}_S(x, y) = \int_S \mathbf{J}(x, y) H_0^{(2)} \left(k_m \sqrt{(x - x')^2 + (y - y')^2} \right) dx' dy', \tag{207}$$

where $H_0^{(2)}$ is the Hankel function of order zero and of the second kind. For both two-dimensional and the three-dimensional cases, such algorithms can be used to reconstruct $\mathbf{J}$ from the scattered field $\mathbf{E}_S$. Here, the reconstructed current is the image which appears as the convolution between the point-spread function of the focusing system and the induced current distribution in the organ. The *method of angular spectrum* may be used for reconstruction of the current distribution from the scattered field [72, 94].

6.2 Complex Permittivity of a Lossy Dielectric Medium

Assuming the total electric field I flowing through an arbitrary surface S, one can write [88]

$$I = \int_S \mathbf{J} \cdot d\mathbf{s}, \tag{208}$$

where $\mathbf{J}$ is current density in amperes per square meter. The current density $\mathbf{J}$ is, in its turn, defined as

$$I = Nq\mathbf{u}, \tag{209}$$

where q is electric charge, $\mathbf{u}$ the velocity of the electric charge and N, number of charge carriers per unit volume. The product Nq is free charge per unit volume. In the case of conduction currents possessing more than one kind of charge carriers (electrons, ions and holes) with different velocities, Eqn. (209) should be written as

$$\mathbf{J} = \sum_i N_i q_i \mathbf{u}_i, \tag{210}$$

for $i = 1, 2, ..., M$ and $M \in \mathrm{N}$. For most conducting materials, the average velocity is directly proportional to the applied electric field intensity $\mathbf{E}$. For metallic conductors

$$\mathbf{u_e} = -\mu_e \mathbf{E}, \tag{211}$$

where μ_e is the electron mobility in $m^2/V \cdot s$. Combining Eqns. (209) and (211) yields

$$\mathbf{J} = -\rho_e \mu_e \mathbf{E}, \tag{212}$$

where $\rho_e = -Ne$ is the charge density for drifting charges (electrons) which is denoted by e. Eqn. (212) can now be written as

$$\mathbf{J} = -\sigma \mathbf{E}, \tag{213}$$

where σ is called conductivity. Eqn. (213) is called the *point form of Ohm's law.*

For semiconductors, conductivity is dependent on the concentration and mobility of both electrons and holes, that is [24]

$$\sigma = -\rho_e \mu_e + \rho_h \mu_h, \tag{214}$$

where the subscript h denotes hole. Assume now a lossy medium, defined as an imperfect conductor or imperfect dielectric with $\sigma \neq 0$, distinguished from a perfect dielectric with $\sigma = 0$; a lossy medium is also defined as a medium in which electromagnetic wave loses power as it propagates due to poor conduction. In addition, a dielectric is [88]:

- linear, if the permittivity ϵ does not change with an applied $\mathbf{E}$ field,
- homogeneous, if ϵ does not change from point to point and
- isotropic if ϵ does not change with direction.

Consider now a linear, homogeneous, isotropic, lossy dielectric medium which is charge free ($\rho_v = 0$). For so-called time-harmonic fields, Maxwell's curl equations become

$$\nabla \times \mathbf{E} = -j\omega \mathbf{H}, \tag{215}$$

and

$$\nabla \times \mathbf{H} = (\sigma + j\omega)\mathbf{E}. \tag{216}$$

where $\omega = 2\pi f$ is the angular frequency (rad/s), f being the frequency in hertz. By time-harmonic fields, the time factor $e^{j\omega t}$ is suppressed. From Eqn. (216):

$$\nabla \times \mathbf{H} = j\omega(1 - \frac{j\sigma}{\omega\epsilon})\mathbf{E} = j\omega\epsilon_c \mathbf{E}, \tag{217}$$

where

$$\epsilon_c = \epsilon(1 - j\frac{\sigma}{\omega\epsilon}),, \tag{218}$$

or

$$\epsilon_c = \epsilon' - j\epsilon'',, \tag{219}$$

and $\epsilon' = \epsilon$, $\epsilon'' = \sigma\omega$; the new variable, ϵ_c is called *complex permittivity* of the medium.

6.3 Direct Methods in Biological Imaging

For the direct electromagnetic formulation, a classical approach considering a 2D version of the problem may be used as an alternative. A 3D version of the problem would otherwise be to describe the field properties using

the Maxwell's equations which leads to a heavy 3D vectorial problem. In the 2D formulation, the biological object under test is considered to be nonmagnetic with constant dielectric properties along its vertical axis. The whole strategy in this approach is to convert the electromagnetic scattering problem into a radiating problem in the free space and a, so called, 2D scalar Electrical Field Integral Equation (EFIE). The implicit time dependence of $e^{-j\omega t}$, with ω as the radial frequency is also introduced. The homogeneous and inhomogeneous wave equations in this context are [42]

$$(\nabla^2 + k_1^2)E^i(\mathbf{r}) = 0, \tag{220}$$

and

$$(\nabla^2 + k^2(\mathbf{r}))E(\mathbf{r}) = 0, \tag{221}$$

respectively. Here, $E^i(\mathbf{r})$, as the incident field, is the propagation of a TM-polarized, single-frequency, time-harmonic electromagnetic wave, see Fig. 15; the total electric field is denoted by $E(\mathbf{r})$. The constant wavenumber k_1 inside the homogeneous media, and the wavenumber k are respectively as

$$k_1 = \omega\sqrt{\mu_0\epsilon_1^*}, \tag{222}$$

and

$$k^2(\mathbf{r}) = \omega^2\mu_0\epsilon^*(\mathbf{r}), \tag{223}$$

where ϵ_1^* is the complex permittivity inside the homogeneous media, and $\epsilon^*(\mathbf{r})$ the complex permittivity of the inhomogeneous region. For the two-dimensional mathematical formulation it is assumed that the OUT with the complex dielectric permittivity is not dependent on the z coordinate in the media, see Fig. 15 The total field, $E(\mathbf{r})$, as a superposition of the incident field and the scattered field $E^s(\mathbf{r})$ can be written as

$$E(\mathbf{r}) = E^i(\mathbf{r}) + E^s(\mathbf{r}). \tag{224}$$

Introducing a new constant $C(\mathbf{r})$ as

$$C(\mathbf{r}) = k^2(\mathbf{r}) + k_1^2 \tag{225}$$

together with the above equations will result into the following wave equation

$$(\nabla^2 + k_1^2)E^s(\mathbf{r}) = -C(\mathbf{r})E(\mathbf{r}). \tag{226}$$

Associated with the scattered field $E^s(\mathbf{r})$ in Eqn. (226), an equivalent current $J(\mathbf{r})$ can be defined as

$$J(\mathbf{r}) = C(\mathbf{r})E(\mathbf{r}). \tag{227}$$

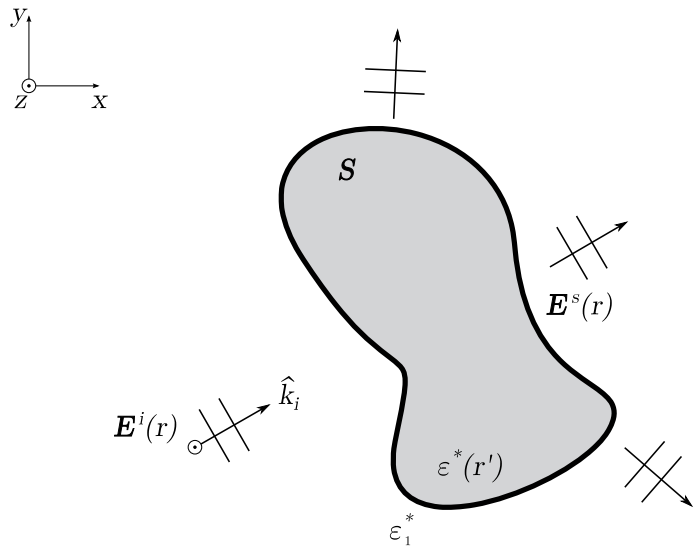

Figure 15: Two-dimensional visualization of the object under test to measure the complex dielectric permittivity.

In fact, this equivalent current produces the scattered field and the wave equation above can now be written as [42]

$$(\nabla^2 + k_1^2)E^s(\mathbf{r}) = -J(\mathbf{r}). \tag{228}$$

A Green's function formulation for the inhomogeneous wave equation in (228) can be deduced to solve $E^s(\mathbf{r})$, that is

$$(\nabla^2 + k_1^2)G(\mathbf{r}, \mathbf{r}') = -\delta(\mathbf{r} - \mathbf{r}'), \tag{229}$$

where $\delta(\mathbf{r} - \mathbf{r}')$ is the Dirac delta function; the associated Green's function is

$$G(\mathbf{r}, \mathbf{r}') = \frac{j}{H_0^{(1)}}(k_1|\mathbf{r} - \mathbf{r}'|), \tag{230}$$

where $H_0^{(1)}$ is, as previously mentioned, the zero-order Hankel function of the first kind. By the aid of the Green's function formulation above, and the principle of superposition, the scattering field can be obtained by

$$E^s(\mathbf{r}) = \int\int_S G(\mathbf{r}, \mathbf{r}')C(\mathbf{r}')E(\mathbf{r}')d\mathbf{r}'. \tag{231}$$

Considering (224) and (231), the total field is finally expressed as the following integral formulation [42]:

$$E(\mathbf{r}) = E^i(\mathbf{r}) + \int\int_S G(\mathbf{r}, \mathbf{r}')C(\mathbf{r}')E(\mathbf{r}')d\mathbf{r}'. \tag{232}$$

Since the complex permittivity is known and the incident field $E^i(\mathbf{r})$ is given, the scattered field $E^s(\mathbf{r})$ will be computed as the direct formulation of the electromagnetic scattering problem. In such context, Eqns. (231) and (232) can be solved, for example, by the method of moments (MoM), see previous chapters. Using this numerical method, two different two-dimensional configurations, by planar or cylindrical situated dipoles, are solved in [42]. Assuming constant fields and dielectric properties in a rectangular cell as the OUT, the incident and the scattered field will be discretized as

$$E^i(\mathbf{r_n}) = \sum_{j=1}^{N}(\delta_{nj} - G(\mathbf{r_n}, \mathbf{r_j})C(\mathbf{r_j}))E(\mathbf{r_j}), \quad n = 1, 2, ..., N, \tag{233}$$

and

$$E^s(\mathbf{r_m}) = \sum_{j=1}^{M}(\delta_{nj} - G(\mathbf{r_m}, \mathbf{r_j})C(\mathbf{r_j}))E(\mathbf{r_j}), \quad m = 1, 2, ..., M, \tag{234}$$

where the region, i.e., the OUT, is discretized into N cells and also M receiving points for the observed scattered field; the Green's function G can be computed analytically as depicted in [29]. Numerical solution of this direct scattering problem will be used for creating image reconstruction algorithms for the inverse problem using which the unknown permittivity contrast distribution of the OUT will be found. Concerning biological image reconstruction by microwave methods, there are different approaches which are generally based on either *radar techniques* or *tomographic formulation* [60, 16, 17].

7 Numerical Results and Conclusions

7.1 Current Distribution along the Horizontal Dipole Antenna above Real Ground

In the case of a thin horizontal dipole antenna (HDA) above lossy half-space (LHS) of known electrical parameters, thorough analysis is performed. The approach is based on the electric-field integral equation method, and formulation of the Hallén's integral equation (HIE), [10]. This equation is then solved for the current, which is assumed in a polynomial form Popović[73], using the point-matching method (PMM) [10]. This way obtained system of linear equations involves improper Sommerfeld's integrals, which express the influence of the real ground, and are here solved approximately using simple, so-called OIA and TIA, approximations (Rančić and Rančić[76, 77], Rančić and Aleksić[78, 80], Rančić[79]). Both types of approximations are in an exponential form, and therefore, are similar to those obtained applying the Method of Images. Approximate method for the analysis of horizontal dipole antenna has been applied for the purpose of the current distribution and input admittance evaluation for the HDA positioned in the air at arbitrary height above LHS, which is considered a homogenous medium. This analysis is focused on validation of the applied method for the cases of interest in the EMC studies. The analysis has been performed in a wide frequency range, and for different positions of the antenna, as well as for various values of the LHS's conductivity. It has been proven, based on the comparison with the exact model from Arnautovski-Toseva *et al.*[8, 7], that the methodology used here yields very accurate results in the observed parameters' ranges. This indicates a possibility of applying this method for analysis of different wire structures in the air above LHS, and more importantly, very close to the ground where the finite conductivity's influence is the greatest. Thorough analysis is performed in order to observe the influence of different parameters of the geometry, and the ground, on current distribution and the input impedance/admittance of the HDA. Furthermore, the verification of the method is done by comparison to the exact model based on the full-wave theory (Arnautovski-Toseva *et al.*[8, 7]), and experimental data from Nicol and Ridd[69]. Obtained results indicate a possibility of applying the described methodology to inverse problems involving evaluation of electrical parameters of the ground (or detection of ground type change) based on measured input antenna impedance/admittance.

Described numerical procedure is applied to near-field analysis of the

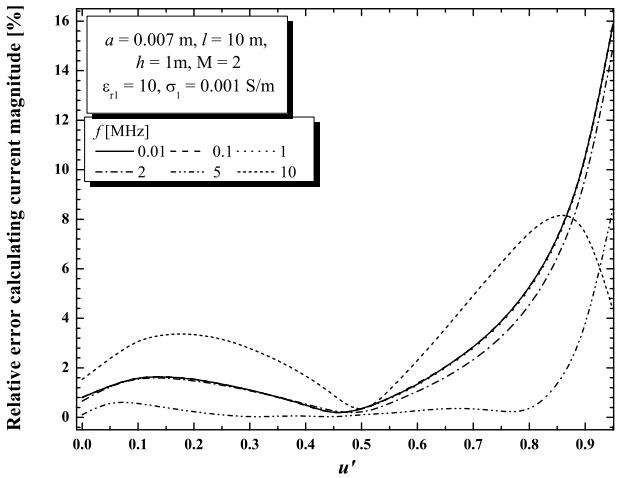

Figure 16: Relative error of the current magnitude along the HDA arm.

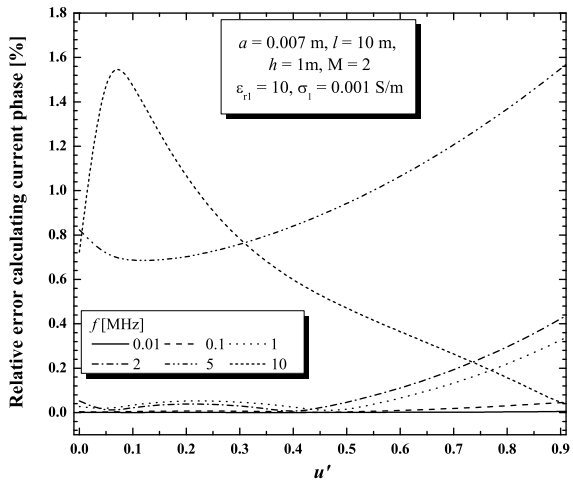

Figure 17: Relative error of the current phase along the HDA arm.

symmetrical HDA fed by an ideal voltage generator of voltage U.

Firstly, results of the relative error of current distribution calculation are given in Figs. 16 and 17. The conductor is $2l = 20$ m long with the cross-section radius of $a = 0.007$ m, and it is placed at $h = 1.0$ m above

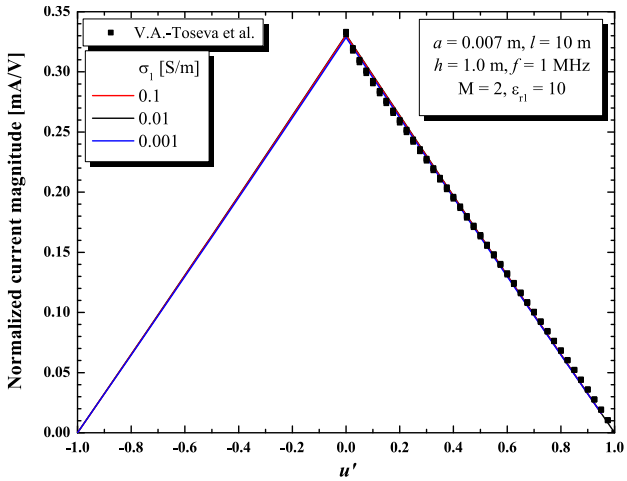

Figure 18: Relative error of the current magnitude along the HDA for different ground conductivities.

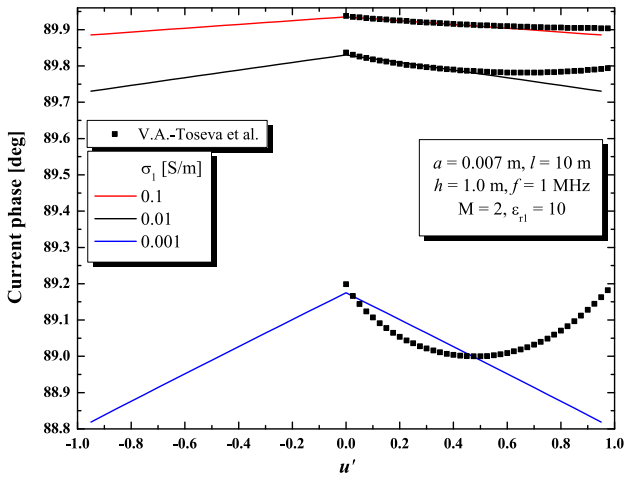

Figure 19: Relative error of the current phase along the HDA for different ground conductivities.

lossy ground with electrical permittivity $\epsilon_{r1} = 10$. In this case, the variable parameter is the frequency that takes values from a wide range (10 kHz to 10 MHz). The relative error is shown separately for the current magnitude

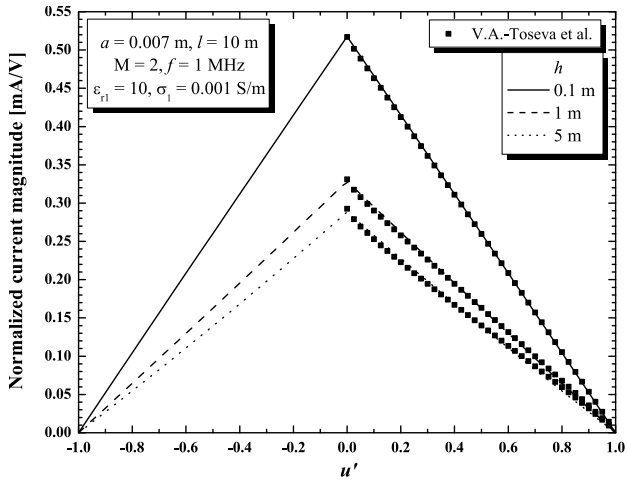

Figure 20: Relative error of the current magnitude along the HDA above LHS at different heights.

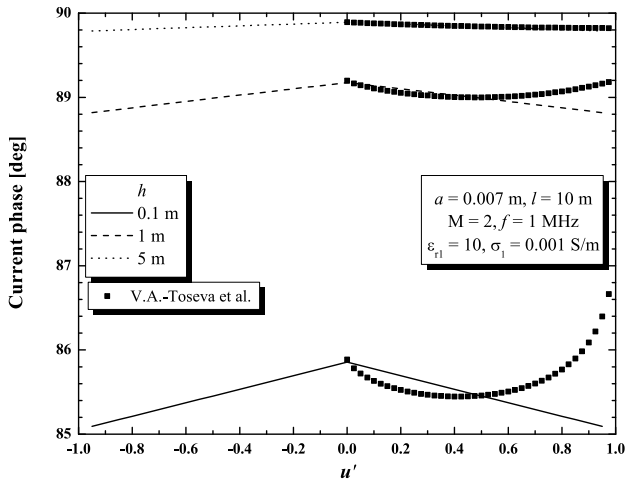

Figure 21: Relative error of the current phase along the HDA above LHS at different heights.

and phase along the HDA arm for the case of the specific conductivity of $\sigma_1 = 0.001$ S/m. As a reference set of data, those from Arnautovski-Toseva

et al.[8, 7] are taken.

Current distribution's magnitude and phase at 1 MHz, can be observed from Figs. 18 and 19. The HDA has the same dimensions as previously, and it is placed at $h = 1.0$ m above lossy ground with electrical permittivity $\epsilon_{r1} = 10$. The value of the specific conductivity has been taken as a parameter: $\sigma_1 = 0.001, 0.01, 0.1$ S/m. Comparison has been done with the results from Arnautovski-Toseva *et al.*[8, 7].

Further, the influence of the conductor's position on the current distribution has been analyzed. The results are graphically illustrated in Figs. 20 and 21 together with the ones from Arnautovski-Toseva *et al.*[8, 7]. Three cases were observed that correspond to heights $h = 0.1, 1.0, 5.0$ m. The current has been calculated at frequency of 1 MHz, and analysis has been done for the following values of the specific ground conductivity: $\sigma_1 = 0.001, 0.01, 0.1$ S/m. HDA dimensions are the same as previously. Next ex-

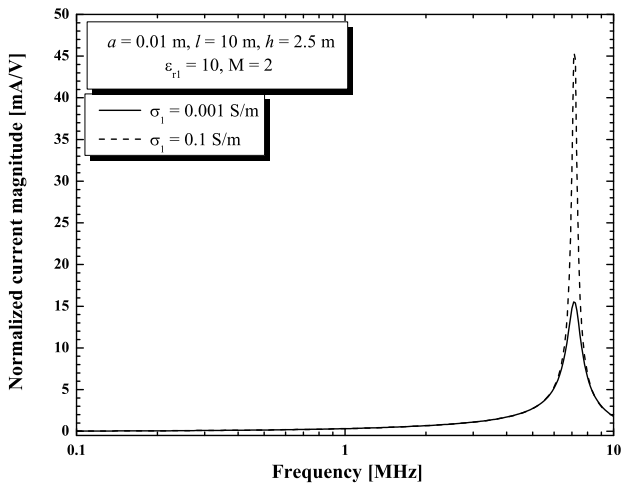

Figure 22: HDA current magnitude at point A for different ground conductivities.

ample explores the dependence of the current (its magnitude and phase) on different ground conductivities calculated at the feeding point A($l = 0$ m), which can be observed from Figs. 22 and 23. Two cases are considered: solid line represents the value of $\sigma_1 = 0.001$ S/m, and the dashed one corresponds to $\sigma_1 = 0.1$ S/m. Fig. 22 corresponds to HDA height of $h = 2.5$ m, and Fig. 23 to $h = 5.0$ m. The same influence for height $h = 0.5$ m is given in Rančić and Aleksić[80].

Similarly, the dependence of the current (its magnitude and phase) at

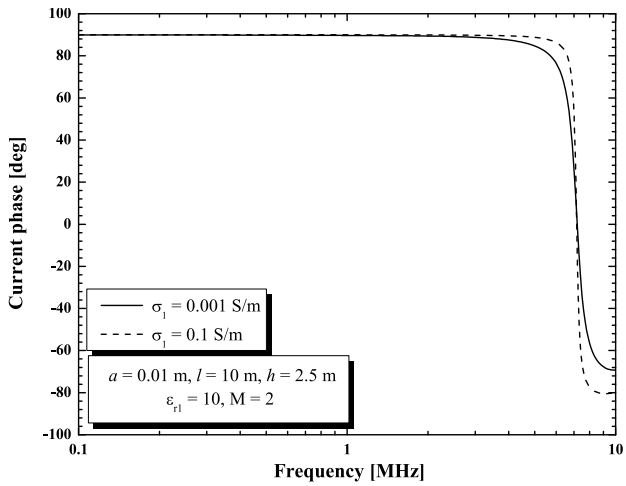

Figure 23: HDA current phase at point A for different ground conductivities.

specific points along the HDA arm in the frequency range from 10 kHz to 10 MHz, is presented in Figs. 24 and 25. The antenna is $2l = 20$ m long with a cross-section radius of $a = 0.01$ m, and considered heights are: $h = 0.5, 2.5, 5.0$ m. Electrical parameters' values of the ground are: electrical permittivity $\epsilon_{r1} = 10$, and specific conductivity $\sigma_1 = 0.1$ S/m. Current is calculated at points: A($l = 0$ m), B($l = 2.5$ m), C($l = 5.0$ m), and D($l = 7.5$ m). This example for $\sigma_1 = 0.001$ S/m and $h = 0.5$ m is given in Rančić and Aleksić[80].

Finally, Figs. 26 and 27 show comparison between theoretical calculations and the results of the admittance measurements for the frequency range of $7 - 12$ MHz (Nicol and Ridd[69]). Observed HDA is 15 m long suspended at height of 0.3 m above the LHS. Two boundary cases of the ground are observed: a perfect dielectric (blue data), and a highly conducting plane (black data). Corresponding results obtained by the Method of Images are also shown (open circles). It can be observed that the better accordance is achieved using the method described here, which was expected since the observed antenna is very close to the ground (for the frequency of 10 MHz, height of 0.3 m corresponds to $0.01\lambda_0$), and the accuracy of the Method of Images decreases when the antenna is at height less than $h/\lambda_0 = 0.025$ (Popović and Petrović[75]).

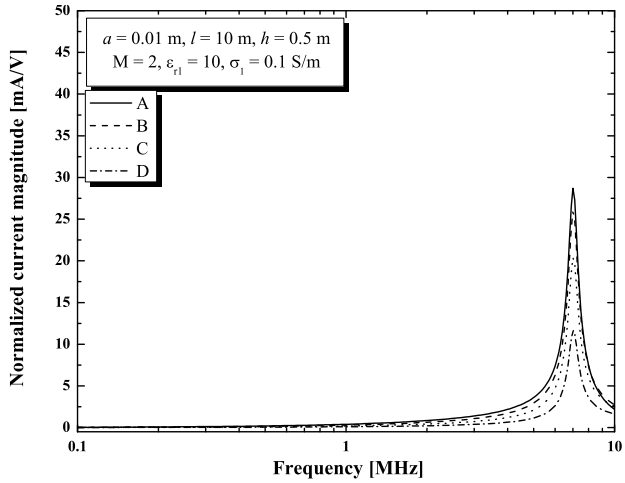

Figure 24: HDA current magnitude at different points along the antenna.

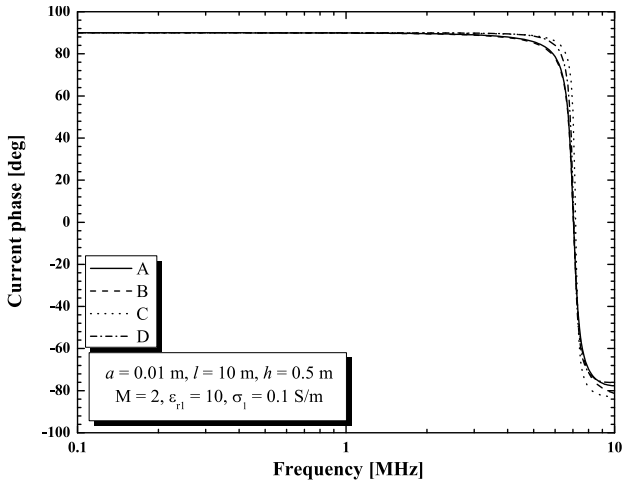

Figure 25: HDA current phase at different points along the antenna.

7.2 Semi-Norm Analysis for the FDTD Algorithm

To determine the order of convergence in the 2D-FDTD algorithm, an error analysis is used. Let P be an observation point in the 2D-FDTD domain. This point is symbolized as $\bigotimes$ in Fig. 28.

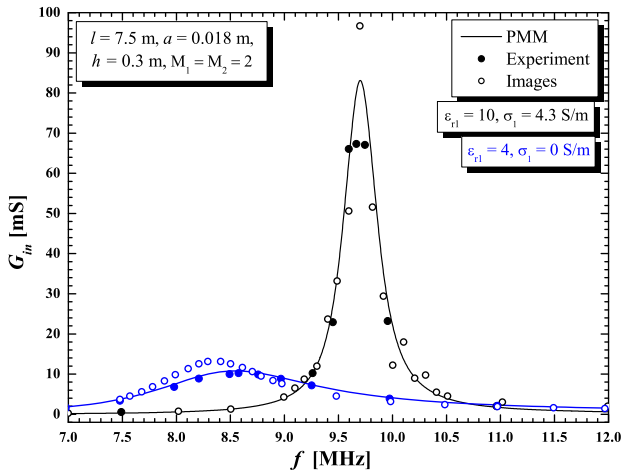

Figure 26: HDA input conductance versus frequency.

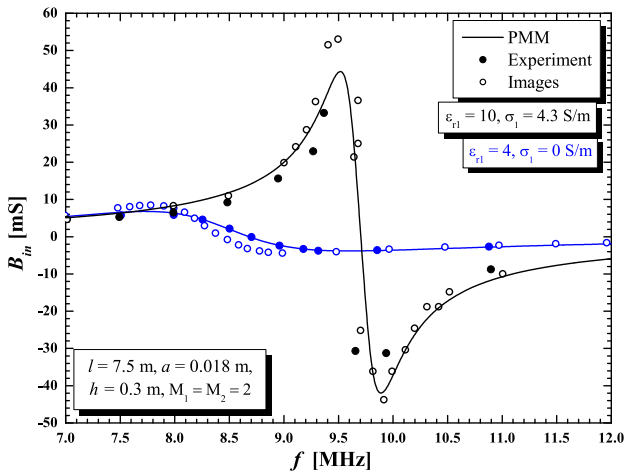

Figure 27: HDA input susceptance versus frequency.

A good way to visualize errors when they are expected to behave like some power of the spatial discretization, is to write the error ϵ as [59]

$$\epsilon(h) \approx C\,(h)^k\,, \tag{235}$$

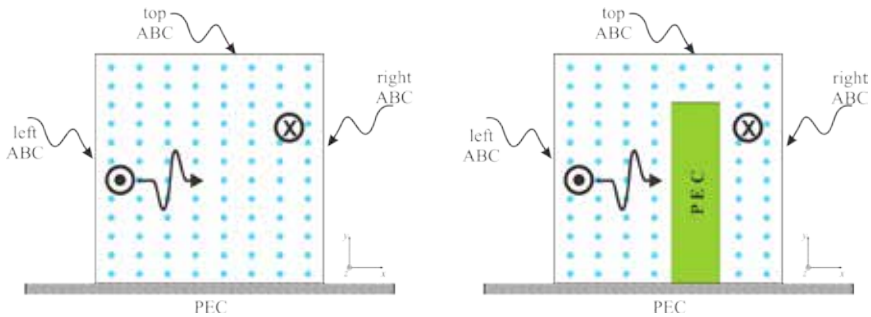

Figure 28: Absorbing boundary condition in form of MUR1 for the 2D-FDTD in two cases: without (left), or with (right) a PEC obstacle.

where h is the cell size and C is a constant independent of h. The linear equation of $\eta = k\xi + m$ was built to determine the real constants k and C. In this analysis, k constitutes the order of spatial convergence in the 2D-FDTD algorithm. In this linear equation $\eta = \ln\left(|||u_h - u_{\frac{h}{2}}|||\right)$, $m = \ln(C)$, and $\xi = \ln(h)$. Based on computer implementation, numerical values for ξ and η can, in vector form, be written as

$$\xi = \ln(h) = [-3.4012 \ -4.0943 \ -4.7875 \ -5.4806]\,, \tag{236}$$

$$\eta = \ln\left(|||u_h - u_{\frac{h}{2}}|||\right) = [-3.2597 \ -4.6670 \ -6.0616 \ -7.4570]\,. \tag{237}$$

The next step in determining the order of convergence k in the 2D-FDTD algorithm, is to choose a constant value for the time-step Δt equal to $4ns$. To find the order of the spatial convergence k, in a least-squares sense, the two vectors in (236) and (237) should be fitted. As a result, the polynomial coefficients for the linear equation of $\eta = k\xi + m$ will be determined as $k = 2.0178$ and $m = 3.5997$, respectively. This verifies that the 2D-FDTD algorithm is point-wise convergent by the order of 2 in the spatial discretization.

7.3 GPU Parallelism of the 2D-FDTD Algorithm

In order to speedup the simulation process of the 2D electromagnetic problem by the FDTD method, parallelism was used. The problem to be solved was resembling so-called Breast Phantom in biological applications [42]. Computer simulations, based on theoretical analysis, confirm stability and convergence of the 2D-FDTD algorithm, implemented by CPUs and GPUs.

Discretization/meter	Octave	C	CUDA
30	40.83	1.37	1.63
60	44.53	5.25	1.68
120	63.03	20.26	2.23
240	127.17	79.50	4.75
480	899.91	317.76	15.30
960	3779.71	1322.28	55.84

Table 1: Simulation time per second for the Octave, C, and CUDA implementations for different discretization levels

Discretization/meter	C	CUDA
30	29.74	25.05
60	8.49	26.58
120	3.11	28.26
240	1.60	26.80
480	2.83	58.83
960	2.85	67.69

Table 2: Speedups by the C and CUDA implementations compared to the implementation in Octave

Although CPUs were easy to program, it was shown that they didn't offer much in the parallelism process due to the FDTD algorithm. FPGAs, on the contrary, offered high performance parallelism but the implementation was complicated. On the other hand, FPGAs are not generally as accessible as either GPUs or CPUs. These were two reasons to exclude parallelism by FPGAs. In this thesis, the first parallelism performance aspect was based on the elapsed time for implementations in Octave, C, and CUDA. This is depicted in Table 1. The second aspect was the speedup factor for these three different implementation environments. This is depicted in Table 2, where the speedup factor for C and Octave is compared to the Octave's implementation. Finally, the third aspect of performance in this work is with respect to implementation quality when the discretization level is increasing. As it is shown in Table 3, in this kind of performance analysis, the number of computed cells per second is measured with respect to increasing discretization level. The efficiency level of the C implementation stay almost still for different discretization levels while the CUDA's implementation performance grows prominently, see Table 3. The computing performance grows

Discretization/meter	Octave	C	CUDA
30	2.24	65.55	22.22
60	8.10	68.68	214.93
120	22.85	71.10	645.74
240	45.29	72.45	1213.10
480	25.60	72.51	1506.18
960	24.38	69.70	1650.43

Table 3: Millions of cells computed per second for different discretization level implemented in Octave, C, and CUDA

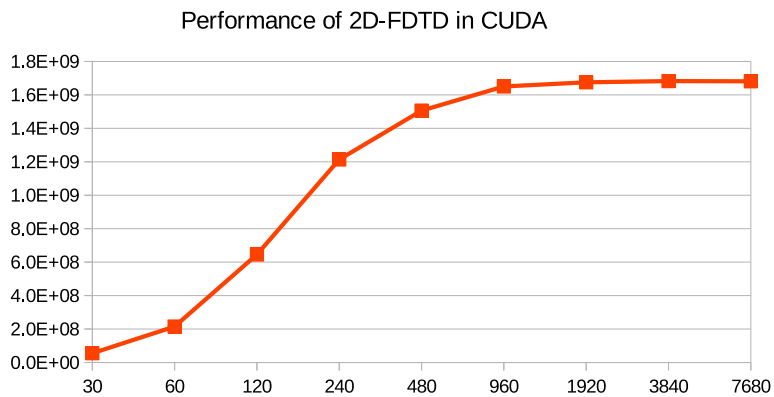

Figure 29: Efficiency of the CUDA implementation for different levels of discretization (horizontal axis) vs number of cells computed per second (vertical axis).

from 22 millions cells per second to about 1650 millions cells per second for different discretization levels. Although efficiency of the C implementation is significantly higher than that of the Octave's, the CUDA's implementation is strikingly more efficient. However, for greater levels of discretization, computations implemented in CUDA are shown to stay around 1680 millions cells per second, see Fig. 29. Validation of the FDTD solution of the electromagnetic scattering problem was based on a semi-norm analysis in the previous section and in [66]. Accordingly, this value should converge to 2. As a matter of fact, it was shown that the order of convergence in the parallelized implementation of the FDTD code was, as well, very close to 2.

7.4 Antenna Analysis Applying the PEEC Method

Test Object: Orthogonal $\frac{\lambda}{2}$ Dipole

For implementation of the Grid-PEEC, a test environment was provided in which the test was preformed with different numbers of executors (1, 2, 6, 12 and 20). All of the executors were running on Dell Optiplex GX260, P4-2.0 GHz, 640 Mb RAM, and Gigabit network card. The manager was run on an IBM Thinkpad R50p with a 1.5 GHz Centrino, 512 Mb RAM, and a 100 Mbit/s network card. The executors where all located in the same computer lab and the manager in a nearby office. The bandwidth of the network between the two rooms is 100 Mbit/s. The Grid-PEEC program was run on the same computer as the manager. This section shows the results for a $\frac{\lambda}{2}$ dipole discretized using orthogonal cells thus enabling the usage of analytic calculation routines for partial elements. These computations are performed in approximately μs and therefore no speed up can be expected du to the slow connection of computers on the grid. Consider the results for the calculation of partial elements as shown in Fig. 30. It is clear that grid computations are not suitable for these type of structures.

Test object: Nonorthogonal Transmission Line

This section present results for a simple nonorthogonal transmission line (TL). The test object is generic in the sense that another object discretized in the same manner would give the same speed up. The TL is differential fed with a unitary current source and the near- and far- end is terminated using 50 Ω resistances.The TL is discretized using 200 nodes and the near- and far- end responses are calculated. The structure requires the calculation of

- 200 self and 19 900 mutual coefficients of potentials (cops) using a 5-5-1 Gauss-Legendre quadrature rule and
- 198 self and 19 503 mutual partial inductances using a 5-5-2 Gauss-Legendre quadrature rule.

The old code calculated the cops in 10 seconds and the partial inductances in 320 seconds. The grid-PEEC calculation times for the partial elements are shown in Fig. 31 for an increasing number of executors. It is clear that the partial element calculation time is not improved by the grid-PEEC application.

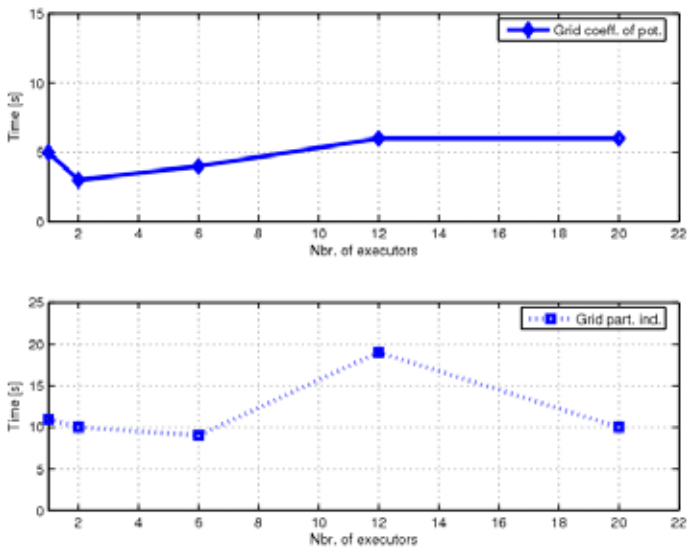

Figure 30: Calculation time for orthogonal partial elements when increasing the number of executors, (top) coefficients of potentials and (bottom) partial inductances.

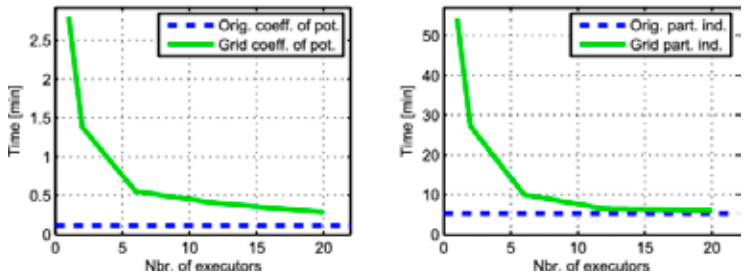

Figure 31: Speed up when increasing the number of executors. (Left) shows the lack of speed up for calculating coefficients of potentials while (right) shows the lack of speed up for calculating partial inductances.

Solution of Frequency Domain System

The frequency sweep is performed from 1 MHz to 10 GHz using 1 000 points. The old code performed the 1 000 calculations (solutions) in 65 minutes on the manager computer (IBM-R50). The grid-PEEC execution time for the frequency sweep is shown in Fig. 32 (left) for an increasing number of executors. From the figure, it is clear that the frequency sweep time is

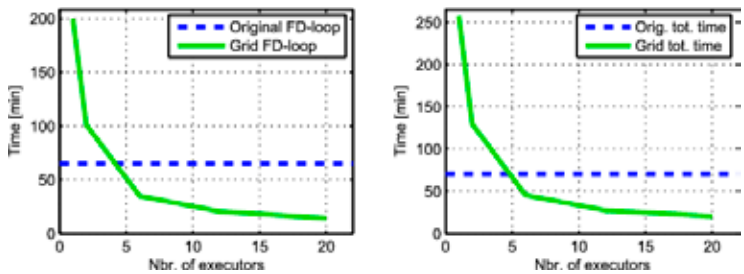

Figure 32: Speed up when increasing the number of executors. (Left) shows the speed up for the repeated frequency domain solution while (right) shows the speed up for the total grid-PEEC solver.

clearly improved by the grid-PEEC application. However, five executors are required to improve the calculations, and by using 20 executors the time is reduced by 78%.

Total Solution Time

Even if the grid code does not speed up the partial element calculations, as seen in Fig. 31, the overall solution time is improved due to the dominance of the solution time for the frequency domain circuit equations which are clearly improved.

7.5 The PEEC Method and CIM

This section gives two examples for PEEC models utilizing the theory described in previous sections.

$\frac{\lambda}{2}$Dipoles

The first example is a horizontal, thin wire dipole of length 50 mm and radius 0.01 μm, located above a PEC-plane as studied in [1]. For numerical

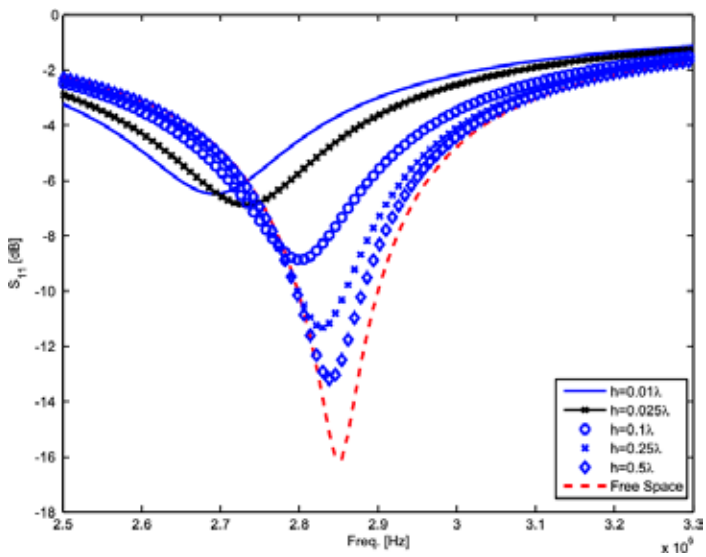

Figure 33: Resonance frequency results for a $\frac{\lambda}{2}$dipole above a PEC plane modeled using a combination of PEEC and IM.

modeling, a PEEC-based solver utilizing the modified computation of the partial elements to account for a PEC plane at $z = 0$ is used. Fig. 33 shows the computed driving point impedance of the dipole at various heights above the PEC-plane which compares well with the results from [1]. Fig. 34 shows

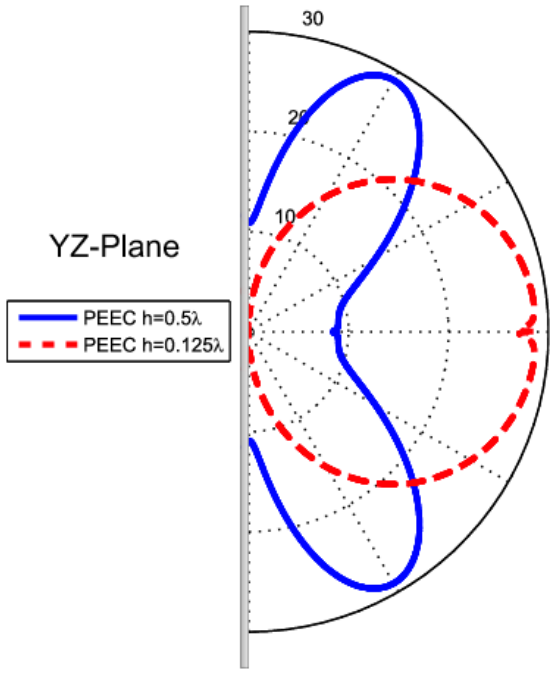

Figure 34: Electric field for different heights above a PEC-plane for a $\frac{\lambda}{2}$dipole modeled using a combination of PEEC and CIM.

the computed electric field strengths for two different heights above the PEC-plane. These results compare well with results from [10].

Dual-Band Antenna (PIFA)

The second numerical example is the dual-band, PIFA (Planar Inverted F Antenna), studied in [63]. The antenna consists of two interconnected, by an LC-trap, antenna elements (20 × 10 mm and 10 × 10 mm) above a PEC-plane. Using the traditional PEEC method, the antenna can be studied by modeling the PEC-plane. However, here we show the results obtained by using the theory from above compared to a free-space situation (no PEC-plane). The PIFA-antenna is designed to have resonance frequencies around 900 and 1 800 MHz depending on the LC-trap. Using one of the suggested L-C-combinations in [63], the Image-PEEC solver gives the result presented in Fig. 35. The resonance frequencies are 1 000 and 1 750 MHz without

altering the L-C-combination which has to be considered well in comparison with the published results.

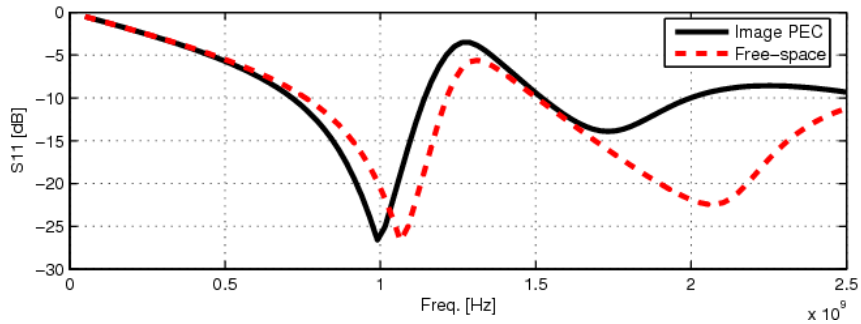

(a)

Figure 35: Resonance frequencies for a dual-band antenna (PIFA) above a PEC plane.

Z-Section Test

Based on the coupled formulation of the PEEC method and the CIM, a so-called Z-section test was done where the system was consisted of two rails, a ground plane, and a discontinuity, see Fig. 36. The computational time was considerably reduced by approximating the ground effects and the reduced number of unknowns, in comparison to the case where the ground were gridded. Some of the case studies showed computational speed ups for

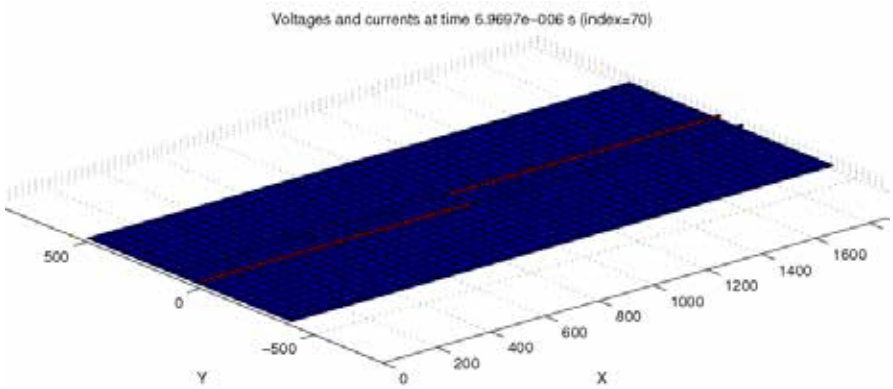

Figure 36: Voltages and currents in a Z-section test.

EM problems containing large ground planes where the PEEC method and the CIM were applied. These results are as follows:

- In the case of the PIFA test from paper A, the frequency domain, quasi-static solution by 100 steps and gridded ground plane resulted into 585 + 322 unknowns. This was solved by regular PEEC in 1 minute, 44 seconds. Removed ground plane resulted into 155 + 91 unknowns by the solution time of 3 seconds.

- In the case of the Z-section test, mentioned in Chapter 4, the frequency domain, quasi-static solution by 100 steps and gridded ground plane resulted in 2270 + 1275 unknowns. This was solved by the regular PEEC in 56 minutes. Removed ground plane resulted in 200 + 204 unknowns. This was solved in 5 seconds.

It should be mentioned that the speed ups were strongly application dependent.

8 Summaries of the Papers

The thesis includes six papers, namely, paper **A**: "Antenna analysis using PEEC and the complex image methods" (Monsefi, Ekman, 2006a); paper **B**: "Optimization of PEEC based electromagnetic modeling code using grid computing" (Ekman, Monsefi, 2006b); paper **C**: "Sommerfeld's integrals and Hallén's integral equation in data analysis for horizontal dipole antenna above real ground" (Monsefi, Rančić, Aleksić, Silvestrov, 2014a); paper **D**: "HF analysis of thin horizontal central-fed conductor above lossy homogeneous soil" (Monsefi, Rančić, Aleksić, Silvestrov, 2014b); paper **E**: "Analysis of shielded coupled microstrip line with partial dielectric support" (Perić, Ilić, Aleksić, Raičević, Monsefi, Rančić, Silvestrov, 2014c); paper **F**: "Solution of 2D electromagnetic scattering problem by FDTD with optimal step size, based on a discrete norm analysis" (Monsefi, Carlsson, Rančić, Otterskog, Silvestrov, 2014d). **G**: "GPU Implementation of a Biological Electromagnetic Scattering Problem by FDTD. Submitted to *Proceedings of 16th ASMDA Conference, 30 June - 4 July 2015, Piraeus, Greece.* (Monsefi, Carlsson, England, Otterskog, Rančić, Carlsson, Silvestrov, 2015a).

8.1 Paper A

The partial element equivalent circuit (PEEC) method has been developed from VLSI inductance calculations in the early 70s. The method is still evolving and new application areas are continuously reported. In this paper we show how the PEEC method is utilized to model antenna characteristics by the use of the appropriate Green's functions. By applying the complex image methods due to a layered medium, the potential, generated by a source, will be the same as the sum of potentials by a combination of the source itself and image sources including both real and image locations. Calculated and analytical results are compared for dipoles while more complex antenna designs are compared with published results by other researchers. Fast and accurate results encourage for further work.

8.2 Paper B

This paper deals with the optimization of an existing frequency domain, nonorthogonal partial element equivalent circuit based electromagnetic analysis code using the freeware Alchemi toolkit in a Windows environment. The purpose is to speed up both the calculation of the nonorthogonal partial elements and the solution of the frequency domain systems. The technology

with this type of heterogeneous grid computing was shown to be very young and extensive work, including the construction of a linear algebra library, was required to enable satisfactory results.

8.3 Paper C

Increase of the radiation power in different frequency bands during the last decades, has called for a study of harmful effects on the living organisms and electronic equipment of the radio frequency energy. An accurate determination of the near field strength, electric as well as magnetic, in the vicinity of higher-power transmitting antennas is necessary for assessing any possible radiation hazard. In that sense, it is of great importance to account for the influence of the finite ground conductivity on the electromagnetic field structure in the surroundings of these emitters. The estimation of this influence has been intensively studied, and a number of approaches has been applied in that sense, ranging from the exact full-wave based ones to different forms of approximate, less time-consuming, ones. Although the approximate methods introduce a certain level of calculation error, their simplicity is of interest in the electromagnetic compatibility (EMC) studies. For that reason, finding an approximate, but satisfyingly accurate method, applicable to wide range of parameters is often a goal of researches done in this field.

In this paper, the authors perform an analysis of a thin horizontal dipole antenna (HDA) above real ground of known electrical parameters. The approach is based on the electric-field integral equation method, and formulation of the Hallén's integral equation (HIE). This equation is then solved for the current, which is assumed in a polynomial form, using the point-matching method (PMM). This way obtained system of linear equations involves improper Sommerfeld's integrals, which express the influence of the real ground and are here solved approximately using simple, so-called OIA and TIA, approximations (one- and two-image approximations). Both types of approximations are in an exponential form, and therefore are similar to those obtained applying the Method of Images. It should be kept in mind that the goal of this approach is to develop approximations that have a simple form, whose application yields satisfyingly accurate calculations of the Sommerfeld's type of integrals, and are widely applicable, i.e. their employment is not restricted by the values of electrical parameters of the ground, or the geometry.

Thorough analysis is performed in order to observe the influence of different parameters of the geometry, and the ground, on current distribu-

tion and the input impedance/admittance of the HDA in a wide frequency range. Furthermore, the verification of the method is done by comparison to the exact model based on the full-wave theory, and experimental data. Obtained results indicate a possibility of applying the described methodology to inverse problem involving evaluation of electrical parameters of the ground (or detection of ground type change) based on measured input impedance/admittance of the antenna.

8.4 Paper D

In this paper, the authors perform HF analysis of a thin horizontal conductor fed in its center, and arbitrarily positioned above lossy homogeneous ground of known electrical parameters. The approach is based on the electric-field integral equation method, and formulation of the Hallćn's integral equation. This equation is then solved for the current using the point-matching method. The Sommerfeld's integrals that express the influence of the lossy ground, and that appear in these calculations, are solved approximately. Thorough analysis is performed in order to observe the influence of different parameters of the geometry and the ground on current distribution in the specified frequency range. Furthermore, the verification of the method is done by comparison with the exact model based on the full-wave theory.

8.5 Paper E

A shielded coupled micro-strip line with partial dielectric support is analyzed using the hybrid boundary element method (HBEM) and the finite difference method (FDM). The HBEM is a combination of the equivalent electrodes method (EEM) and the boundary element method (BEM). The microstrip line characteristic parameters: the effective relative permittivity and the characteristic impedance are determined. "Odd" and "even" modes are taken into account. The results are compared with corresponding ones found in the literature.

8.6 Paper F

To solve the electromagnetic scattering problem in two dimensions, the Finite Difference Time Domain (FDTD) method is used. The order of convergence of the FDTD algorithm, solving the two-dimensional Maxwell's curl equations, is estimated in two different computer implementations: with and without an obstacle in the numerical domain of the FDTD scheme. This constitutes an electromagnetic scattering problem where a lumped sinusoidal

current source, as a source of electromagnetic radiation, is included inside the boundary. Confined within the boundary, a specific kind of Absorbing Boundary Condition (ABC) is chosen and the outside of the boundary is in form of a Perfect Electric Conducting (PEC) surface. Inserted in the computer implementation, a semi-norm has been applied to compare different step sizes in the FDTD scheme. First, the domain of the problem is chosen to be the free-space without any obstacles. In the second part of the computer implementations, a PEC surface is included as the obstacle. The numerical instability of the algorithms can be rather easily avoided with respect to the Courant stability condition, which is frequently used in applying the general FDTD algorithm.

8.7 Paper G

A shielded coupled micro-strip line with partial dielectric support is analyzed using the hybrid boundary element method (HBEM) and the finite difference method (FDM). The HBEM is a combination of the equivalent electrodes method (EEM) and the boundary element method (BEM). The micro-strip line characteristic parameters: the effective relative permittivity and the characteristic impedance are determined. "Odd" and "even" modes are taken into account. The results are compared with corresponding ones found in the literature.

References

[1] M. F. Abedin, M. Ali. "Effects of EBG Reflection Phase Profiles on the Input Impedance and Bandwidth of Ultrathin Directional Dipoles". *IEEE Trans. on Ant. and Prop.*, vol. 53, No. 11, Nov. 2005.

[2] Alchemi. [.NET Grid Computing Framework] Homepage (2005-05-17). [Online]. Available: http://www.alchemi.net/

[3] G. Antonini, A. Orlandi, A. Ruehli. "Speed-up of PEEC Method by using Wavelet Transform", in *Proc. of the IEEE Int. Symposium on EMC*", Washington, DC, USA, 2000.

[4] G. Antonini. "The Fast Multipole Method for PEEC Circuit Analysis", in *Proc. of the IEEE Int. Symposium on EMC",* Minneapolis, MN, USA", 2002.

[5] B. Archambeault, C. Brench, O. Rahami. *EMI/EMC Computational Modeling Handbook*, Kluwer Academic Publishers 1998.

[6] G. B. Arfken, Hans J. Weber. *Mathematical Methods for Physicists*, Academic Press, 2001.

[7] V. Arnautovski-Toseva, K. El. Khamlichi Drissi, K. Kerroum, S. Grceva, L. Grcev. "Comparison of Image and Transmission Line Models of Energized Horizontal Wire above Two-Layer Soil", *Automatika* 53, 38-48 (2012).

[8] V. Arnautovski-Toseva, K. El. Khamlichi Drissi, K. Kerroum. "Comparison of Approximate Models of Horizontal Wire Conductor above Homogeneous Ground", in Proc. of *EuCAP 2012* Prague, Czech Republic, 678-682 (2012).

[9] K. Atkinson, W. Han. *Theoretical Numerical Analysis*, A Functional Analysis Framework. Springer-Verlog, New York, Inc., 2001.

[10] C. A. Balanis. *Antenna Theory: Analysis and Design*, John Wiley & Sons, Inc., 1982.

[11] C. A. Balanis. *Advanced Engineering Electromagnetics*, John Wiley & Sons, Inc., 1989.

[12] P. R. Bannister. "Extension of Quasi-Static Range of Finitely Conducting Earth Image Theory Technique to other Ranges", *IEEE Trans. on AP* 26, 3, 507-508 (1978).

[13] A. Banos. *Dipole Radiation in the Presence of a Conducting Half Space*, New York: Pergamon, p. 35, 1969.

[14] J. Blöbaum. "Optimization methods for an inverse problem with time-harmonic electromagnetic waves: an inverse problem in electromagnetic scattering. Inverse Problems" **5**, 463-482 (1989).

[15] J. C. Bolomey, A. Izadnegahdar, L. Jofre, C. Pichot, G. Peronnet, M. Solaimani. "Microwave Diffraction Tomography for Biomedical Applications", *IEEE Transactions on Microwave Theory and Techniques*, vol. 30, No. 11, November 1982.

[16] J. Bond, X. Li, S. C. Hagness. "Microwave imaging via space-time beamforming for early detection of breast cancer," *IEEE Trans. Antennas Propag.*, vol. 51, pp. 1690-1705, Aug. 2003.

[17] J. Bond, X. Li, S. C. Hagness. "Numerical and experimental investigation of an ultrawideband ridged pyramidal horn antenna with curved launching plane for pulse radiation", vol. 2, pp. 259-262, 2003.

[18] A. Bondeson, T. Rylander, P. Ingelström, *Computational Electromagnetics*, Springer, New York, 2005.

[19] P. A. Brennan, A. E. Ruehli. "Efficient Capacitance Calculations for thr Three-dimensional Multiconductor Systems", *IEEE Trans. Microwave Theory Tech.*, vol. 21, no. 2, pp. 76-82, Feb. 1973.

[20] P. A. Brennan, N. Raver, A. E. Ruehli. "Three-dimensional Inductance Computation with Partial Element Equivalent Circuits", *IBM Journal of Research and Development*, vol. 23, no. 6, pp. 661-668, Nov. 1979.

[21] The Cactus Code Server Homepage (2005-05-17). [Online]. Available: http://www.cactuscode.org/

[22] J. Carlsson. *Computation of EMC properties of Slots and Printed Circuit Boards*, PhD Dissertation, Chalmers University of Technology and SP Swedish National Testing and Research Institute, Sweden 1998.

[23] W. Cheney, D. Kinacid. *Numerical Analysis*, Second Edition, ISBN 0-534-33892-5, 1996.

[24] D. K. Cheng. *Field and Wave Electromagnetics*, Addison-Wesley Publishing Co., Reading, Mass., 1989.

[25] D. K. Cheng. *Fundamentals of Engineering Electromagnetics*, Addison-Wesley Series in Electrical Engineering, Nov. 1993.

[26] W. C. Chew. *Waves and Fields in Inhomogeneous Media*, New York: IEEE PRESS Series on Electromagnetic Waves, 1995.

[27] D. Colton, R. Kress. *Inverse Acoustic and Electromagnetic Scattering Theory*, 2nd Edn. Springer-Verlog Berlin Heidelberg New york, 1998.

[28] D. B. Davidson. *Computational Electromagnetics for RF and Microwave Engineering*, Cambridge University Press, New York, 2005.

[29] A. J. Devaney. "The Limited-View Problem in Diffraction Tomography", *Inverse Problems.* 5, 4, 510-510, 1989.

[30] J. Ekman. *Electromagnetic Modeling Using the Partial Element Equivalent Circuit Method*, Ph.D. dissertation, Luleå University of Technology, 2003.

[31] J. E. Garrett. *Advancements of the Partial Element Equivalent Circuit Formulation*, PhD dissertation, The University of Kentucky, 1997.

[32] S. D. Gedney. *Introduction to the Finite-Difference-Time-Domain (FDTD) Method for Electromagnetics*, Morgan & Claypool Publishers, Kentucky, USA, 2010.

[33] D. N. Ghosh, L. S. Couchman. *Inverse Problems and Inverse Scattering of Plane waves*, Academic Press, Orlando, Florida, USA, 2001.

[34] The Globus Alliance Homepage (2005-05-17). [Online]. Available: http://www.globus.org/

[35] Grid Computing and Distributed Systems (GRIDS) Laboratory Homepage (2005-05-17). [Online]. Available: http://www.gridbus.org/

[36] F. Grover. "Inductance Calculations: Working Formulas and Tables", Van Nostrand, 1946.

[37] R. F. Harrington. *Field Computation by Moment Methods*. Robert E. Kreiger, Malabar, FL, 1987.

[38] H. Heeb, A. E. Ruehli. "Approximate Time-Domain Models of Three-Dimensional Interconnects", in *Proc. of the IEEE Int. Conference on Computer-Aided Design*, Santa Clara, CA, USA, 1990, pp. 201–205.

[39] H. Heeb, A. E. Ruehli. "Three-dimensional interconnect analysis using partial element equivalent circuits", *IEEE Trans. Circuits and Systems*, vol. 39, pp. 974-982, Nov. 1992.

[40] M. T. Heath. *Scientific Computing: An Introductory Survey*. McGraw-Hill International Editions, Compter Science Series, Singapore 1997.

[41] J. Held, D. Johansson. *Optimization of Experimental Computational Electromagnetic Code & Grid Computing for PEEC*, Bachelors thesis, Luleå University of Technology, 2005.

[42] T. Henriksson. *Contribution to Quantitaive Microwave Imaging Techniques for Biological Applications*, PhD dissertation, Mälardalen University, Sweden, 2009.

[43] F. B. Hildebrand. *Introduction to Numerical Analysis*, Second Edition, Dover Publications, Inc., New York, 1987.

[44] C. Ho, A. Ruehli, P. Brennan. "The modified nodal approach to network analysis", *IEEE Trans. on Circuits and Systems*, pages 504–509, June 1975.

[45] C. Hoer, Love. "Exact inductance Equations for rectangular Conductors with Applications to More Complicated Geometries", *Journal of Research of the National Bureau of Standards - C. Engineering and Instrumentation*, 69C(2):127-137, 1965.

[46] HPC2N - High Performance Computing Center North (2006-05-20). [Online]. Available: http://www.hpc2n.umu.se/

[47] X. Hu, J. White, J. H. Lee, L. Daniel. "Analysis of Full-wave Conductor System Impedance over Substrate Using Novel Integration Techniques." *DAC 2005, June 13-17, 2005, Anaheim, California, USA.*

[48] A. Ishimaru. *Electromagnetic Wave Propagation, Radiation and Scattering*, Engelwood Cliffs, NJ: Prentice-Hall, 1991.

[49] J. Jin. *The Finite Element Method in Electromagnetics.*, Second Edition, John Wiley & Sons., New York, USA, 1993.

[50] C. Johnson. *Numerical Solution of Partial Differential Equations by the Finite Element Method.* Studentlitteratur, ISBN 91-44-25241-2, 1987.

[51] A. Kirsch, R. Kress. "On an integral equation of the first kind in inverse acoustic scattering". In: *Inverse problems* (Canon and Hornung, eds). ISNM 77, 93-102 (1986).

[52] A. Kirsch, R. Kress. "A numerical method for an inverse scattering problem". In: *Inverse problems* (Engl and Groetsch, eds). Academic Press, Orlando, 270-290 (1987).

[53] A. Kirsch, R. Kress. "An optimization method in inverse acoustic scattering". In: *Boundary elements IX, Vol 3. Fluid Flow and Potential Applications.* Springer-Verlog, Berlin Heidelberg New York, 3-18 (1987).

[54] R. Kress, A. Zinn. "Three dimonsional representation in inverse obstacle scattering". In: *Mathematical Methods in Tomography* (Hermans et al, eds). Springer-Verlog Lecture Notes in Mathematics **1497**, Berlin Heidelberg New York, 125-138 (1991).

[55] R. Kress, A. Zinn. "Three dimensional reconstructions from near-field data in obstacle scattering". In: *Inverse Problems in Engineering sciences* (Yamaguti et al, eds). ICM-90 Satellite Conference Proceedings, Springer-Verlog, Tokyo Berlin Heidelberg, 43-51 (1991).

[56] R. Kress, A. Zinn. "On the numerical solution of the three dimensional inverse obstacle scattering problem". J. Comp. Appl. Math. **42**, 49-61 (1992).

[57] G. Kristensson. *Spridningsteori med tillämpningar*, Studentlitteratur, Lund, Sweden, 1999.

[58] P. K. Kythe. *Boundary Element Methods.* CRC Press, Boca Raton, FL, 1995.

[59] R. J. Leveque. *Finite Difference Methods for Ordinary and Partial Differential Equations*, SIAM, Washington, 2007.

[60] X. Li, S. K. Davis, S. C. Hagness, D. W. van der Weide, B. D. Veen. "Microwave imaging via spacetime beamforming: Experimental investigation of tumor detection in multilayer breast phantoms", *IEEE Trans. Microw. Theory Tech.,* vol. 52, pp. 1856-1856, Aug. 2004.

[61] J. C. Lin. "Frequency optimization for microwave imaging of biological tissues" *in Proc. IEEE,* vol. 73, no. 2, pp. 374-375, 1985.

[62] J. D. Logan. *Applied Mathematics*, 3rd ed. John Wiley & Sons, 2006.

[63] G. K. H. Lui, R. D. Murch. "Compact Dual-Frequency PIFA Designs Using LC Resonators", *IEEE Trans. on Ant. and Prop.*, 49(7):1016-1019,

[64] D. Melendy, A. Weisshar. "A New Scalable Model for Spiral Inductors on Lossy Silicon Substrate", Oregon State University, Department of Electrical and Computer Engineering, 2003.

[65] F. Monsefi. *Mathematical Modeling of Electromagnetic Disturbances in Railway System*, licentiate thesis, Luleå University of Technology, 2006.

[66] F. Monsefi, L. Carlsson, M. Rančić, M. Otterskog, S. Silvestrov. "Solution of 2D electromagnetic scattering by FDTD with optimal step size, based on a discrete norm analysis", *Proceedings of 10th International Conference on Mathematical Problems in Engineering, Aerospace and Sciences-ICNPAA 2014*, Narvik, Norway, 2014.

[67] J. R. Mosig. "Arbitrary shaped Microstrip structures and Their analysis with a Mixed Potential Integral Equation", *IEEE Trans. on Microwaves Theory Tech.*, vol. MTT-36, pp. 314-323, Feb. 1988.

[68] G. Mur. "Absorbing boundary conditions for the finite-difference approximation of the time-domain electromagnetic field equations", *IEEE Transactions on Electromagnetic Compatibility*, Vol. 23, pp. 377-382, 1981.

[69] J. L. Nicol, P. V. Ridd. "Antenna Input Impedance: Experimental Confirmation and Gological Application", *Can. J. Phys.* 66, 818-823 (1988).

[70] Numerical Electromagnetics Code NEC2 unofficial home page. [online]. Available: http:/www.nec2.org/

[71] A. F. Peterson, S. L. Ray, R. Mittra. *Computational Methods for Electromagnetics*. IEEE Press, New York, USA, 1998.

[72] C. Pichot, L. Jofre, G. Peronnet, A. Izadnegahdar, J. Ch. Bolomey. "An angular spectrum method for inhomogeneous bodies reconstruction in microwave."

[73] B. D. Popović. "Polynomial Approximation of Current along thin Symmetrical Cylindrical Dipoles", *Proc. Inst. Elec. Eng.* 117, 5, 873–878 (1970).

[74] B. D. Popović, D. Ž. Djurdjević. "Entire-Domain Analysis of Thin-Wire Antennas near or in Lossy Ground", *IEE Proc., Microw. Antennas Propag.* 142, 213-219 (1995).

[75] B. D. Popović, V. V. Petrović. "Horizontal Wire Antenna above Lossy Half-Space: Simple Accurate Image Solution", *International journal of numerical modeling: Electronic networks, devices and fields* 9, 194-199 (1996).

[76] M. P. Rančić, P. D. Rančić. "Vertical Dipole Antenna above a Lossy Half-Space: Efficient and Accurate Two-Image Approximation for the Sommerfeld's Integral", in Proc. of *EuCAP 2006* Nice, France, paper No121 (2006).

[77] M. Rančić, P. Rančić. "Horizontal Linear Antennas above a Lossy Half-Space: A New Model for the Sommerfeld‘s Integral Kernel", *Int. J. El. Commun. AEU* 65, 879-887 (2011).

[78] M. Rančić, S. Aleksić. "Horizontal Dipole Antenna very Close to Lossy Half-Space Surface", *Electrical Review* 7b, 82-85 (2012).

[79] M. Rančić. *Analysis of Wire Antenna Structures in the Presence of Semi-Conducting Ground*, Ph.D dissertation, Faculty of electronic engineering, University of Niš, Niš, Serbia (2012).

[80] M. Rančić, S. Aleksić. "Analysis of Wire Antenna Structures above Lossy Homogeneous Soil", in Proc. of *21st Telecommunications Forum (TELFOR)* Belgrade, Serbia, 640-647 (2013).

[81] J. F. Roach. *Green's Functions.* 2nd ed. Cambridge University Press. New York, 1982.

[82] A. E. Ruehli. *An Integral Equation Equivalent Circuit Solution to a Large Class of interconnect System* , PhD. Dissertation, The University of Vermont, USA, 1972.

[83] A. E. Ruehli. "Inductance Calculations in a Complex Integrated Circuit Environment", *IBM Journnal Development*, vol. 16, no. 5, pp. 470-481, Sep. 1972.

[84] A. E. Ruehli, P. A. Brennan. "Efficient capacitance calculations for three-dimensional multiconductor systems", *IEEE Trans. on Microwave Theory and Techniques*, 21(2):76-82, February 1973.

[85] A. E. Ruehli. "Equivalent Circuit Models for Three-dimensional Multiconductor Systems", *IEEE Trans. Microwave Theory Tech.*, vol. 22, no. 3, pp. 216-221, Mar. 1974.

[86] A. E. Ruehli. "Circuit Models for Three-dimensional Geometries Including Dielectrics"*IEEE Trans. microwave Theory Tech.*, vol.40, no.7, pp. 1507-1516, Jul. 1992.

[87] A. E. Ruehli. *et al.*, "Nonorthogonal PEEC Formulation for Time- and Frequency- Domain EM and Circuit Modeling", *IEEE Trans. on EMC*, vo. 45, no. 2, pp. 167-176, May 2003.

[88] M. N. O. Sadiku. *Numerical Techniques in Electromagnetics.* CRC Press, Inc. 1992.

[89] M. N. O. Sadiku. *Elements of Electromagnetics*, Fourth Edition, Oxford University Press, New York, 2007.

[90] "The Self and Mutual Inductance of linear Conductors", *Bulletin of the National Bureau of Standards*, 4(2):301-344, 1908.

[91] S. Y. Semenov, R. H. Svenson, A. E. Boulyschev, A. E. Souvorov, V. Y. Borisov, Y. Sizov, A. N. Starostin, K. R. Dezern, G. P. Tatsis, V. Y. Baranov. "Microwave Tomographi. Two-Dimensional System for Biological Imaging", *IEEE Transactions on Biomedical Engineering*, Vol. 43, NO. 9, September 1996.

[92] R. M. Shubair, Y. L. Chow. "A Closed Form Solution of Vertical Dipole Antennas above a Dielectric Half-Space", *IEEE Tran. on Antenna and Prop.*, Dec., 1993.

[93] G. Sparr. *Kontinuerliga System*, Lund Institute of Technology, Department of Mathematics, Sweden. Lund 1984.

[94] J. J. Stammes. "Focusing of two-dimensional waves", *J. Opt. Soc. Amer.,* vol. 71, no. 1, pp. 15-31, 1981.

[95] D. M. Sullivan. *Electromagnetic Simulation Using the FDTD Method*. John Wiley & Sons, Inc., 2000.

[96] L. N. Trefethen. *Finite Difference and Spectral Methods for Ordinary and Partial Differential Equations*, SIAM, New York, 1996.

[97] L. Tsang, J. A. Kong, K-H. Ding. *Scattering of Electromagnetic Fields*, John Wiley & Sons, New york, 2000.

[98] J. R. Wait, K. P. Spies. "On the Image Representation of the Quasi-Static Fields of a Line Current Source above the Ground", *Can. J. Phys.* 47, 2731–2733 (1969).

[99] S. Wolfgang. *Total Variation Regularization for Linear Ill-posed Inverse Problems: Extensions and Applications*, PhD Dissertation, Arizona State University, December, 2008.

[100] J. J. Yang, Y. L. Chow, D. G. Fang. "Discrete complex images of a three-dimonsional dipole above and within a lossy ground", *IEE Proceedings-H*, vol. 138, No. 4, Aug. 1991.

[101] K. S. Yee. "Numerical Solution of initial Value Problems Involving Maxwell's Equations in Isotropic Media", *IEEE Trans. Antennas and Propagation*, vol. 14, pp. 302-307, 1966.